CHEMICAL REVIEWS

REVIEW

pubs.acs.org/CR

# Theoretical Studies of Plasmonics using Electronic Structure Methods

Seth M. Morton, Daniel W. Silverstein, and Lasse Jensen*

Department of Chemistry, The Pennsylvania State University, 104 Chemistry Building, University Park, Pennsylvania 16802, United States

## CONTENTS

1. Introduction 3962
2. Absorption Properties of Small Metal Clusters 3963
   2.1. Alkali Metals 3963
   2.2. Noble Metal Clusters 3964
   2.3. Monolayer-Protected Metal Clusters 3966
   2.4. Microscopic Origin of Plasmons 3966
   2.5. Optical Properties of Quantum Nanoparticle Dimers 3968
3. Enhanced Absorption of Molecules near Metal Clusters 3968
   3.1. Enhanced Electronic Excitations 3968
   3.2. Surface-Enhanced Infrared Absorption 3970
4. Surface-Enhanced Fluorescence 3970
5. Surface-Enhanced Raman Scattering 3974
   5.1. Early History of SERS 3974
   5.2. The Electromagnetic Mechanism 3975
   5.3. The Chemical Mechanism 3976
      5.3.1. The Resonance Raman Mechanism 3976
      5.3.2. The Charge-Transfer Mechanism 3977
      5.3.3. The Nonresonant Chemical Mechanism 3977
   5.4. Unifying the Description of SERS 3978
      5.4.1. Combined Quantum and Classical Method for SERS 3979
6. Chiroptical Properties of Small Metal Clusters 3979
   6.1. Circular Dichroism 3979
      6.1.1. Chiral Core Model 3980
      6.1.2. Dissymmetric Field Model 3981
      6.1.3. Chiral Footprint Model 3981
   6.2. Vibrational Raman Optical Activity 3983
7. Nonlinear Optical Properties 3984
   7.1. Surface-Enhanced Hyper-Raman Scattering 3984
8. Conclusion 3986
Author Information 3987
Biographies 3987
Acknowledgment 3987
References 3988

## 1. INTRODUCTION

There has been a great interest in understanding the interactions between light and noble metal nanoparticles ever since Michael Faraday's study of the ruby-red color of colloidal gold in the mid-1800s.[1] The property that makes the nanoparticles so special is their ability to support surface plasmons (collective oscillations of the conduction electrons). Excitation of these plasmons leads to a strong absorption band in the UV−visible region and is thus responsible for nanoparticles' brilliant optical properties. The plasmon wavelength can be tuned by adjusting the size, shape, and surroundings of the nanoparticle.[2,3] This feature makes them uniquely suited for a wide range of applications in catalysis, optics, chemical and biological sensing, and medical therapeutics.[4−8]

Today, advances in colloidal synthesis methods and nanofabrication techniques, such as e-beam and nanosphere lithography, combined with detailed characterization methods[9−14] enable nanoparticles with tunable shapes and sizes, and therefore tunable optical properties, to be obtained. In addition, the characterization of the nanoparticles by detailed quantitative electromagnetic simulations has provided an unprecedented understanding of correlation between shape, size, and environment with the optical properties of the nanoparticles.[9,10,12,13] This in turn has resulted in a wide range of applications in ultrasensitive chemical and biological sensing[15−21] due to new techniques like plasmon resonance sensing,[22,23] surface-enhanced Raman scattering (SERS),[5,15,24,25] and surface-enhanced fluorescence (SEF).[26,27]

Classical electrodynamics methods provide accurate and efficient simulations of optical properties assisting in the rationalization of experimental findings and prediction and design of novel nanostructured materials with specific optical properties. Several numerical simulation methods, such as Mie theory,[28] discrete dipole approximation (DDA),[29,30] and finite difference time domain (FDTD),[31,32] exist and have been widely used to model nanospheres, nanodisks, nanorods, nanoprisms, and other complex geometrical configurations. The optical spectrum of small metal particles (sizes below the wavelength of the light) are dominated by a broad resonance interpreted as a surface plasmon resonance (or Mie resonance), which can be considered as a collective excitation of the conducting electrons.[5,33,34] Within classical electrodynamics, the optical properties of metallic nanoparticles are well understood if the size is large enough such that a local dielectric constant is appropriate. However, as the size of the particle becomes smaller than the mean free path of the conduction electrons (∼50 nm for Au and Ag), the dielectric constants have a size dependence that needs to be included if accurate optical properties are to be determined.[4,5,34−36] This becomes critical for particles with dimensions smaller than ∼10 nm and leads to a significant broadening of the plasmon peak. These deviations are usually accounted for by modifying the dielectric constant of the metal particle empirically to account

**Special Issue:** 2011 Plasmonics

**Received:** August 17, 2010
**Published:** February 23, 2011

for the enhanced electron-surface scattering in small nanoparticles, and this approach has been shown to improve upon the classical results.[5,37] Recent studies have also highlighted the importance of using a fully nonlocal dielectric constant for correctly describing the optical properties of nanoparticles with dimensions smaller than 10 nm.[38,39]

As the size of metal particles decreases further to dimensions comparable to the Fermi wavelength of the electron (~0.5 nm for Au or Ag), the electronic motion becomes confined and the electronic energy levels become discrete. This smaller size is associated with optical, electronic, and chemical properties differing from those of the larger nanoparticles.[4,40,41] Due to quantum confinement, these small metal clusters show molecular-like electronic structures, and the characteristic plasmon bands are replaced with discrete electronic transitions.[42−44] Thus, investigating small metal clusters by optical spectroscopy provides a way of understanding the electronic structure of these systems.[4,5,33,34,45−53]

Recent advances in nanoscience have demonstrated that small Au and Ag nanoclusters (<2 nm) can be synthesized with precise control of the number of metal atoms and ligands.[14,54−56] Small noble metal (Cu, Ag, Au) particles are of great interest to study due to their complicated physical and chemical properties.[3,5,34,50] Small Ag and Au clusters stabilized by encapsulation in organic dendrimers have been shown to exhibit strong fluorescence at room temperature.[57,58] Furthermore, small silver clusters have been shown to produce enhanced Raman signal characteristic of the scaffold used to stabilize the clusters in solution.[59,60] Thus, these nanoclusters are of great interest due to their unique optical and electronic properties, and their small size makes them particularly suitable for biological sensing.[59−62]

The electronic states of a metal are typically considered as a continuum and are described in terms of their band structure. However, since metal clusters exhibit a strong dependence on size and configuration due to quantum size effects, the discreteness of the electronic states becomes important as the size of metal particles become smaller. Kubo showed that the spacing between energy levels increases inversely with the volume of the particle.[64,65] This can be realized by considering a free electron model where the energy gap, the so-called Kubo gap ($\delta$), near the Fermi energy ($E_f$) is given by

$$\delta = \frac{4E_f}{3N} \quad (1)$$

where $N$ is the number of valence electrons. If the gap is smaller than the thermal energy, $k_BT$, the particle will be metallic, and if the gap is larger than $k_BT$, the particle will be insulating. The dependence of the gap on the size of the particle is illustrated in Figure 1. For very small particle sizes, the electronic energy levels are discrete and thus are molecular-like in nature. At the point where the Kubo gap becomes similar to the thermal energy, the discreteness of the energy levels starts to influence the properties of the metal cluster. For example, at room temperature the number of valence electrons needed for the gap to be similar to the thermal energy for silver is around 287 ($E_f$ = 5.51 eV). This corresponds roughly to a nanoparticle with a size on the order of 2 nm, and in this regime, the exact nature of the electronic structure becomes important and is dominated by quantum size effects.

The focus of this review is to highlight recent advances in applying electronic structure methods to study and understand optical properties of metal clusters ranging from small clusters to large nanoparticles. First, optical response of metal nanoparticles will be described in detail to explain the origin of plasmons. The application of those plasmon resonances is then discussed with respect to enhancements of linear absorbance, Raman scattering, fluorescence, infrared absorption, optical activity, and nonlinear optical processes. A brief outline of potential future work is given to conclude this review.

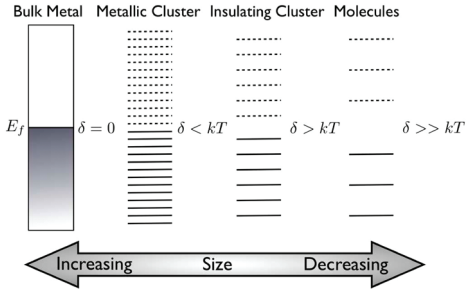


**Figure 1.** Evolution of the band gap and the density of states as the number of atoms in a system increases (from right to left). $\delta$ is the so-called Kubo gap. Adapted with permission from ref 63. Copyright Wiley-VCH Verlag GmbH & Co. KGaA.

## 2. ABSORPTION PROPERTIES OF SMALL METAL CLUSTERS

### 2.1. Alkali Metals

The optical properties of small alkali metal clusters have been of great interest since the early experiments by Knight and coworkers[33,48,66,67] showing that clusters with 2, 8, 18, 20, 34, 40, etc. atoms, the so-called magic numbers, were more stable. These magic numbers could be explained based on a simple jellium model where the metal cluster is modeled by uniform, positively charged spheres with electronic shells, that is, 1s, 1p, 1d, 2s, 1f, 2p, etc., filled with valence electrons.[34,53,68,69] Since then the photoabsorption spectra of size-selected sodium clusters with a small number of atoms ($n = 3-40$) have been studied extensively.[33,45,46,48,51] While the smallest clusters ($n < 6$) showed absorption spectra more characteristic of molecules with several distinct transitions, the larger clusters show spectra dominated by a broad resonance containing most of the oscillator strength. The resonance corresponds to the collective dipole oscillation of the valence-electron cloud against the positive ionic background.[33] Thus, the photoabsorption spectra of the sodium clusters evolve from discrete transitions in the small cluster to more collective excitations resembling the response of larger nanoparticles. For this reason, the initial interpretations of absorption spectra were done in terms of the surface plasmon resonance.[33,34,45,48]

The surface plasmon resonance, $\omega_p$, for a finite metallic spherical cluster much smaller than the wavelength of the light is given classically by the Drude model as[33,34,45,48]

$$\omega_p^2 = \frac{4\pi\rho e^2}{3m_e} \quad (2)$$

where $\rho$ is the valence electron density of the cluster. Since the electron density can be related to the polarizability as $\rho = 3N_e/(4\pi\alpha)$, we can write the plasmon resonance as[33,34,45,48]

$$\omega_p^2 = \frac{N_e e^2}{m_e \alpha} \quad (3)$$

where $N_e$ is the number of valence electrons in the cluster. The polarizability for spherical metal clusters as a function of size can,

to a good approximation, be described by a jellium model[70]

$$\overline{\alpha}_{atom} = \frac{(N^{1/3} r_{WS} + \delta)^3}{N} \quad (4)$$

where $N$ is the number of atoms in the metal cluster, $r_{WS}$ is the Wigner−Seitz radius of the bulk metal, and $\delta$ represents the spill-out of the electrons from the surface of a metallic sphere. This simple model could be extended to spheroidal particles by taking into account that the clusters can have different polarizabilities along their axes.[34] This ellipsoidal shell model (ESM) has been shown to work reasonably well for small sodium clusters.[33,45,48] However, for small lithium clusters, this model was found to give poor results[51] but could be corrected by adopting an effective number of valence electrons of $N_e^{eff} = 0.77N_e$.[51,71] As the size of the particle increases, the polarizability reaches the classical limit of a conducting sphere, that is, $\alpha = r_{WS}^3$. From this, we see that the polarizability of a small sphere is increased compared with the bulk limit due an increase in the effective radius caused by the spill-out of the valence electrons. This increase in the polarizability as the size of the cluster is reduced was indeed observed experimentally for small Na and K clusters.[67,71−74] Since the plasmon resonance is inversely proportional to the polarizability, the spill-out effect would also lead to a red-shift in the plasmon resonance compared with the bulk Mie results as the size of the cluster decreases. This red-shift in the plasmon response of the small clusters was also observed experimentally.[33,45,46,48,51] While the simple EMS model was fairly successful in explaining the main features and broad resonance of the photoabsorption spectra and providing an intuitive explanation for its origin, the model could not account for additional fine structure in the spectra. Since both $Na_8$ and $Na_{20}$ are closed-shell structures (and thus spherical), the EMS model predicts only one resonance. While only one broad peak is found for $Na_8$, the experiments show an additional band that is blue-shifted compared with the main absorption in $Na_{20}$. Additionally, the EMS model was found to predict resonances in good agreement with experiments for clusters with $n = 6−12$ whereas larger discrepancies were found for larger clusters.

Due to the small size of the metal clusters, it is not surprising that classical models fail to account for all the observed features since quantum effects are expected to be crucial. Therefore, to account for quantum effects, there have been numerous simulations of the photoabsorption properties of small alkali metal clusters, since their small size made them amenable to treatment using high-level electronic structure.[46,47,49−52,75−81] Generally, the agreement between experiment and electronic structure theory is very good, allowing for a detailed understanding of not only the main peaks but also the fine structure in the absorption spectra. Thus, the interplay between the accurate theoretical models and the experimental results lead to a more detailed understanding of the electronic configurations and, at least for smaller clusters, a determination of the ground-state geometries. For larger clusters, contributions from more than one structure should not be excluded. Most of these studies were done at zero temperature, but first-principles simulations have shown that quantum and thermal fluctuations also have a significant effect on the photoabsorption spectra.[80,82−84]

Another property of alkali metal clusters for which a strong dependence on cluster size is observed is the static polarizability.[67,71−74] The experiment carried out by Knight et al. for the direct measurement of the polarizability of Na and K clusters by electron deflection of a molecular beam has revealed the size-dependence of the polarizability of these metal clusters. It has been shown that minima in the polarizability values for $Na_n$ clusters occur when $n = 2$, 8, or 20, which correspond to shell-closing in the simple jellium model. Again, due to their small size, many examples of calculations of the static polarizability for alkali clusters using first-principles methods exist in the literature.[76,78,85−92] In general, there is good agreement between theory and experiments, especially if one considers the evolution of the polarizability with respect to the size of the clusters. The theoretically estimated polarizability for sodium clusters is in general found to be too low compared with experiments, whereas for lithium clusters, the opposite is true. For sodium clusters, it was shown that the inclusion of temperature effects into the calculations could explain the discrepancy.[87,88] In the case of lithium clusters a recent high-level correlated electronic structure theory study showed that the main reason for the discrepancy is that density functional theory (DFT) overestimates the Li−Li bond length in these clusters.[77]

The excellent agreement between first-principles results and experiments naturally suggests that the photoabsorption spectra of small clusters is best described in terms of distinct molecular transitions. Therefore, the concept of a surface plasmon is questionable for the small metal clusters discussed here.[50] However, a recent study using quantum fluid dynamics and time-dependent density functional theory (TDDFT) showed that the electronic excitation can be interpreted as density oscillations even for very small clusters.[93,94] This is illustrated in Figure 2 where the density change due to the lowest excitation in $Na_2$ clearly shows a density increase at one end of the molecule and a decrease at the other. Thus, the description of excitations in small metal clusters in terms of transitions between distinct molecular states agrees with the notion of collective electronic excitations arising from the oscillations of the valence electrons.

### 2.2. Noble Metal Clusters

While the alkali clusters behave like almost perfect free-electron metals, the electronic structure of noble metal clusters is more complicated due to the influence of d-electrons. Thus, understanding the electronic and optical properties of noble metal clusters remains a challenge. Experimentally, optical absorbance spectra were first obtained by photofragmentation of mass-selected $Ag_n^+$ ($n \leq 21$) clusters.[95] Small neutral $Ag_n$ ($n = 2−39$) clusters have also been characterized by embedding the clusters in rare-gas matrices.[96−98] Similar to small Na clusters, it has been observed that silver clusters have large peaks on their absorbance spectra as cluster size increases.[96,98] These plasmon-like peaks are characterized by broad widths and large intensity and thus are dominant features of the absorbance spectra. The absorbance spectra for the $Ag_n$ clusters ($n = 2−39$) show similar characteristics to one another in two different size regimes. For smaller clusters in the range from $n = 2$ to $n = 6$, the spectra are characterized by several comparable intense absorption lines. The remaining silver clusters ($n = 7−39$) are likewise grouped together with similar features on their absorption spectra. For the larger clusters, the spectrum becomes primarily dominated by one peak located between 3.40 and 4.00 eV.

Similar to the Na clusters, the absorption spectra for small Ag clusters was initially interpreted in terms of collective excitation of the valence electrons.[36,95,96,98] However, in contrast to alkali metal clusters, which showed a red-shift of the plasmon resonance for small clusters, small Ag clusters show a blue shift of the

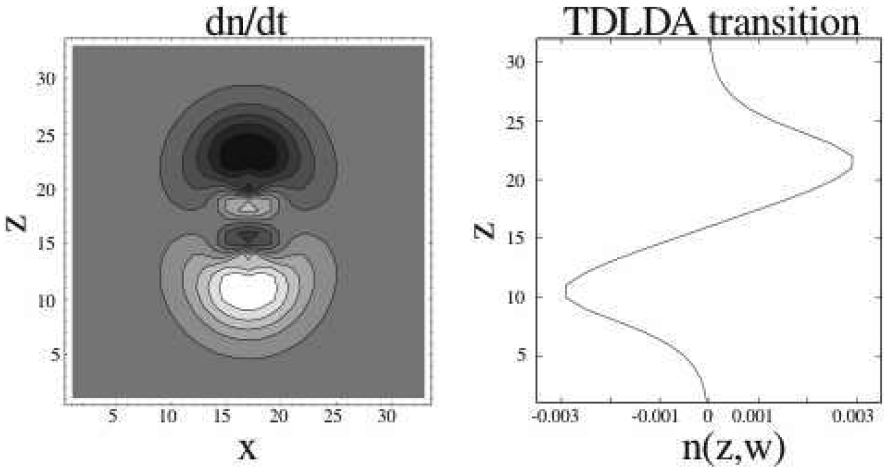


**Figure 2.** (left) Change in valence electron density using quantum fluid dynamics, where dark shading indicates a density increase and light shading a decrease for the lowest excitation in $Na_2$. (right) Integrated electron density along the bond axis using TDDFT for the lowest excitation in $Na_2$. Reprinted from ref 93 with kind permission from Springer Science and Business Media. Copyright 2001.

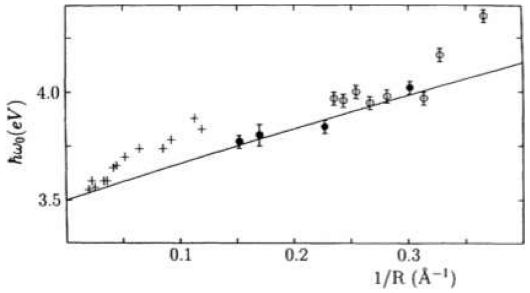


**Figure 3.** Blue shift of plasmon resonance in small Ag clusters as the size decreases. Reprinted with permission from ref 95. Copyright 1993 by the American Physical Society.

resonance as the size of the metal cluster decreases (see Figure 3). As described above, the red-shift for Na clusters was caused by the spill-out of the valence electrons. Using a Drude model for the Ag clusters (which only takes into account the 5s electrons) cannot describe the observed blue shift in peak position as the cluster size is decreased. Thus, in order to correctly describe this effect, it is essential to include the interband transitions from the 4d electrons to the free electron bands at the Fermi level. The d electrons form a size-dependent polarizable background, which screens the interactions between the valence electrons, effectively shifting the collective excitation frequencies to lower energies relative to those predicted from a simple Drude model.[36] Since the d electrons are more strongly localized and therefore do not exhibit spill-out effects, the screening at the surface is reduced. To account for this, the optical properties of the Ag clusters were modeled using a two-layer dielectric model where the inner sphere was described by a bulk dielectric function, which includes the effects of the d electrons, and an external layer described by a Drude dielectric function that includes the spill-out of the 5s electrons.[36] This model showed that the blue shift of the plasmon frequency is a result of two opposite trends, that is, the screening due to the d-electrons and the spill-out effect from the s electrons. As the size of the Ag cluster decreases, the surface to volume ratio increases which reduces the d electron screening and increases the plasmon frequency, compensating for the spill-out effect.

First-principles modeling has provided accurate and efficient descriptions of the electronic structure and optical properties of Ag nanoclusters of different sizes.[5,34,50,99−104] Absorbance spectra have been modeled theoretically using *ab initio* techniques for neutral $Ag_n$ clusters ($n = 2-8$) and cationic $Ag_n^+$ clusters ($n = 2-4$) using the framework of linear response equation-of-motion coupled cluster (EOM-CC) method.[105,106] TDDFT has also been used to examine optical properties for small and medium $Ag_n$ ($n = 2-22$) clusters.[97,107−109] A comparison between TDDFT and many-body method based on solving the Bethe−Salpeter equation (BSE) for calculating the optical excitation of small $Ag_n$ ($n = 1-8$) clusters has also been discussed.[109] While TDDFT was found to generally be in good agreement with experiments, poor agreement was found for the BSE method, especially for the larger clusters. This was explained by the nonlocality of the BSE kernel and correlations involving 4d electrons. Recently, the absorption properties of $Ag_n$ ($n = 4-20$) clusters was also studied using long-range corrected TDDFT, which showed improved agreement with experiments and EOM-CCSD results compared with traditional DFT functionals.[110] Overall, very good agreement between theory and experiments is found, especially for smaller clusters, enabling a detailed understanding of the optical properties of the Ag clusters to be achieved.

The importance of the d electrons on the absorption spectra of the Ag clusters can be understood in detail since the first-principles methods explicitly account for their interaction on the electronic structure. TDDFT has been used to characterize the contribution of the d electrons to the excitation energies in small Ag clusters.[107,108] Absorption spectra are affected by the d electrons through two mechanisms. First, the d electrons screen the s electrons, which leads to a quenching of the oscillators. They also contribute directly to the electronic transitions. Both processes are illustrated in Figure 4. On average, the screening is found to quench the oscillator strengths by 55% using TDDFT and around 65% from experiments compared with the values characteristic for s-electrons in alkali metals. In general, the oscillator strengths obtained within the time-dependent local density approximation (TDLDA) are approximately 15% smaller than those obtained in EOM-CC calculations.[107,108] One possible explanation for the underestimation of oscillator strengths below a certain threshold is that TDDFT calculations involving

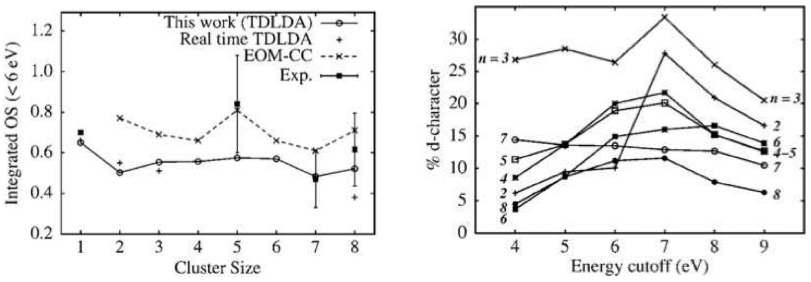


**Figure 4.** (left) Reduction of oscillator strength due to d electrons. (right) Contribution of d electrons to excitations in small Ag clusters. Reprinted with permission from ref 108. Copyright 2005 by the American Physical Society.

traditional exchange−correlation (XC) functionals find many spurious low-lying charge-transfer states. While these spurious states do not carry any significant oscillator strength, they do push some oscillator strength to higher energies. Thus, a reduction in the total oscillator strength is observed below a given threshold. It was recently shown that long-range corrected TDDFT, which correctly describes charge-transfer states, predicts significantly fewer states and higher oscillator strengths than traditional functionals like PBE.[110] The long-range corrected functionals were also found to predict absorption spectra in better agreement with both experiments and EOM-CC results than the traditional functionals.

In contrast to Na and Ag clusters, fewer experimental studies that focus on understanding the size dependence of the optical properties of small Au clusters have been presented.[111−116] There have been several theoretical studies of the optical properties of small and medium sized Au clusters.[99,103,117−123] Experimentally, near-UV depletion spectra of $Au_n^- \cdot Xe$ ($n = 7-11$) have been determined and compared with TDDFT simulations.[116] It was found that spectra were characterized by molecular-like absorption features without the strong transition near 530 nm found for the plasmon resonance in larger nanoparticles. TDDFT predictions of the optically allowed transitions for the most stable isomers of the corresponding Au cluster anions were found to be consistent with the experimental observation. TDDFT results show that in small Au clusters the screening of the s electrons by the d electrons is stronger than that for Ag clusters and leads to quenching of the oscillator strengths by 40%.[103] Also, the d electron contribution to the excitations is increased in Au clusters compared with Ag clusters. The stronger mixing of the d electrons in the excitations is due to the smaller energy difference between the s and d levels in Au clusters. This is caused by relativistic effects and is essential to include in order to correctly describe the optical properties of Au clusters. This is in contrast to Ag clusters where relativistic effects play a minor role. While most studies only account for scalar relativistic effects, a few studies have highlighted the importance of also including spin−orbit effects in the simulations of the optical properties of Au clusters.[120,121]

## 2.3. Monolayer-Protected Metal Clusters

Small monolayer protected Au and Ag nanoclusters (<2 nm) can be synthesized with precise control of the number of metal atoms and ligands,[14,54−56,124−126] and clusters with composition $Au_{20}(SR)_{16}$, $Au_{25}(SR)_{18}$, $Au_{38}(SR)_{24}$, $Au_{102}(SR)_{44}$, $Au_{140-156}(SR)_{\sim 50-60}$, where SR is the thiolated organic ligand used to stabilize the cluster, are found to be particularly stable. A breakthrough in the characterization of these small monolayer projected Au clusters was the total structural determination of the Au nanoclusters $Au_{102}(SR)_{44}$ and $Au_{25}(SR)_{18}^-$ through X-ray crystallography presented recently.[14,54−56] Electronically, the stability of the $Au_{25}(SR)_{18}^-$ clusters can be understood in terms of the "superatom" model.[127] The superatom model describes the electronic stability of small metal clusters based on a jellium model. In this model, structures with filled shells, that is, number of valence electrons given by the magic numbers 2, 8, 18, etc., are predicted to be particularly stable. Experiments and DFT simulations have shown that the $Au_{25}(SR)_{18}^-$ cluster can be viewed as consisting of a $Au_{13}^{5+}$ core surrounded by six anionic $RS-(Au-SR)_2^-$ units.[54−56] This leads to a shell-closing of eight electrons in the core, which should bring extra stability according to the superatom model. The superatom model has also been used to understand the stability of larger Au clusters,[127] although a recent study using DFT has shown that the model cannot account for the thermodynamic stability of the gold nanoparticles.[128]

The fact that the crystal structure of the $Au_{25}(SR)_{18}^-$ clusters was available enabled a complete correlation between its structure and its optical properties.[56,129,130] The simulated absorption spectrum calculated using TDDFT was found to be in very good agreement with experiments, enabling a detailed understanding of the individual bands observed. As shown in Figure 5, the optical spectrum is characterized by three main transitions. The first transition at 1.52 eV is the HOMO to LUMO transition, which can be characterized as an intraband band transition (sp ← sp), the second transition at 2.63 eV arises from mixed intraband (sp ← sp) and interband (sp ← d) transitions, while the transition at 2.91 eV arises predominantly from an interband transition (sp ← d). While initially the lowest transition at 1.52 eV was described in terms of the electronic and geometric structure of the $Au_{13}$ core, recent work has shown that the optical absorption spectra are not separable into core and ligand contributions.[129]

## 2.4. Microscopic Origin of Plasmons

Although the optical properties of small metal clusters could with some success be understood in terms of collective oscillations of the valence electrons using a simple Drude model, a superior description was obtained by adapting electronic structure methods. For the smallest clusters, this naturally lends itself to interpreting the optical properties in terms of discrete molecular-like transitions. However, for larger clusters a comprehensive analysis of the excitations using electronic structure theory becomes cumbersome because the excited states form a quasi-continuum so that a large number of molecular transitions contribute to the observed absorption band. This raises the question of at what point is it best to describe the transition in terms of collective excitations or plasmons rather than in terms of individual molecular transitions. Or said in another way, how many electrons are needed to support a plasmon? While the

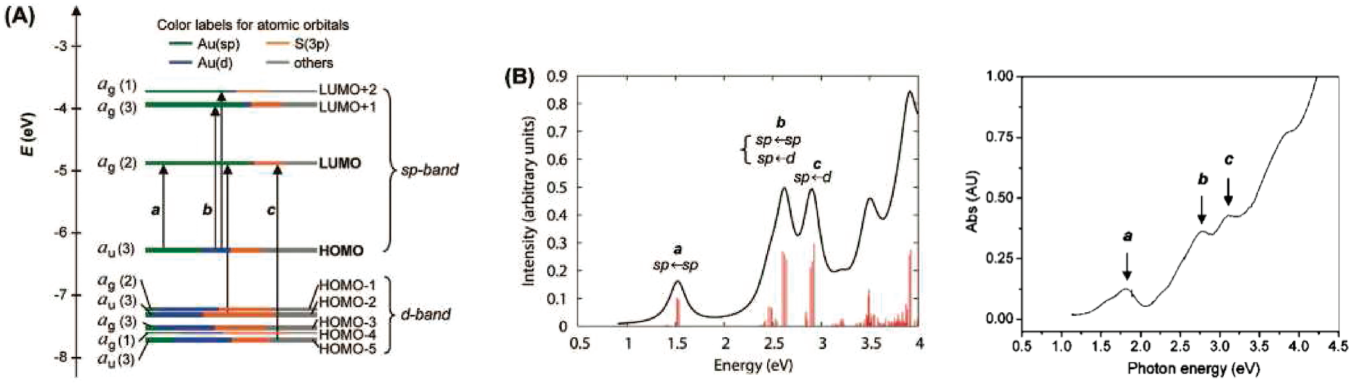


**Figure 5.** (A) Orbital energy level diagram for the model $Au_{25}(SH)^{-}_{18}$. (B) Simulated absorption spectrum of $Au_{25}(SH)^{-}_{18}$. (C) Experimental absorption spectrum of $Au_{25}(SR)^{-}_{18}$. Reprinted with permission from ref 56. Copyright 2008 American Chemical Society.

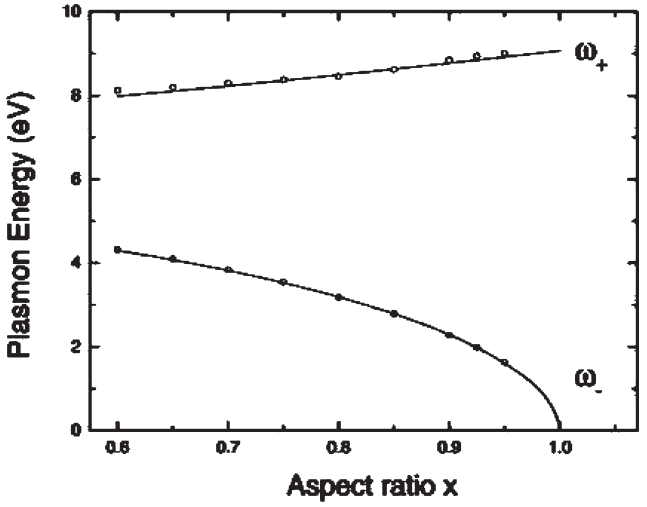


**Figure 6.** TDLDA simulations of the optical properties of nanoshells. Symmetric ($\omega_-$) and antisymmetric ($\omega_+$) plasmon resonances calculated using TDLDA are represented by ○. Solid lines correspond to Mie theory results. Reprinted with permission from ref 132. Copyright 2003 American Chemical Society.

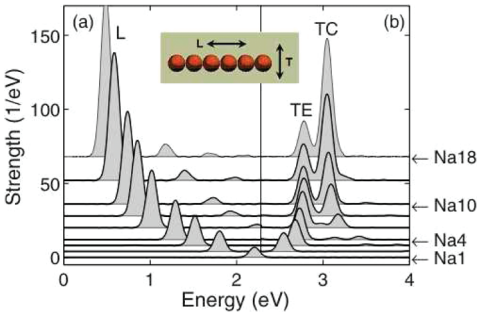


**Figure 7.** Evolution of plasmon in 1D atomic chains of Na as the number of atoms in a system increases: (a) longitudinal and (b) transverse directions. Reprinted with permission from ref 135. Copyright 2007 by the American Physical Society.

experimental and theoretical studies of the absorption spectra of small size-selected clusters provide direct insights into the size evolution of the plasmon resonance, the different cluster shapes and structures complicate the comparison with larger spherical nanoparticles. Therefore, several studies using electronic structure theory have focused on understanding the size evolution of plasmons for simple geometric nanoparticles.[118,122,131−136]

Since the plasmon resonance of large nanoparticles is typically described in terms of classical electrodynamics such as Mie theory, it is important to understand at what point quantum mechanical methods agree with classical electrodynamics. The optical properties of large nanoparticles can efficiently be calculated using TDLDA, employing a jellium model where the ionic background charge of the particles is replaced by a uniform charge density that terminates at the nanoparticle surfaces. This model was shown to be able to successfully describe the optical properties of small sodium clusters.[53,68,69] Using this model, one can simulate the optical properties of spherical nanoparticles with up to $10^5$ electrons, which are large enough that the results can be compared directly with classical results.[132,137,138] This model was recently used to study the structural tunability of the plasmon resonance in metal nanoparticles consisting of a thin metal nanoshell around a dielectric core with overall diameters between 4 and 32 nm. The TDLDA results of the dependence of two dipolar resonances on the ratio of the particle radius to the shell thickness was in excellent agreement with predictions based on Mie theory, as shown in Figure 6.

Electronic structure theory that goes beyond the simple jellium model is computationally very demanding and thus unable to treat the large nanoparticles needed for a direct comparison with classical results. However, by study of nanoclusters with a highly symmetric tetrahedral shape, it was possible to systematically follow the evolution of the cluster spectra from $Ag_{20}$ to $Ag_{120}$ since these clusters are characterized by an especially narrow absorption line shape.[131] This allowed the size dependence of the absorption wavelength and width of the absorption spectra to be extrapolated, making it possible to connect the TDDFT results with classical electromagnetic theory results that are obtained for larger clusters based on DDA simulations. Also, a TDDFT study of the optical properties of charged gold octahedral clusters with 6−146 atoms has been used to explore the blue shift in the main absorption band with decreasing cluster size.[139]

Electronic excitations in linear atomic chains of metals atoms consisting of Na, K, Ag, and Au have been studied using TDDFT.[134−136] The 1D nature of the atomic chains provides a simple system in which the formation and development of collective excitations in the absorption spectra as a function of

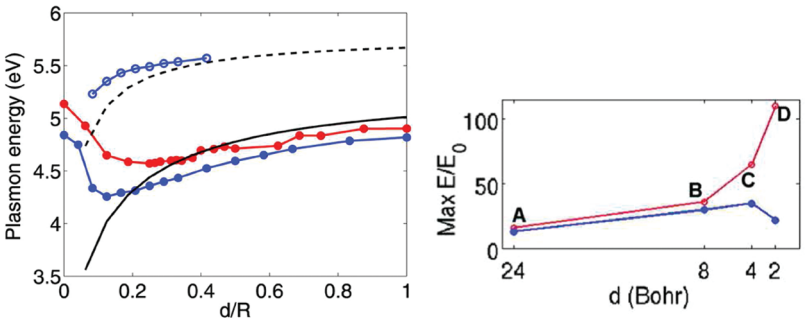


**Figure 8.** Optical properties of nanodimers calculated using TDLDA and Mie theory: (left) plasmon resonances plotted with respect to the ratio of the particle gap (d) and particle radius (R) and (right) electric field enhancement as a function of particle gap. For the left panel, data for $R = 16$ bohr (red) and 24 bohr (blue) are shown for dipolar (●) and quadrupolar (○) plasmon energy. Mie theory results are shown with solid (dipolar) and dashed (quadrupolar) lines. For the right panel, data for Mie theory (red) and TDLDA (blue) are shown. Reprinted with permission from ref 144. Copyright 2009 American Chemical Society.

chain length can be studied. These studies showed that the collective oscillations in the chain converge into a single plasmon resonance in the longitudinal direction but split into two separate transverse modes. One mode, termed the "surface" plasmon, was localized at the end of the chain, whereas the second mode was found at the center of the chain and thus termed the "bulk" plasmon (see Figure 7). In Ag chains, the screening due to the d electrons reduced the energies and intensities of the transverse modes but had little effect on its longitudinal resonance. In the Ag chain, the longitudinal excitations are dominated by 5s electrons, whereas the transverse modes are strongly mixed with the d electrons. Thus, the interband p ← d transitions are responsible for the anisotropic screening.

In addition, classical models based on interacting frequency-dependent charges and dipoles have also been explored to calculate the optical properties of large Ag clusters.[140−143] These models are parametrized based on TDDFT calculations of small Ag clusters and thus include quantum size effects. These models have been shown to bridge the gap between first-principles modeling and the classical electrodynamics descriptions.

### 2.5. Optical Properties of Quantum Nanoparticle Dimers

There is tremendous interest in understanding the quantum nature of nanoparticle aggregrates, since aggregates provide a unique way of tuning the optical response by varying the distance between the nanoparticles.[144−150] Additional interest stems from the extremely large localized electric fields that can be found in the gap between nanoparticles (the so-called hot spots) when the plasmons are excited. As the gap between the particles decreases, the coupling increases, leading to the very high electric fields. The very high electric fields are typically found for separations below 5 nm where one would expect nonlocal dielectric effects to be important.[39,151] This becomes even more apparent when the gap is reduced even further so that the particles are nearly touching.[144−146,148−150] In this regime, the classical description breaks down and electrons can tunnel between the nanoparticles, an effect that requires a quantum mechanical description. Thus, there have been several electronic structure studies of nanoparticle dimers using either jellium models[144] or TDDFT for dimers of small clusters.[145,147,150]

Classically, as the distance between the two nanoparticles is reduced, the dipole plasmon resonance is found to red-shift continuously and a sharp increase in the local field in the gap is observed. However, a recent quantum calculation using a jellium model found that for separations smaller than 1 nm, quantum mechanical effects begin to significantly influence the plasmonic response of the dimer.[144] For larger interparticle separation distances, the quantum calculations agree with the predictions of the classical approach for both plasmon energy and field enhancement, as indicated in Figure 8. The major effect is the onset of electron tunneling between the two nanoparticles, resulting in significantly smaller hybridization and a strong reduction of the electromagnetic field enhancements across the junction. Thus, for small separations, it becomes essential to adapt a quantum mechanical description in order to predict reliable electric field enhancements.

## 3. ENHANCED ABSORPTION OF MOLECULES NEAR METAL CLUSTERS

The plasmon resonance of metal nanoparticles described in the previous section has important consequences when molecules are near the metal surface. Large electric fields in proximity to the metal nanoparticle, brought about by surface plasmon resonances, lead to dramatic enhancements in the optical response of molecules. When a molecule interacts with electromagnetic radiation, absorption of photons can occur. Relevant research in the field of enhanced absorption processes is divided into two areas characterizing electronic excitations and vibrational excitations. Understanding these processes is fundamental for investigations of other surface-enhanced spectroscopies. Therefore, developing methods that can resolve the electronic structure of molecules based on linear absorption represents an important first step to comprehend more complicated optical properties described in later sections of this review.

### 3.1. Enhanced Electronic Excitations

Enhancement of electronic excitations (or more generally, surface-enhanced absorption) involves a phenomenon where molecules near a metal nanoparticle or small metal cluster scaffolds experience a greater capacity to absorb photons. Enhanced absorption was first reported for the dyes rhodamine B and nile blue on Au and Cu films by Glass et al.[152] Garoff et al.[153] expanded on that work to examine the absorption of rhodamine 6G on silver-island films using both measured spectra and analysis using Mie theory.[154] Application of the theory in that work allowed for the analysis of distribution of energy absorbed from the incident radiation between the silver film and dye molecule. Craighead and Glass[155] applied the effective-medium theory of Garnett[156] in a study that allowed the authors to

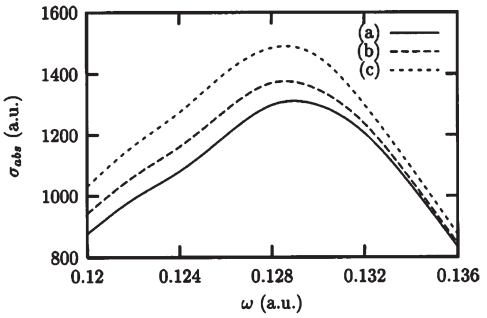


**Figure 9.** Absorbance cross section of 20 Å silver nanoparticles that are uncoated (a), coated with 20 molecules of the merocyanine dye $H_2NCH{=}CHCHO$ (b), and coated with 20 molecules of the merocyanine dye $H_2N(CH{=}CH)_2CHO$ (c). Reprinted with permission from ref 159. Copyright 2001 American Institute of Physics.

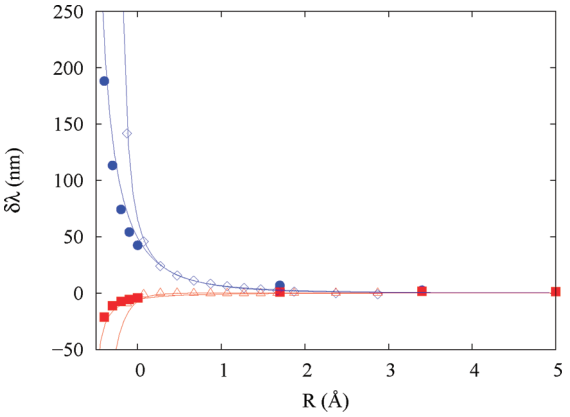


**Figure 10.** Shift in the wavelength ($\delta\lambda = \lambda(R{=}x) - \lambda(R{=}\infty)$) in the excitation energies for the two strongest excitations for R6G on $Ag_{2057}$ (blue dots and red squares) and CV on $Au_{2057}$ (blue diamonds and red triangles). The distance $R = 0$ defines the equilibrium position for the two molecules with respect to the nanoparticle. Reprinted with permission from ref 160. Copyright 2010 American Institute of Physics.

characterize the observed splitting of the plasmon resonance of silver resulting from adsorption of dyes on the surface. This section overviews investigations that describe enhanced absorption for species both chemisorbed and physisorbed to metal surfaces.

DFT and TDDFT have been applied to study tryptophan−silver cluster systems,[61,62] as well as complexes of both di- and tripeptides with silver clusters.[157,158] These investigations demonstrate that the optical properties of the complex are associated with charge transfer in both directions between the molecule and metal. This indicates that the enhanced absorption results from strong electronic interactions between both parts of the complex. Bonding between the metal cluster and biomolecules also results in complicated electronic structure, as demonstrated by the analysis presented by Compagnon et al.[61]

Corni and Tomasi[159] studied enhancements of the polarizability of merocyanine dyes physisorbed to silver and copper nanoparticles with various shapes. In this model, the molecules were represented using Hartree−Fock (HF) theory, while the metal nanoparticles were described using their dielectric functions. It was shown that the imaginary part of the molecular polarizability is enhanced in this method, resulting in an increased absorption for the molecule when it is near a metal nanoparticle. Furthermore, the authors find that the image field generated by the molecule-induced metal polarization has a much smaller effect on the molecular polarizability than the reflected field of the metal. In Figure 9, the absorbance cross section is plotted for 20 Å silver nanoparticles with and without dye molecules surrounding them. When the dye molecules were adsorbed to the silver nanoparticles, an increase in the absorbance of the metal nanoparticles themselves and a small red shift in the absorbance maximum were observed as well.

Morton and Jensen[160] examined the linear response of rhodamine 6G (R6G) and crystal violet (CV) physisorbed to quasi-spherical gold and silver nanoparticles. Their model included a quantum mechanical description of the molecule using TDDFT and an atomistic representation of the nanoparticle based on the capacitance−polarizability interaction model.[141,161] For the strongest molecular excitation of both molecules, it was demonstrated that the metal nanoparticle causes an increase in oscillator strength of 10−20%. The shift of the excitation energy with respect to the excitation energy of the free molecule as a function of distance between the molecule and nanoparticle is shown in Figure 10. Because the electric field of the metal nanoparticle decays quickly as the distance from its surface is increased, the convergence of the molecular excitation energy as distance from the metal surface is increased follows physical intuition. This work also discussed how orientation of the molecule on the surface and adsorption site on the nanoparticle affect the excitation energy and oscillator strength for different excitations.

Numerous other studies have described interactions of molecules with metal nanostructures. Arcisauskaite et al.[162] applied a quantum mechanical/molecular mechanical method (QM/MM) to study charge transfer excitation energies for pyridine−silver complexes using the CAM-B3LYP exchange−correlation functional.[163] This study concluded that the charge transfer excitation energies were more strongly perturbed by silver atoms near the metal surface. Jørgensen et al.[164] described a multiconfigurational self-consistent reaction field (MCSCRF) method applied to the linear response of CO near a metal surface represented as a perfect conductor. The authors examined the lowest four excitations of CO, noting that the excitation energies shift and that transition dipole moments may increase or decrease depending both on the distance between the molecule and surface and on the metal's dielectric constant. Lopata and Neuhauser[165] studied the interactions of a polar molecule with an array of collinear spherical gold nanoparticles with a split field finite-difference time-domain (FDTD) random phase approximation (RPA) approach. Comparing results when the molecule is present to when it was absent indicated that the molecule scatters incident energy transferred between the nanoparticles and also that the molecule enhances the electric field between nanoparticles. Masiello and Schatz[166] applied a many-body Green's function approach with TDDFT to study the adsorption of pyridine on silver nanoparticles of various shapes. This study demonstrates that varying the nanoparticle shape, local surface plasmon resonance, and molecule−metal orientation and separation shifts molecular excitation energies and changes the molecule's polarizability. Corni and Tomasi[167] studied the interactions between molecules and a metal surface, along with how the excitation energies change when a solvent modeled including the polarizable continuum model (PCM) was used. Inclusion of representations of both the metal nanoparticle and solvent environment is an important step in comparing theoretical models to experimental results so that enhanced spectroscopies may be understood.

Recent work by Chen et al. has indicated that a hybrid method, involving a quantum mechanical description of a molecule with real-time TDDFT and classical electrodynamics description of a metal nanoparticle, can account for enhanced absorption of molecules near a nanoparticle.[168] With the N3 dye, it was shown that the model accounts for the strongest enhancement of absorption as the molecule is closer to the surface. Interestingly, binding the metal nanoparticle changed the relative intensities of different molecular absorption peaks.

Further description of the enhancement of absorption will be examined in section 4, in relation to enhanced fluorescence. The remainder of this section focuses on enhancement of infrared absorption specifically.

### 3.2. Surface-Enhanced Infrared Absorption

Surface-enhanced infrared absorption (SEIRA) is a technique where molecular absorption of infrared photons is enhanced in proximity to nanostructured metal surfaces. The first SEIRA investigation was performed by Hartstein et al.[169] for molecular monolayers coated with either Ag or Au metal films in an attenuated-total-reflection (ATR) geometry. It was demonstrated that each molecule studied (4-nitrobenzoic acid, benzoic acid, and 4-pyridinecarboxylic acid) had the same enhancement of their IR spectra on the order of $10^4$. This finding indicated that the enhancement was not from a chemical mechanism, but rather from plasmon resonances of the metal deposited on the monolayers.

A general review of SEIRA that describes many experimental studies not discussed here was presented by Osawa nearly 10 years ago.[170] SEIRA has been investigated on nonmetallic substrates such as silver halide fibers[171] and dielectric nanoparticles of $Al_2O_3$ and SiC.[172] Xue et al.[173] used SEIRA to characterize bonding orientations of *p*-nitrobenzoate to a Pt surface and also examined the electrooxidation reaction of methanol involved in direct methanol fuel cells. Nishikawa et al.[174] studied the effects of low reflective substrates for characterizing organic films, finding that the best SEIRA signals were obtained for those substrates with low refractive indices. Other SEIRA studies have focused on detection of biomolecules[175−177] and examining electrochemical reactions, such as the reduction of nitrite.[178]

One feature that is generally observed is the asymmetric peak shape of different normal modes on the SEIRA spectrum.[179−185] Krauth et al. examined asymmetric line shapes of the modes of CO adsorbed to iron films coated on MgO(001) surfaces.[179] The observed Fano-like line shape[186] for the main IR absorbance line has been explained by resonance of the vibrations of CO and electronic transitions between the metal and CO molecule, by applying the electron−hole pair model of Langreth.[187,188] However, it should be noted that this band asymmetry has been shown to occur for molecules such as n-heptane[183] that can only physisorb to a metal surface, meaning the chemical mechanism does not necessarily cause the Fano-like line shape.

Persson and Ryberg applied the coherent potential approximation (CPA) to study the chemical enhancement mechanism of SEIRA for disordered monolayers of isotopic mixtures of CO on Cu(100) surfaces.[189] In this model, vibrating molecules were allowed to interact with each other via oscillating dipole fields. Comparisons between the model and experimental data showed that good agreement exists for the surface coverage dependent frequency shifts and integrated peak absorptance, which validated the model. Estimates of the chemical enhancement resulted from an increase in the dynamic dipole moment by a factor of 2−3, attributed to charge oscillations between the orbitals of the CO molecule and metal.

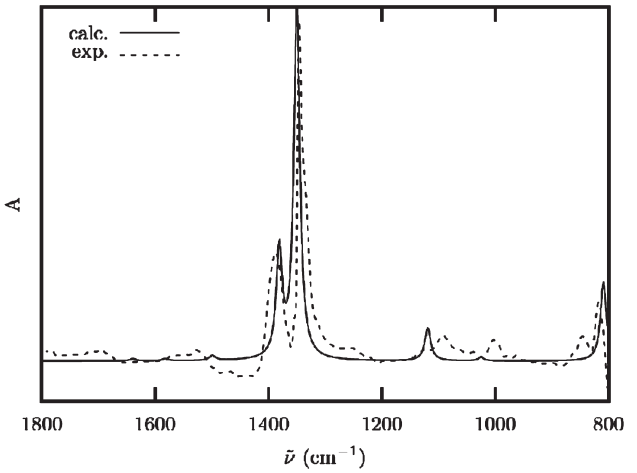


**Figure 11.** Simulated (—) SEIRA spectrum for *p*-nitrobenzoate on a spherical 2 nm conductor and measured (− − −) SEIRA spectrum for *p*-nitrobenzoate on 4 nm thick silver-island film from ref 191. Calculated spectrum is for the perpendicular orientation of *p*-nitrobenzoate on the metal surface. Reprinted from ref 190 with kind permission from Springer Science and Business Media. Copyright 2006.

Corni and Tomasi[190] have simulated SEIRA spectra using DFT for *p*-nitrobenzoate. IR spectra were calculated for molecular orientations perpendicular to the metal surface and tangential to it as well and were subsequently compared with SEIRA spectra measured by Osawa and Ikeda.[191] The calculated spectrum for molecules oriented perpendicular to the surface is shown in Figure 11. Comparison of the different orientations of the *p*-nitrobenzoate on the metal surface indicated that perpendicular molecules absorb more strongly than those that are tangential. The authors stress that this does not mean that all of the molecules are perpendicular to the surface, though.

## 4. SURFACE-ENHANCED FLUORESCENCE

Four decades ago, Drexhage et al. noted that the fluorescence of a $Eu^{3+}$ complex could be altered by the presence of a flat metallic surface.[192] Since then, several studies have shown that fluorescence of molecules can be markedly enhanced by placing molecules near a metal surface, leading to surface-enhanced fluorescence[24,26,27,193−205] (SEF), sometimes referred to as metal-enhanced fluorescence (MEF). The fluorescence can be enhanced by the strong local field near a metal surface due to the excitation of surface plasmons. The interactions between the molecule and metal surface alters the decay rates leading to enhanced fluorescence and the possibility of using radiative decay engineering in designing new sensing systems. This is particularly important for bioanalytical applications since the intrinsic fluorescence of a biological molecule may be amplified so that fluorescent tags are not required.[206−208] However, unlike other surface-enhanced phenomena, fluorescence is optimally enhanced when it is not adsorbed directly onto the surface; in fact, the fluorescence is quenched when the molecule is too close to the surface.

The fluorescence efficiency of a molecule is expressed in terms of the fluorescence quantum efficiency, $\Phi^{FQE}$, given by

$$\Phi^{FQE} = \frac{\gamma}{\Gamma} \quad (5)$$


dx.doi.org/10.1021/cr100265f |*Chem. Rev.* 2011, 111, 3962–3994

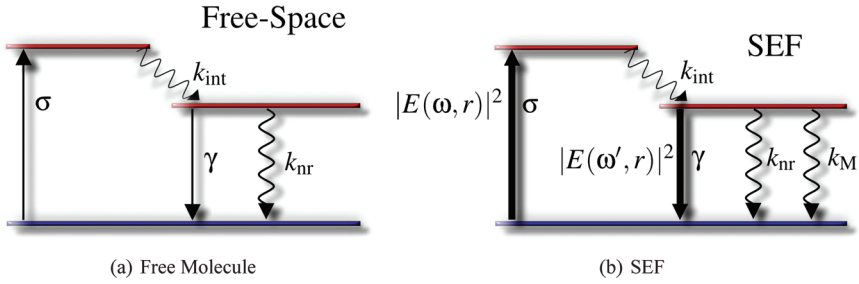


**Figure 12.** Jablonski diagram comparing the decay paths of a molecule (a) in free space and (b) on a metal. In this figure, $\sigma$ represents the absorption cross-section, $\gamma$ is the radiative decay rate, $k_{nr}$ is the free molecule nonradiative decay rate, $k_M$ is the nonradiative decay rate into the metal, and $k_{int}$ is the rate of internal conversion. The terms $|E(\omega,r)|^2$ and $|E(\omega',r)|^2$ represent the electric field enhancement due to the metal at the incident laser frequency, $\omega$, and the emission frequency, $\omega'$, respectively. Adapted from ref 27 with permission from Elsevier. Copyright 2001.

where $\gamma$ is the free molecule radiative transition rate and $\Gamma$ is the total decay rate. A simplified Jablonski diagram describing free-space fluorescence is given in Figure 12a. The free molecule transition rate is given by Fermi's golden rule[209,210] as

$$\gamma = \frac{2\pi}{\hbar}|\mu_{eg}|^2\rho_g \quad (6)$$

where $\mu_{eg}$ is the transition dipole moment between an electronic excited state e and the ground state g and $\rho_g$ is the density of photons at the final state g. The total decay rate is given by

$$\Gamma = \gamma + k_{nr} + k_{int} + k_{pc} \quad (7)$$

where $k_{nr}$ is the nonradiative decay rate (collisional, thermal, and vibrational losses), $k_{pc}$ is the rate of photochemical processes (i.e., irreversible photobleaching), and $k_{int}$ is the rate of internal conversion. In the following, we will use "$\gamma$" to indicate a radiative transition and "$k$" to indicate a nonradiative transition. Typically $k_{int}$ is very fast compared with the other processes, so it can safely be ignored.[193] We include the absorption cross-section $\sigma$ in Figure 12a to highlight the fact that the molecule must first absorb a photon to enter the excited state.

The effect of the metal on the fluorescence of a molecule is typically discussed in terms of either the additional decay channels available to the molecule[27,211] or the enhancement of the free molecule decay rates,[26,212−214] which is based on the idea proposed by Purcell in relation to NMR.[215] Here, we will adapt the approach of Garoff et al.[216] and describe the change in radiative decay rate by a multiplicative enhancement but the change in nonradiative decay rate as an additive enhancement. For a molecule near a metal surface, the total decay rate of the fluorophore is given by[216]

$$\Gamma = \gamma|E(\omega',r)|^2 + k_{nr} + k_{pc} + k_M \quad (8)$$

where $|E(\omega',r)|^2$ is the electric field enhancement factor around the metal evaluated at the metal−molecule distance $r$ and the emission frequency $\omega'$ and $k_M$ is the nonradiative decay due to the metal. Note that we will use $\omega$ as the laser frequency in this discussion. The modified Jablonski diagram for SEF is seen in Figure 12b, where it is clear that the effect of the metal is either through the enhanced local field due to the plasmon ($|E(\omega,r)|^2$ for $\sigma$ and $|E(\omega',r)|^2$ for $\gamma$) or through the nonradiative decay due to the metal $k_M$. One should note that in the limit of $r = \infty$, that is, free-space conditions, then $\Gamma = \Gamma^{Free}$, where $\Gamma^{Free}$ is the free-space decay rate as defined in eq 7. It is interesting that the presence of the metal may cause $\Phi^{FQE}$ to increase toward one

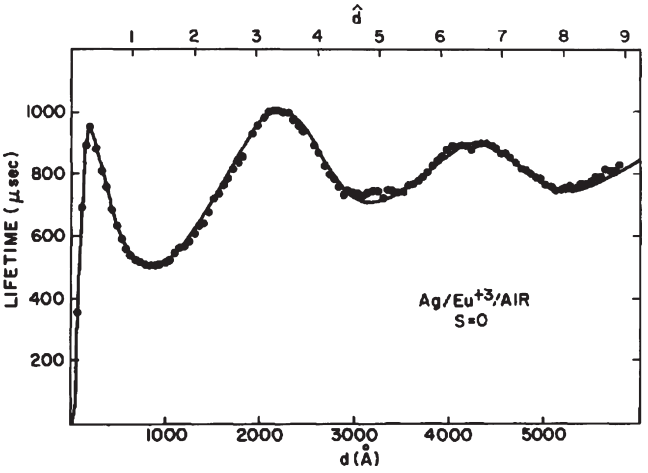


**Figure 13.** Change in $\Gamma$ of a $Eu^{3+}$ complex with distance from a silver mirror. Note the oscillations and the rapid quenching at very small distances. The dots are the experimental points found by Drexhage et al., and the solid line is CPS theory. Reprinted with permission from from ref 219. Copyright 1975 American Institute of Physics.

but also decreases the lifetime $\tau = 1/\Gamma$ in the process. This is contrary to conventional fluorescence, where typically the two quantities move in unison, so that one must choose between good quantum efficiency or rapid photobleaching,[27,200] since decreasing $\Gamma$ will increase the efficiency of photobleaching ($k_{pc}/\Gamma$).[216−218] It is also common to discuss SEF in terms of the enhancement factor EF = $\Gamma/\Gamma^{Free}$ (sometimes called the Purcell factor or normalized decay rate).

Drexhage et al.[192] showed that for a $Eu^{3+}$ complex on a silver mirror, the fluorescence lifetime oscillates with distance from the surface. This was the first experimental evidence of altering the fluorescence lifetime of a molecule on a flat surface, although it had been predicted earlier by Purcell and shown to be possible in a microcavity.[215] This oscillation of the lifetime can be seen in Figure 13. Drexhage proposed a simple explanation for the oscillations based on the method of images: when the light radiating directly from the dipole is in phase with the light reflecting off the mirror, they will interfere constructively, whereas if the two are out of phase, they will interfere destructively. While this proved to be acceptable for distances >1000 Å, it was insufficient to describe effects at shorter distances. Following, that several theories were proposed, both quantum[220,221] and classically based.[222−224]

Chance, Prock, and Silbey (CPS)[219,225−228] provided a theory based on solving Maxwell's equations for a two-mirror system


dx.doi.org/10.1021/cr100265f |Chem. Rev. 2011, 111, 3962–3994

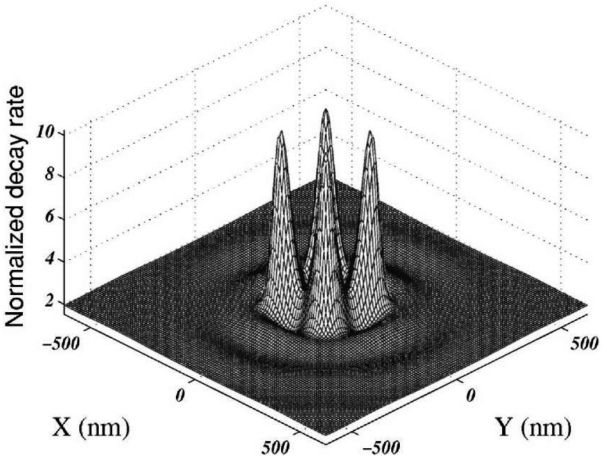


**Figure 14.** A plot of EF on top of a parallelepiped-shaped gold particle. This illustrates that EF is greatest on regions of high local curvature (i.e., corners), also called hot spots. Reprinted with permission from ref 230. Copyright 2001 by the American Physical Society.

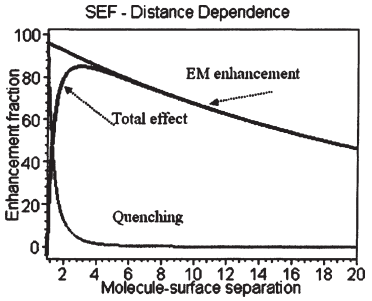


**Figure 15.** An approximate representation of the contribution of $|E(\omega',r)|^2$ (EM enhancement) and $k_M$ (quenching) to the overall SEF effect as a function of distance. It is only at small metal−molecule distances that $k_M$ becomes important. Reprinted from ref 204 with kind permission from Springer Science+Business Media. Copyright 2005.

that was able to quantitatively describe the experimental findings (see Figure 13). They showed that the expression for the decay rate of a fluorophore on a flat metal mirror can be decomposed into a radiative and a nonradiative component. It was also shown that previous formulations (i.e., the image method) only accounted for the radiative component and therefore failed at small $d$. Nonradiative decay was suggested to be due in part to coupling of the emission to surface plasmon modes in the metal. Furthermore, it was found that there was a large increase in the nonradiative decay at the surface plasmon frequency. They also demonstrated that the plasmon frequency could be shifted by changing the thickness of the film. CPS theory has been highly successful in describing the fluorescence decay on flat metal surfaces, the reason being, as pointed out by Johansson and coworkers,[229] that SEF is almost purely electromagnetic in nature. For a thorough review of the classical theories of SEF, we refer the readers to the recent review by Fort and Grésillon.[193]

As one might imagine, the main ways that the metal can enhance fluorescence is through the term $|E(\omega',r)|^2$. This primarily results from the enhanced electric field due to the excitations of the plasmons in the metals, although $|E(\omega',r)|^2$ is weakly affected by image radiation.[228] Rahmani et al.[230] used a mixture of linear response theory and the coupled dipole approximation to determine the effect of local geometry on the enhancement factor, EF, of a nearby molecule based on $|E(\omega',r)|^2$. They tested the method on parallelepiped-shaped (rhomboid) dielectric and metal particles on a dielectric or metal planar surface. They found, especially for the metals, that the largest enhancements occur in the areas of highest local curvature. This is clearly shown for the case of a silver nanoparticles on a gold substrate (Figure 14), where the largest enhancements were found at the corners of the structure. This agrees with other works[231] indicating that $|E(\omega',r)|^2$, and thus EF, is largest at sharp points (hot spots).

The effect of the metal on the fluorescence of the molecule through the nonradiative term $k_M$ is primarily due to electron−hole coupling between the molecule and the metal at close metal−molecule separation, $r$. This means that nonradiative decay is primarily a nonplasmonic phenomenon, as clearly demonstrated recently by Muñoz-Losa et al.[232] by comparing decay rates determined from full QM to those based on bulk dielectric constants. For a flat surface, $k_M$ is proportional to $1/r^3$ or $1/r^4$, depending on thickness,[228,233] whereas for a spheroid, it is proportional to $1/r^6$.[216] A common method to model $k_M$ is using the $1/r^6$ dipole approximation of Förster. However, simple dipole−dipole coupling has been shown to break down at small distances, indicating that higher-order multipoles are required for an adequate model.[234] A more rigorous electronic structure model was developed by Persson,[233,235−237] who examined the formation of electron−hole pairs in a metal by the presence of a vibrationally excited molecule. In this method, the metal was represented by a simple jellium model, except that the dielectric function at the surface was smeared out to represent a more realistic surface electronic distribution. The molecule was represented by a two-state dipole according to Fermi's golden rule. Li and Tully[238] have developed a method to determine the decay rate of a particular excited state of a molecule using real-time electronic structure dynamics and by monitoring electron charge. They demonstrate this method using a single H atom on a $Li_{66}$ three-layer flat surface where they were able to determine $k_M$ for the lowest charge-transfer state by fitting a single exponential to the decay curve.

Due to the strong connection between SERS, surface-enhanced resonance Raman scattering (SERRS), and SEF, general models aimed at describing all of these phenomena have been presented. Weitz et al.[211] presented a theory to connect SERS, SERRS, and SEF results for rhodamine-6G (R6G) and basic fuchsin (BF). They compared results for the molecules on silica and silver island films with a four-level (two electronic states, each with two vibronic levels) model. They showed that for molecules with large intrinsic $\Phi^{FQE}$, such as R6G, EF is actually less than one. This is in contrast to BF, a molecule with low intrinsic $\Phi^{FQE}$, where EF was ~3. This was shown to be the result of the enhancement of the radiative rate with respect to the addition of nonradiative emission into the metal. Pettinger[239,240] used a similar four-level model to examine the role of energy transfer in these surface-enhanced spectroscopies.

Johansson et al.[229,241] used a two-state model within a displaced harmonic oscillator approximation in conjunction with Mie theory[28] to determine the electromagnetic enhancement to SERS and SEF for a molecule between two nanoparticles. They found that the enhancement in SERS is proportional to $|E|^4$, as expected and that the SEF enhancement factor is proportional to $|E(\omega,r)|^4/|E^*(\omega',r)|^2$. Note that we use $|E^*(\omega',r)|^2$ to indicate that Johansson et al. included $k_M$ into the $|E(\omega',r)|^2$ term. They found that except for short distances (<200 Å) where decay into

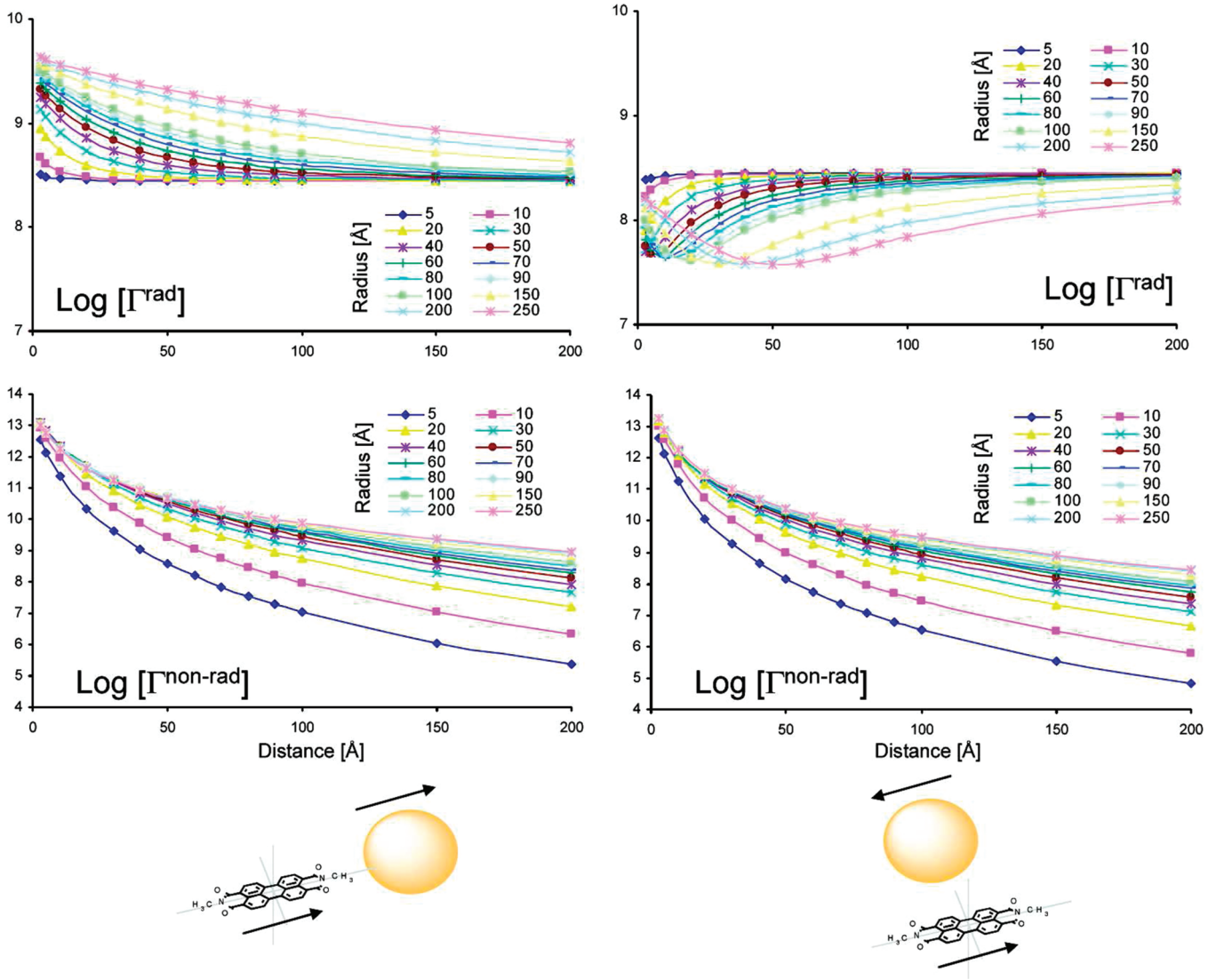


**Figure 16.** Plots of the radiative decay rate ($\Gamma^{rad}$ in the figure, $\gamma$ in the text) and nonradiative decay rate ($\Gamma^{non\text{-}rad}$ in the figure, $k_M$ in the text) for two different molecular orientations with respect to a gold nanosphere: (left) the longitudinal (L) orientation; (right) the transversal (T) orientation. Notice that the radiative decay is affected by orientation, but the nonradiative decay is not. Reprinted with permission from ref 247. Copyright 2009 American Chemical Society.

the spheres becomes important, $E^*(\omega',r)$ is roughly the same as $E(\omega,r)$, and therefore SEF scales roughly as $|E(\omega,r)|^2$. However, for a single nanoparticle at close distances, $E^*(\omega',r)$ becomes greater in magnitude than $E(\omega,r)$. This is the reason for the observed maximum in the EF close to the surface before quenching of the fluorescence dominates (see Figure 15). Interestingly, they find that $E^*(\omega',r)$ is equal in magnitude whether the molecule is on a single sphere or between two spheres, whereas $E(\omega,r)$ is much larger in the gap between two spheres, indicating that fluorescence is unlikely to be fully quenched in a dimer system. This could potentially lead to the SERS background continuum sometimes noted in the literature.[242]

Most studies of SEF use either a point dipole approximation or a two-level system when modeling the molecule. However, one method that has been used to extend this approximation is to use a quantum mechanical description of the molecule combined with PCM for the metal.[167,232,243−249] To do this, the original PCM model was modified so as to represent first a planar, semi-infinite metal surface[167,244] and then later a metal nanoparticle of arbitrary shape.[245] The interactions between the molecule and the metal are solved fully self-consistently. In this way, the model accounts for the changes in the molecular properties due to the metal nanoparticle such as the transition dipole moment ($|\mu_{eg}|^2$ term from eq 6). A recent study using the PCM model by Vukovic et al. has focused on understanding the molecular orientation and distance, nanoparticle size, shape, and composition, and number of nanoparticles on the fluorescence of a molecule.[247] Since this work presents several important findings related to SEF, we will discuss it in more detail.

Vukovic et al. showed that for a molecule oriented so that its transition dipole moment points toward the nanoparticle (longitudinal, L, left cartoon in Figure 16), $\gamma$ ($\Gamma^{rad}$ in Figure 16) increases with decreasing distance from the particle. However, if the molecule is rotated 90° (transversal, T, right cartoon in Figure 16), then $\gamma$ decreases with decreasing distance. This is because depending on the molecular transition dipole orientation,

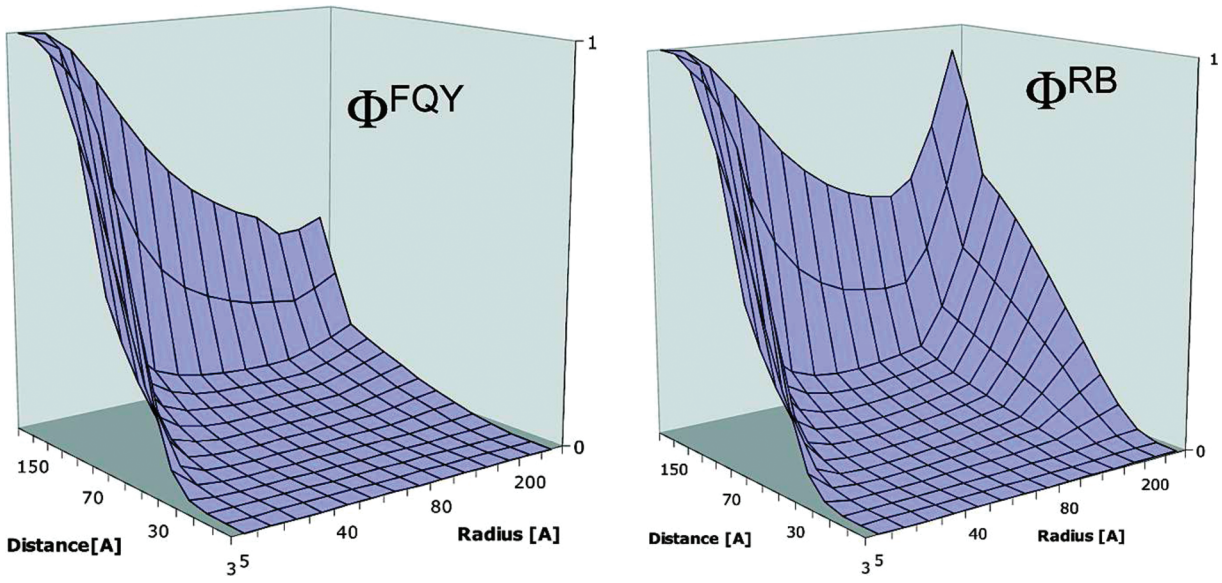


**Figure 17.** (left) The fluorescence quantum efficiency ($\Phi^{FQE}$) and (right) the relative brightness ($\Phi^{RB}$) of the molecule for various metal−molecule separations and metal sizes. Notice that for larger metal radii, $\Phi^{FQE}$ does not predict an increase in fluorescent photons due to increased absorption but $\Phi^{RB}$ does. Reprinted with permission from ref 247. Copyright 2009 American Chemical Society.

the induced metal dipole can be parallel (L orientation) or antiparallel (T orientation) to the molecular transition dipole. As a result, the transition dipole moments of the metal and the molecule for the L orientation interact constructively, whereas for the T orientation they are actually destructive, accounting for the observed trends shown in Figure 16. This is similar to results found using classical theory.[250] It should also be noted that the enhancement of $\gamma$ at small distances was found to be proportional to the radii of the metal spheres. They further found that the magnitude of $k_M$ (denoted by $\Gamma^{non\text{-}rad}$ in the figure) does not change appreciably with orientation, nor with metal radii, as seen in Figure 16. The primary determining factor for $k_M$ is the metal−molecule separation.

Vukovic et al. also point out that the use of $\Phi^{FQE}$ or EF may not be enough to completely describe the SEF enhancement and suggest the use of relative brightness, $\Phi^{RB}$, which is defined as[247]

$$\Phi^{RB} = \Phi^{FQE}\frac{\sigma}{\sigma^{Free}} \quad (9)$$

where $\sigma^{Free}$ is the absorption cross-section for the free molecule. This is because $\Phi^{FQE}$ and EF take into account only $\gamma$ and $k_M$ and do not include the enhancement of $\sigma$ due to the metal. This is shown in Figure 17, where both $\Phi^{FQE}$ and $\Phi^{RB}$ are plotted against metal−molecule separation and metal radii for the L orientation. It is easily seen that for small metal radii both measures give qualitatively the same results. However, for larger metal radii, $\Phi^{RB}$, is found to be larger than $\Phi^{FQE}$. At small distances, $k_M$ is much larger than $\gamma$, even for large metal radii, and therefore considering $\Phi^{FQE}$ or EF would lead one to interpret this as a poor separation for SEF. However, inclusion of the enhancement of $\sigma$ illustrates that the fluorescence is not completely quenched. In the same way, $\Phi^{RB}$ is larger between a nanoparticle dimer because $k_M$ increases linearly but $\gamma$ and $\sigma$ increase nonlinearly. This mirrors the result found by Johansson et al.[229,241] using the two-state model discussed previously. Finally, they showed that silver yields larger enhancements than gold, primarily because silver is less absorptive than gold at the emission wavelength and thus leads to weaker $k_M$.

## 5. SURFACE-ENHANCED RAMAN SCATTERING

SERS is currently the only method that can simultaneously detect a single molecule and provide its chemical fingerprint.[242,251−255] This has potentially high impact on biological sensing such as DNA detection,[15−21,256−259] early detection of chemical and biological warfare,[260−267] real-time glucose sensing for diabetes,[7,268−270] and nondestructive art analysis.[271−278] SERS refers to the strong enhancement by factors as large as $10^6$−$10^{12}$ of the Raman signal of molecules in close proximity to nanostructures that exhibit plasmons.[279−281] In recent years, SERS has been transformed into a powerful analytic technique[15,18−21,282] due to advances in nanofabrication[9−14,254] and an increased understanding of plasmonic properties of nanomaterials.[3,29,283,284] A major breakthrough was the discovery of single−molecule SERS, which provides evidence of the enormous sensitivity of the technique, and its applications to understand surface chemistry at the nanoscale.[242,251−254,285−292] However, even 35 years after its initial discovery, it is still not completely understood due to its highly complex nature and required experimental conditions, such as roughened surfaces, nanoparticle junctions and aggregates, and chemical interactions. Here we will highlight recent advances in understanding SERS using electronic structure methods.

### 5.1. Early History of SERS

In 1974, Fleischmann, Hendra, and McQuillan[279] observed that the Raman intensity of pyridine on a roughened silver electrode in the presence of $Cl^-$ could be modulated by adjusting the potential of the electrode. This was attributed to the pyridine molecules preferentially adsorbing to the silver at a certain potential, and thus they interpreted the enhancement as arising from an increased surface concentration of analyte. In 1977, Jeanmaire and Van Duyne[280] (JVD) observed enhancements of pyridine on roughened silver electrodes of $10^5$−$10^6$. They


dx.doi.org/10.1021/cr100265f |Chem. Rev. 2011, 111, 3962–3994

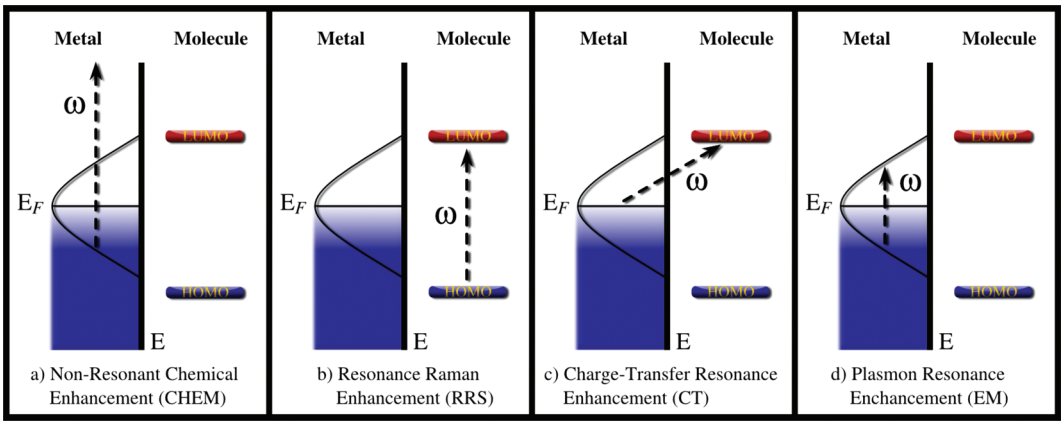


**Figure 18.** A cartoon representation of the mechanism of SERS, here using crystal violet on a gold nanotriangle as a representative example: EM = electromagnetic mechanism; RRS = resonance Raman scattering; CT = dynamic charge transfer; CHEM = nonresonant chemical mechanism. Adapted from ref 104 by permission of The Royal Society of Chemistry.

demonstrated that the enhancements could not be explained by surface coverage alone. Consequently, they proposed that an electric field arising from the roughened electrode surface enhances the Raman intensity. Albrecht and Creighton[281] (AC) independently noted the discrepancy between surface coverage and enhancement but proposed instead that the enhancement originated from new or broadened electronic states caused by interactions with the metal surface creating a resonance Raman (RR) like effect. Interestingly, JVD observed that the enhancement increased with increasing excitation energy, while AC observed the opposite trend. These findings spurred great interest in this new phenomenon[293−310] and soon it was given the acronym "SERS" by Van Duyne.[311−313]

Most early theories of SERS focused on simple classical models. King, Van Duyne, and Schatz[314] proposed an image dipole model where the adsorbate is approximated by a single dipole over a smooth surface with no chemical interaction between the two. Using this model, they could qualitatively predict the dependence of the enhancement on incident frequency as found by JVD.[280,301] Moskovits[309] suggested that roughening the electrode surface creates colloids on the smooth metal surface with finite radii that exhibit size-dependent resonances (like surface plasmons). Moskovits used this idea to explain the discrepancy between the frequency dependence that JVD and AC observed for the Raman enhancement in terms of differing surface plasmon resonances. Hexter and Albrecht[307] and Tsang, Kirtley, and Bradley[305] suggested that these surface plasmons couple to molecular electronic states to form new resonances not accessible in normal Raman scattering. A similar mechanism was proposed by Burstein et al.,[304] where instead of a continuum-type charge transfer, charge transfer from discrete electron−hole states occurred. Gersten, Birke, and Lombardi[303,308] discussed a variation in which charge transfer occurred directly from the metal to the molecule. Otto[300,310,315,316] argued the existence of a local enhancement due to an electronic interaction between metal and molecule and that it is likely that SERS signal is dominated by a small number of molecular SERS active sites.[317,318] For a more detailed history of the discovery of SERS, the reader is referred to the review by Tian, Ren, and Wu.[319]

Resulting from the experimental observations, two main methods of explaining the larger enhancements of SERS arose, one being an electromagnetic mechanism (EM)[24,211,296,297,301,306,309,320−323] and the other being a chemical mechanism (CM).[304,315,324−327] In its most general terms, CM arises from overlap between the metal and adsorbate wave functions, whereas EM is classical in nature and does not rely on this overlap.[25,320] Today, it is well accepted that EM arises due to resonances between the incident laser and the surface plasmons of the metallic nanostructured surface.[3,321,322,328−332] EM typically is the largest contributor to SERS, yielding enhancements anywhere between $10^4$ and $10^8$. In contrast to EM, the nature of CM enhancement is less clear.[104,327,333−335] It is generally accepted that there is a dynamic charge-transfer (CT) mechanism that arises from a resonance between the incident laser and a metal to molecule or molecule to metal excitation. Additionally, if the incident laser is resonant with an intermolecular excitation, the molecule will experience resonance Raman scattering (RRS). Although this is strictly not a surface effect, the metal does influence the RRS enhancement. CT and RRS have individually been known to contribute enhancements anywhere from 10 to $10^6$. Finally, there is a small enhancement that is gained simply by placing the molecule onto a metal surface, which is due to relaxation of the electronic structure of the molecule; this is called the nonresonant chemical mechanism (CHEM) and is expected to only yield enhancements on the order of $10^2$ or less. Of course, the two mechanisms EM and CM are not mutually exclusive but work together in concert to produce the overall SERS effect. However, depending on the specific system, the importance of individual mechanisms may vary. A cartoon illustrating the different enhancement mechanisms is presented in Figure 18 and discussed in more detail below.

### 5.2. The Electromagnetic Mechanism

As mentioned above, EM is a result of surface plasmon resonances on the nanoparticle surface and is therefore considered to be independent of the nature of the molecule or the chemical bond between the metal and molecule. As such, many successful studies of EM have been performed utilizing classical electrodynamics methods such as Mie theory,[28] DDA,[29,30,330,336] and FDTD.[31,32] It can be shown that the enhancement factor due to EM can be written as[104,296,337]

$$\mathrm{EF_{EM}} = |\mathbf{E}(\omega)|^2|\mathbf{E}(\omega')|^2 \qquad (10)$$

where $\mathrm{EF_{EM}}$ is the electromagnetic mechanism enhancement factor, $\mathbf{E}(\omega)$ is the frequency-dependent electric field at incident frequency $\omega$, and $\mathbf{E}(\omega')$ is the frequency-dependent electric field

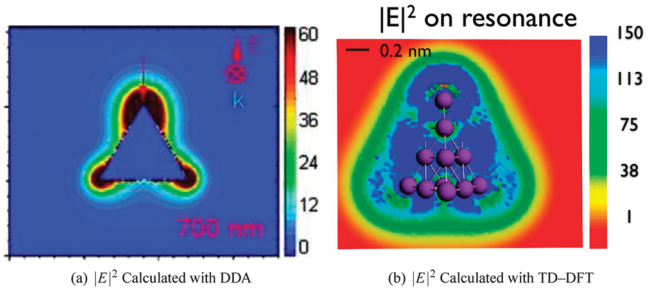


**Figure 19.** (a) DDA calculation of the electric field enhancement $|E|^2$ around a nanotriangle, highlighting the fact that the greatest enhancement is at the tips. Reproduced with permission from ref 328. Copyright 2004 American Institute of Physics. (b) TD-DFT calculation of $|E|^2$ for a tetrahedral $Ag_{20}$ cluster. The two methods yield qualitatively the same results. Reproduced from ref 104 by permission of The Royal Society of Chemistry.

at the Stokes shifted frequency $\omega'$. However, since the Stokes shift is usually small compared with the wavelength of laser, eq 10 is typically simplified as

$$EF_{EM} = |\mathbf{E}(\omega)|^4 \quad (11)$$

The local electromagnetic field due to plasmon excitations is largest in regions with high local curvature and in particular in the junction between dimers of nanoparticles, the so-called hot spots. This is illustrated in Figure 19a where Hao and Schatz[328] used DDA to simulate the EM enhancements around triangular nanoparticles. Compared with the large amount of literature on using classical methods to simulate EM, much less has been presented on using electronic structure theory to simulate EM. However, as discussed previously, the discrete electronic transitions observed in small metal clusters can be used as an analogue for plasmon frequencies[110] and thus serve as a model system for understanding EM. This is illustrated in Figure 19b where the electric field enhancement around a $Ag_{20}$ cluster has been calculated using TDDFT[104] and is qualitatively similar to results calculated with DDA (Figure 19a). Calculations of the EM enhancement generally neglect terms such as the enhanced field gradient near the surface, but Kedziora and Schatz[338] showed that higher order terms, such as dipole−quadrupole, quadrupole−quadrupole, and magnetic-dipole−magnetic-dipole terms can be neglected when calculating the Raman cross sections.

One of the earliest electronic structure methods developed to understand SERS was developed by Maniv and Metiu.[339−341] In their model, they assumed that the enhancement was a result of an image dipole in the roughened metal that scatters inelastically. To model this, they used the random phase approximation in conjunction with a jellium model to represent the metal. An alternative method was proposed later by Pandy and Schatz.[342,343] They used time-dependent Hartree−Fock (TDHF) methods to calculate the resonance polarizability of the $H_2$−$Li_2$ system. In this method, they used a phenomenological damping parameter, $\Gamma$, chosen to mimic that of bulk Li. By calculating the $Li_2$ resonance polarizability derivative at various $H_2$−$Li_2$ distances, they found a distance dependence similar to that expected for EM. This method was later expanded upon by Nakai and Nakatsuji[344] to look at CO on $Ag_2$, $Ag_{10}$, $K_2$, $Pd_2$, and MgO. They found a wavelength dependence that closely followed what is observed experimentally and noted that EM depends strongly on resonances in the metal system. They also noted that orientation of the adsorbate on the metal can significantly alter the enhancement factor.

Pustovit and Shahbazyan[345] presented a different approach to model EM by noting that electrons in the sp band of a nanoparticle do not exhibit a step-like potential as is assumed by methods such as Mie theory. To account for this, they model the outer sp band of the nanoparticle using TDLDA, and the bulk d band with a phenomenological dielectric constant. The molecule is represented simply by its molecular polarizability at some distance from the surface. As a result, this model is able to scale to nanoparticles of moderate size (1.4−4.5 nm) while retaining quantum size effects.

An intriguing phenomenon related to EM is that the location of the maximum $EF_{EM}$ does not coincide with the plasmon resonance peak $\omega$, but rather is slightly blue-shifted.[346] A simple explanation of this can be achieved by considering eq 10. Since $EF_{EM}$ is dependent on both both $\omega$ and $\omega'$, the maximum $EF_{EM}$ should occur halfway between these two values. This is indeed what is observed, which calls into question the validity of the $\omega \approx \omega'$ approximation that is generally assumed. This was also demonstrated recently by Franzen.[347] Zhao et al.[101] recently compared $EF_{EM}$ to the absorption maximum of a Ag−pyridine complex calculated using TDDFT. In contrast to the experimental results,[346] they found that the maximum $EF_{EM}$ was red-shifted from $\omega$. This is likely because the electronic structure methods that were employed assumed $\omega \approx \omega'$.

### 5.3. The Chemical Mechanism

Early observations of SERS from molecules like pyridine on plasmonic metal surfaces showed enhancements of 10−1000 orders of magnitude greater than were expected to originate from EM alone. In fact, by alteration of the applied voltage (which is not expected to change EM), the overall SERS enhancement factor could be increased or decreased.[348] Additionally, SERS was shown to exist for nonplasmonic metals[349] or flat surfaces[293] where EM effects are not expected to be important. These observations pointed toward the existence of a chemical mechanism (CM). CM is also sometimes referred to as the electronic mechanism or first layer effect due to its short-range nature.

The chemical mechanism can be divided into three contributions:

1. A molecular resonance (RRS) mechanism. This is analogous to RRS for a free molecule except that the presence of the surface modifies the enhancements observed. This is not traditionally included as a chemical mechanism, but since it is in fact altered by the metal, we prefer to include it as a chemical mechanism. RRS is typically expected to contribute enhancements of $10^3$−$10^6$.
2. A charge transfer (CT) mechanism,[315,327,335,350] in which the applied field is in resonance with either a metal−molecule or molecule−metal transition and typically provides enhancements around 10−$10^4$. It has been proposed that it may be as large as $10^7$ in some situations, based on recent experimental work.[351]
3. A nonresonant chemical (CHEM) mechanism, which arises simply from the ground-state interaction of the molecule with the metal. This is the weakest of the mechanisms, only leading to enhancements on the order of ∼10−100.

**5.3.1. The Resonance Raman Mechanism.** While resonance Raman scattering (RRS) is not technically a surface phenomenon, we choose to include it because it is important for understanding surface-enhanced resonance Raman scattering (SERRS).

SERRS was often used in early experimental studies of SERS[211,352,353] and more recently in single-molecule SERS studies.[242,251−254] The main features of RRS can be explained by assuming a two-state model that neglects vibronic coupling. In this way, the polarizability derivative with respect to normal mode, $Q_k$ $(\partial\alpha/\partial Q_k)$, can be written as[100,354]

$$\frac{\partial\alpha}{\partial Q_k} \propto -\frac{\mu}{(\omega_e - \omega - i\Gamma)^2}\left(\frac{\partial\omega_e}{\partial Q_k}\right) \tag{12}$$

where $\mu$ is the transition dipole moment for this transition, $\omega_e$ is the energy of this transition, and $\omega$ is the laser energy. Since the Raman cross-section $(I)$ is proportional to $(\partial\alpha/\partial Q_k)^2$, at resonance $(\omega = \omega_e)$, the resonance Raman intensity is approximately given by

$$I \propto \frac{\mu^2}{\Gamma^4}\left(\frac{\partial\omega_e}{\partial Q_k}\right)^2 \tag{13}$$

It is important to note from eq 13 that the RRS intensity depends on the transition dipole moment squared but on the inverse of the excited state relaxation rate to the fourth power. Therefore, a proper choice of $\Gamma$ is crucial when attempting to perform an RRS calculation. The transition dipole moment, excitation energies, and $\Gamma$ are all affected by the presence of the metal. Because of its dependence on $\Gamma$, SERRS is often discussed alongside fluorescence. Molecules that are good candidates for RRS are usually strong fluorophores, and therefore the RRS spectrum is typically overpowered by the fluorescence spectrum.[211,353,355,356] Since the presence of a metal surface simultaneously quenches fluorescence and enhances Raman scattering, strong fluorophores like the prototypical rhodamine-6G are excellent SERS probes. The metal can enhance the transition dipole moment $\mu$ and also increase the relaxation rate $\Gamma$. Thus, for an increase in SERRS intensity to occur, the magnitude of the increase in $\mu^2$ must be greater than that of $\Gamma^4$. Depending on the metal and molecule, the interactions can lead to either a stronger or weaker RRS enhancement.

**5.3.2. The Charge-Transfer Mechanism.** The charge transfer mechanism (CT) is related to RRS since it is a resonance effect between a molecular and a metal electronic state. As a result, it can only occur if the molecule is close enough to the metal for the wave functions of the two systems to overlap. CT is undoubtedly the most controversial and least understood mechanism of SERS, because of the difficulty in determining it experimentally[357−359] and theoretically.[101,360]

Early after the proposal of a chemical effect by Otto,[300,302,310,315] several electronic structure models for CT were introduced. Persson[361] proposed a model based on the broadening of the electronic excited state of the molecule by the metal. Pettinger[239] suggested that CT occurs in a five-step process, whereby the metal absorbs a photon and excites a surface plasmon (or electron−hole pair), which then transfers its energy into the molecule, causing it to be in an electronically excited state. The molecule then inelastically returns the electron to the metal, whereby a photon is emitted by the excited surface plasmon (or recombination of electron−hole pair). However, Arenas et al.[362] demonstrated that this mechanism was not necessary to explain the odd selection rules of CT.

Both Adrian[362] and Lombardi et al.[324] developed models based on the similarity of CT with RRS using the framework of Albrecht.[363,364] Albrecht had derived expressions for RRS as the sum of several terms, the first (A-term) is determined by Franck−Condon overlap between the ground and excited state, and the second (B-term) is determined by Herzberg−Teller coupling. Recently, Otero and co-workers[362,365−370] and Lombardi and Birke[324,371−373] have examined CT in terms of the Albrecht model, although Otero and co-workers focus on the Franck−Condon terms and Lombardi and Birke focus on the Herzberg−Teller contribution. In the work of Otero and co-workers, CT is analyzed in terms of vibrational symmetry and the Peticolas[374] formula, in which the CT active modes can be predicted by the ground and excited state geometries. These calculations provide insight into the selection rules of CT but do not offer predictions of the magnitude of $EF_{CT}$ and also bypass the effect of $\Gamma$. A similar strategy is being employed by Sun and co-workers,[375−381] whereby the electronic origin of CT is visualized using the charge difference density method. Lombardi and Birke recast the Herzberg−Teller view of CT from ref 325 into a time-dependent form that accounts for both metal to molecule and molecule to metal charge transfer and also focuses on vibrational symmetry. They indicate that this model results in $EF_{CT} \propto 1/\Gamma^4$, which is the same result as in eq 13 for RRS, as expected.

Recently, Birke et al.[373] calculated the Raman intensity of pyridine on a $Ag_{10}$ cluster on resonance with CT transitions. It was found that exciting at a CT excitation energy causes previously silent modes to become Raman active, as is found experimentally. They also discussed the effect of including the finite lifetime of the excited states, that is, accounting for the effect of $\Gamma$, in the calculations of the polarizability derivatives.[354,382] They found that in the pre-RRS region, that is, slightly away from a resonance, the effect of including $\Gamma$ was small. However, as expected they showed that the effect of including $\Gamma$ was significant at resonance. In fact, neglecting the finite lifetime lead to unphysically large ($>10^{10}$) Raman intensities. This emphasizes the importance of including the decay rate $\Gamma$ in the calculation of RRS or CT.

**5.3.3. The Nonresonant Chemical Mechanism.** The nonresonant chemical mechanism (CHEM, also referred to as the static chemical mechanism) is very difficult to detect experimentally since it makes the smallest contribution to the overall SERS EF, although there have been recent experimental attempts to quantify it.[383,384] Theoretical studies are expected to be particularly useful in describing this mechanism since it is likely to be dominated by the local environment around the molecule, which can be represented using small metal clusters. For this reason, there are many electronic structure studies of the effect of small metal clusters on the Raman properties of small molecules. In these calculations the Raman intensities are obtained using static molecular polarizabilities ($\omega = 0$), ensuring no resonances, and therefore the only enhancement mechanism is CHEM.

While it is clear that CHEM must arise due to an interaction of the adsorbate with the metal surface,[322] the specific characteristics of the new metal−molecule complex that cause the enhancement are less clear. Tian and co-workers[385] demonstrated that the bonding interaction between metal and molecule can cause the vibrational modes to couple together or shift in frequency, making simple comparisons to neat molecular spectra difficult. They further studied the effect of solvent,[386] transition metals,[387,388] and size and shape of the metal cluster on the Raman properties.[389] Vivoni et al.[390] studied the effect of the adsorbate geometry using an adatom model. Muniz-Miranda, Cardini, and co-workers examined the influence of positively charged metal

clusters[391,392] and coadsorbates.[393] Johansson[394] studied the effect of applied static fields and an increase in the Raman cross section. However, he found that the external field does not significantly affect the molecular polarizability, only the polarizability derivatives. Zhao et al.[395] examined the effect of $Ag_2$ and $Au_2$ dimers on the Raman properties. Morton et al.[396] and Saikin et al.[397] studied how strong bonding (thiols, as opposed to the weak bonding pyridine and pyridine derivatives of the previously mentioned studies) altered CHEM. In particular, the latter showed that CHEM is sensitive to the molecule's orientation on the cluster, as well as the symmetry of the cluster−molecule system. Not surprisingly, they also indicated that a mode containing atoms close to the metal will be affected more than other vibrational modes.

Zhao, Jensen, and Schatz proposed that CHEM may arise from either strong bonding interactions or increased static polarizabilities ($\Delta\alpha$).[101] Later, Morton and Jensen[398] showed that CHEM is not (at least directly) related to properties such as $\Delta\alpha$, bonding energy, static charge transfer, or metal−adsorbate bond length, by using a data set of 37 different substituted pyridines, benzenethiols, small molecules, and silver clusters of various shapes and sizes. Using a two-state approximation to polarizability, they found that CHEM was related to the ratio of the lowest excitation energy of the free molecule and the lowest charge-transfer excitation energy of the metal−molecule complex as

$$EF_{int}^{model} = A\frac{{\omega_X}^4}{{\omega_e}^4} \quad (14)$$

where $EF_{int}^{model}$ is the model enhancement factor for CHEM, $\omega_X$ is the lowest (HOMO−LUMO) excitation energy of the free molecule, $\omega_e$ is the lowest charge transfer excitation energy of the metal−molecule complex, and $A$ is a fitting parameter. The "int" in $EF_{int}^{model}$ represents the integrated enhancement, which was used to eliminate differences in vibrational modes from different molecules so they could be compared directly. This means that eq 14 describes the CHEM enhancement for all modes in general, that is, is not mode specific. A plot of the correlations between this model and TDDFT results for the EF is given in Figure 20. This relationship indicates that molecules in which the LUMO is significantly stabilized upon adsorption, such as those that have strong $\pi$-backbonding, will exhibit the strongest CHEM enhancement.

### 5.4. Unifying the Description of SERS

The work described in the previous sections typically focused on one of the main mechanisms of SERS. However, because the different mechanisms occur in concert, it is important to establish a model that describes their combined effect.

An effective model study to understand the different mechanisms was presented by Zhao, Jensen, and Schatz.[101,399,400] They used a TDDFT approach that includes the finite-lifetime effects of the excited states.[100,354] In this work, the magnitude of CHEM, CT, and EM are all examined for pyridine[101,400] or pyrazine[399] on various Ag clusters. They considered a tetrahedral $Ag_{20}$ complex (pictured in Figure 21), which can be thought of as a relaxed fragment of a fcc lattice. If the molecule is placed on the flat edge (position S for surface), then it can approximate absorption onto a (111) planar surface. Conversely, placement onto the point end (position V for vertex) can approximate adatom adsorption. Thus, very different chemical environments were able to be examined without altering the structure of the cluster. Since the charge transfer excitations and Ag intracluster excitations for these systems are nonoverlapping, they were able to probe CT and EM separately. For normal Raman scattering (NRS), they found that the V complex yields a greater CHEM enhancement than the S complex ($EF_{CHEM}$ = 8 and 4, respectively) because of stronger bonding interactions with the V complex, in agreement with ref 398. They found that the EF when on resonance with a charge transfer excitation for the S complex was roughly $10^4$, and thus $EF_{CT} = 10^3$ since $EF_{CHEM} \approx 10$. For Ag intracluster resonance, they found an EF of around $10^5-10^6$, and thus $EF_{EM} = 10^4-10^5$. Therefore, the hierarchy of enhancement factors found was CHEM < CT < EM, as expected from previous studies. Aikens and Schatz[117] found similar results for a Au analogue for this system, except that $EF_{EM}$ is 1−2 orders of magnitude lower than that for Ag. Interestingly, when two of the $Ag_{20}$ clusters were used to form a junction, it was found that $EF_{CHEM} = 10^5$, while $EF_{EM} = 5$.[399] These results indicate that EM has less of an effect in hot spots for these small clusters.

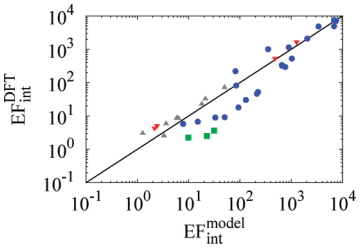


**Figure 20.** A plot of the CHEM enhancement factors calculated from DFT ($EF_{int}^{DFT}$) against the CHEM enhancement factors found from the model in eq 14 ($EF_{int}^{model}$). Each point represents a different metal−molecule system. Reprinted with permission from ref 398. Copyright 2009 American Chemical Society.

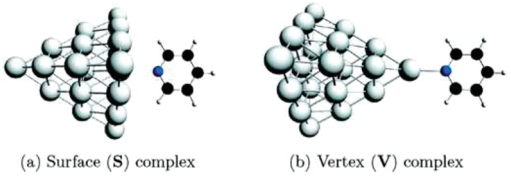


**Figure 21.** Orientation of the (a) S and (b) V complex of the pyridine−$Ag_{20}$ cluster. Reprinted with permission from ref 101. Copyright 2006 American Chemical Society.

Lombardi and Burke[333,371,401] have recently developed a unified expression to explain many of the observations that are seen in SERS. This unified theory for SERS models EM, CT, and RRS simultaneously, and is written (with simplifications and slight change in notation) as

$$R_k(\omega) = \frac{S_k}{((\varepsilon_1(\omega)+2\varepsilon_0)^2+\varepsilon_2(\omega)^2)((\omega_{CT}{}^2-\omega^2)+\Gamma_{CT}{}^2)((\omega_{RRS}{}^2-\omega^2)+\Gamma_{RRS}{}^2)} \quad (15)$$

where $\varepsilon_1(\omega)$ and $\varepsilon_2(\omega)$ are the real and imaginary dielectric components of the metal, $\varepsilon_0$ is the permittivity of free space, $\omega$ is the incident laser frequency, and $\omega_{CT}$, $\omega_{RRS}$, $\Gamma_{CT}$, and $\Gamma_{RRS}$ are the CT and RRS excitation energies and excited state relaxation rates, respectively. The enhancement factor for a specific mode is then given by $EF_k(\omega) = |R_k(\omega)|^2$. The term $S_k$ represents selection rules for the given vibrational mode $k$ based on transition dipole moments and Herzberg−Teller coupling.[402]

The denominator represents the different resonance conditions for the different enhancement mechanisms, where the first term is EM ($\varepsilon_1(\omega) = -2\varepsilon_0$), the middle term is CT ($\omega_{CT} = \omega$), and the last term is RRS ($\omega_{RRS} = \omega$). The equation was later modified to account for the continuum nature of the metal.[401] This expression illustrates that the different mechanisms are not isolated, because the three terms are multiplicative rather than additive. For example, SERRS would be described by having both $\varepsilon_1(\omega) = -2\varepsilon_0$ and $\omega_{RRS} = \omega$ so that there is both a plasmon resonance and a molecular resonance.

**5.4.1. Combined Quantum and Classical Method for SERS.** There is a significant interest in developing a "hybrid method" that combines electrodynamics methods to represent a plasmonic metal at the nanoscale and quantum mechanics to represent the molecule whose properties are of interest. These methods seem to be the most promising procedure for obtaining a unified description of SERS, since they merge the advantage of obtaining fast and accurate descriptions of the plasmonic metal particles while also retaining the electronic structure necessary to describe the molecule. A variety of different hybrid approaches to describe the optical properties of nanoparticle−molecule systems have been presented. Arcisaukaite et al.[162] used a polarizable quantum mechanical/molecular mechanical (QM/MM) method to study the charge-transfer excitation energies of pyridine interacting with small silver clusters. Morton and Jensen[160] recently described a self-consistent hybrid approach that models a metal atomistically via charge−dipole interactions while describing the molecule's electronic structure with TDDFT. Johansson and coworkers[229,241] used a two-state model in conjunction with Mie theory to calculate SERS and SEF. Masiello and Schatz[166,403] recently presented a formal many-body theory combining electronic-structure theory with a continuum-electrodynamics description of the metal and an implementation of the theory within TDDFT to study pyridine interacting with metal nanospheroids with an emphasis on SERS.

Corni and Tomasi[159,404,405] have combined a boundary element method for the metal particles based on PCM with a quantum mechanical description of the molecules for the simultaneous calculation of Raman spectra and Raman enhancement factors. They adapted a cluster−cluster aggregation (CCA) model to create randomly assembled colloidal aggregates of silver spheres in order to replicate experimental conditions. Different aggregation geometries, numbers of spheres, sizes of spheres, and surrounding mediums (vacuum or methanol) of these colloids were sampled to find ones that yielded the largest hot spots. Once suitable hot spots were found (usually between two spheres), a pyridine was placed in the center of the hot spot, and the Raman intensity was calculated. To understand the enhancements, they broke the total EF down into three contributions: $EF_{in}$ is the enhancement due to the incident light interacting with the entire colloidal aggregate, $EF_{hot}$ is the enhancement due only to the particles immediately adjacent to the hot spot, and $EF_{sc}$ is the enhancement due to the scattered light interacting with the entire colloidal aggregate. The total EF is then the product of these three components. Using this model, Corni and Tomasi found that for 20 nm particles of both Ag and Au in methanol, $EF_{in} \approx 400$, $EF_{hot} \approx 7 \times 10^8$, and $EF_{sc} \approx 60$, yielding a total of $EF \approx 2 \times 10^{13}$, which is in agreement with the work of Kneipp et al.[251] They note that simple creation of the hot spot is not enough to create the single-molecule level enhancement, but the surrounding aggregates are in fact needed to further enhance the incident and scattered field.

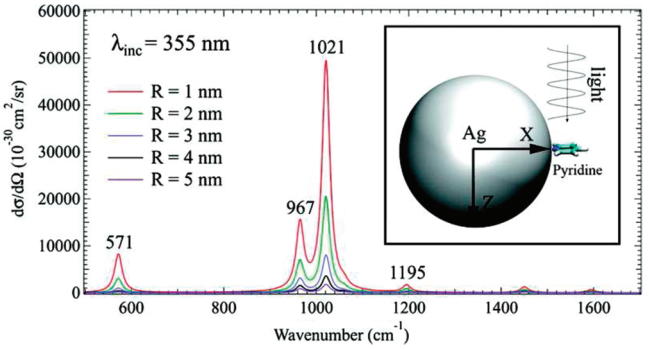


**Figure 22.** Illustration of the FDTD−TDDFT method used by Chen et al.[168] showing the direction of propagating electric field with respect to the metal−molecule system. As the molecule is pulled away from the nanoparticle, the SERS intensity decreases. Reprinted with permission from ref 168. Copyright 2010 American Chemical Society.

Chen et al.[168] have coupled the FDTD with real-time TDDFT. In contrast to traditional TDDFT methods which operate in the frequency domain, the time domain method allows control over the direction of the incident field. They calculate the enhancement of pyridine on a silver sphere with the incident light pointed normal to the plane of pyridine as illustrated in the inset of Figure 22; this was the direction that was found to yield the maximum enhancements. As clearly shown in Figure 22, the maximum EF is around $10^4$ and decays rapidly as the metal−pyridine distance increases. They also show that there is a rather small band of frequencies in which the plasmon can be excited (0.5 eV on either side of the plasmon peak) where Raman enhancement occurs.

## 6. CHIROPTICAL PROPERTIES OF SMALL METAL CLUSTERS

Previous sections have focused on the enhancement of linear optical processes when achiral systems are investigated. This section differs in that the understanding of the enhancement of absorption, infrared absorption, and Raman scattering of molecules and metal nanoclusters is applied to systems that are chiral. Electronic structure calculations have been used to study these processes, facilitating the development of relevant models to understand experimental observations. The discussion in the present section demonstrates how chiral molecules may be studied using absorption (circular dichroism), infrared absorption (vibrational circular dichroism), and Raman scattering (vibrational Raman optical activity) processes.

### 6.1. Circular Dichroism

Optically active systems can be defined by their ability to rotate the plane of polarization of linearly polarized light.[406] Linearly polarized light may be thought of as an equal mixture of left- and right-circularly polarized light. For linearly polarized light that is shone on an optically active system, the left- and right-circularly polarized light is not absorbed equally, resulting in elliptical polarization of the light. This phenomenon is known as circular dichroism (CD), which may be evaluated from the difference in molar extinction coefficients ($\Delta\varepsilon$) between the left- and right-circularly polarized light.[406]

One of the first reports of optical activity for metal nanoparticles was for gold−glutathione (Au−GS) clusters.[407] Linear absorbance confirmed the presence of discrete energy levels,

while CD spectra indicated optical activity for both the Au and glutathione absorption bands. Another study by Schaaff and Whetten[408] placed more emphasis on the optical activity of Au−GS clusters. Using gel electrophoresis, it was indicated that several different compounds were synthesized. Application of both laser desorption mass spectrometry (MS) and electrospray ionization MS allowed the authors to judge the composition of the compounds, finding that the smallest ones contained ∼20−40 Au atoms. These small Au−GS compounds were again shown to have cluster-like electronic structure, based on estimates of the optical gaps (between 1.0 and 1.7 eV) and also observed step structures on the optical absorbance spectra. CD spectra plotted in terms of the anisotropy factor ($\Delta\varepsilon/\varepsilon$) gave comparable values to chiral fullerenes[409,410] and helicenes,[411,412] indicating the strong chiroptical response for Au−GS compounds.

Furthermore, Schaaf and Whetten discussed their observations in terms of several possible mechanisms. At that time, it had been demonstrated in the literature that $Ni_{39}$ clusters took on a low-symmetry ($D_5$) structure.[413,414] The authors used this concept to judge that it may be possible that the metal cluster compounds had chiral Au cores. It was also discussed that the glutathione molecules may adsorb to an achiral metal core in a pattern that results in a chiral Au−GS cluster. Both mechanisms were determined to be plausible since it is difficult to separate the contributions of both effects. The third mechanism was that the adsorption pattern and metal core were achiral, so the optical activity resulted from binding the chiral glutathione molecules. This process was determined to be unlikely because previous findings on fullerenes showed that chiroptical response generated in this way is weak.[409]

In general, three models are used to explain optical activity in metal nanoparticles both with and without ligands present.[415,416] The first is the chiral core model.[408] In this model, optical activity can result from inherent chirality in the metal core or interactions with chiral ligands that cause distortions in the metal cluster. A dissymmetric field model has also been proposed.[417,418] This scheme can be described by having an achiral metal core with chiral adsorption patterns of the ligands, or a vicinal effect resulting from chiral ligands adsorbing to an achiral core in an achiral adsorption pattern. Note that the ligands in these two schemes need not be chiral. The third description is known as the chiral footprint model.[419,420] This results from rearrangement of specific surface metal atoms resulting from the adsorption of the chiral molecule. Studies related to these models are described below.

**6.1.1. Chiral Core Model.** Schaaf and Whetten[408] first described a chiral core model in order to explain their finding of optical activity in Au−GS clusters. Based on their findings, there was enough evidence that this model was a possibility, especially when the finding that $Ni_{39}$ clusters assume low-symmetry structures is considered.[413,414] Studies of metal cluster chirality have also been discussed for 2,2′-bis-(diphenylphosphino)-1,1′-binaphthyl (BINAP)-coated gold and palladium nanoparticles,[421,422] which may be applied to catalysis. López-Lozano et al.[423] found using DFT calculations that different enantiomers of cysteine adsorb with different strengths to Au nanoclusters based on spatial locations of their functional groups, which is important for understanding asymmetric catalysis. Furthermore, it has been demonstrated that large biomolecules like DNA can act as templates for growth of chiral silver nanoclusters.[424,425] Along with these results, numerous studies have approached metal cluster chirality using theory. These are divided into two principle investigation types: chirality from distortions through adsorbate bonding and chirality resulting from asymmetry of the metal core.

Garzón et al.[426] applied DFT calculations to investigate separate components of DNA−gold materials. Even though previous work had indicated that cluster geometries were relatively unperturbed by adsorbates,[427] this study and another by the same authors[428] demonstrated that $Au_{38}$ clusters passivated by methylthiols assume a disordered structure. These investigations lead to more intricate analyses based on simulations of CD spectra.

Román-Velázquez, Noguez, and Garzón[429] applied a polarizability interaction model to study the chiroptical response of chiral $Au_{28}(SCH_3)_{16}$ and $Au_{38}(SCH_3)_{24}$ compounds. Results from the calculations showed that the extinction efficiency correlates with the distribution of atomic distances defining the chiral cluster geometry. The authors also noted that CD spectra simulated with their model could distinguish gold clusters with different Hausdorff chirality measure (HCM)[430] values.

A further step in understanding CD response for $Au_{38}(SCH_3)_{24}$ was performed by Hidalgo et al.[431] using DFT. This study broke down the system by looking at contributions to the CD spectra for two different $Au_{38}(SCH_3)_{24}$ structures and investigating different building blocks of both systems. These components included $Au_{14}$ cores, $Au_{38}$ clusters, $Au_{38}$ clusters passivated with S atoms ($Au_{38}S_{24}$), and the methylthiols themselves without the gold cluster present. CD spectra for the different $Au_{38}(SCH_3)_{24}$ structures and their building blocks are shown in Figure 23. Comparing the CD response for the total cluster (panel a in Figure 23) to that of the $Au_{38}$ clusters alone (panel c in Figure 23) shows that most of the observed optical activity comes from Au atoms themselves. This is strong evidence that the chiral core model leads to optical activity.

More direct evidence of the chirality of metal clusters has resulted from direct investigation of isolated clusters. Garzón et al.[432] found in their structural searches that both $Au_{38}$ and $Au_{55}$ are most stable in amorphous structures, whereas $Au_{75}$ had an ordered Marks decahedron as its minimum energy structure as shown by DFT calculations. Several groups have focused on the $Au_{34}^-$ cluster geometry with respect to its molecular symmetry.[433−435] The preference of that Au cluster for a lower-symmetry structure has been rationalized by surface reconstruction of the metal clusters in order to increase coordination for the metal atoms.[433] It has also been demonstrated using Car−Parrinello molecular dynamics[436] simulations that the $Au_{34}^-$ is a fluxional core−shell system, where the surface shell Au atoms can actively reconstruct by breaking and forming bonds and change coordination number, but the core Au atoms retain a tetrahedral shape.[435] On top of arguments based on the total energy of different $Au_{34}^-$ clusters, the electronic density of states (DOS) calculated using DFT has been used to convincingly illustrate that the chiral geometries are correct, since this arrangement yields the best agreement with experimental photoelectron spectra.[434,435]

Huang et al.[437] investigated $Au_n^-$ clusters ($n$ = 55−64) using a combination of experimental photoelectron spectroscopy (PES) and DFT calculations to understand molecular structures. Based on comparison of the calculated DOS and measured photoelectron spectra, it was evident that the Au clusters had low symmetry in the size range investigated. Interestingly, for structures with $n$ = 56−64, pronounced core−shell structure was present. Structures with $n$ = 59−64 were found by capping six square-defect

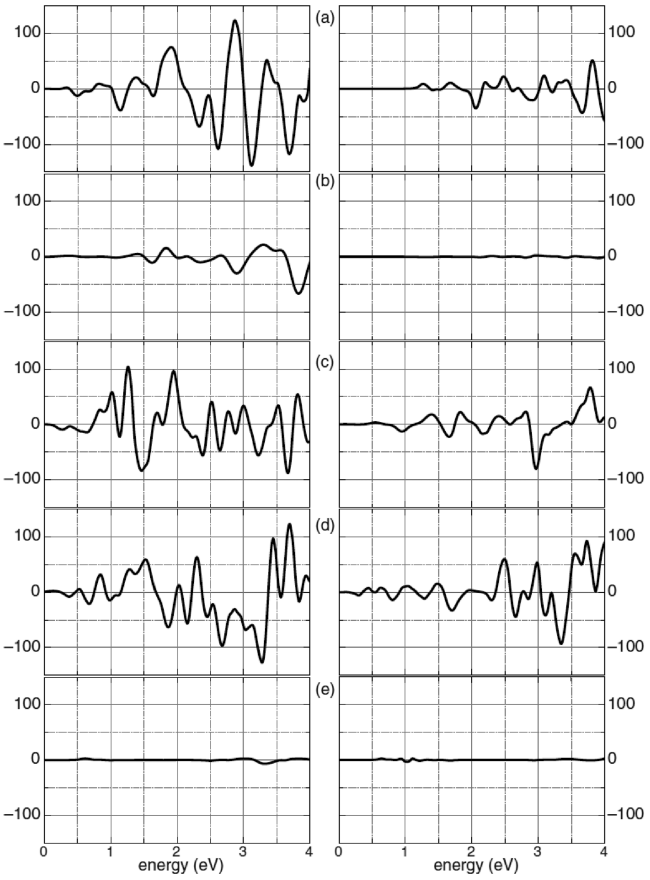


**Figure 23.** CD spectra in $\Delta\varepsilon$ ($M^{-1}$ $cm^{-1}$) for different $Au_{38}(SCH_3)_{24}$ clusters. Results for each individual cluster and their building blocks are shown in the left and right columns, respectively. Panels a−e show CD response for $Au_{38}(SCH_3)_{24}$ clusters, $Au_{14}$ cores, $Au_{38}$ clusters, $Au_{38}$ clusters passivated with S atoms ($Au_{38}S_{24}$), and the methylthiols themselves without the gold cluster present. Reprinted from ref 431 with kind permission from Springer Science+Business Media. Copyright 2009.

sites on the $Au_{58}^-$ surface with adatoms, and even though these structures differed minimally from the $Au_{58}^-$ structure the DOS calculated for these larger clusters agreed very well with measured photoelectron spectra. This indicated a pattern for understanding the growth of large $Au_n^-$ clusters. Surface reconstruction was important in this study to increase coordination between surface Au atoms, which is similar to what was observed for the $Au_{34}^-$ cluster. It was observed that reconstruction resulted in voids in the interior of the clusters, which was attributed to strong relativistic effects of Au motivating each atom to increase its coordination number.

**6.1.2. Dissymmetric Field Model.** Yao and co-workers[417] first described the dissymmetric field model in relation to metal nanoclusters. Optically active gold nanoclusters were synthesized using the chiral molecules D- and L-penicillamine (D-pen and L-pen, respectively), with sizes of 0.57, 1.18, and 1.75 nm (estimated to be ∼6 to ∼150 Au atoms in size) based on small-angle X-ray scattering (SAXS). Absorbance spectra were shown to be structured, which supported that the gold particles were clusters because they lacked features of gold nanoparticles (i.e., surface plasmon resonance). Gold nanoclusters synthesized with D-pen or L-pen showed strong CD response with a mirror image relationship between the CD spectra for individual enantiomers.

To elucidate the cause of the optical activity, the authors performed a few additional experiments. CD measurements showed no optical activity when *meso*-2,3-dimercaptosuccinic acid (DMSA) was attached to the clusters, indicating that D-pen and L-pen were important for causing chirality. Inherent chirality in the gold core was ruled out because the racemic penicillamine had no observed optical activity but would be expected to if the gold clusters rearranged to chiral structures due to adsorption of ligands. The authors determined that the anisotropy factors were similar for the penicillamine-capped gold nanoclusters compared with those transition metal complexes.[438,439] Resulting from this analysis, it was determined that the vicinal effect of the dissymmetric field model most likely resulted in the observed optical activity.

Yao and co-workers[418] also studied the D-pen and L-pen protected gold clusters using CD spectra at different temperatures and in different solvents. Gold clusters used in this study were determined to have sizes of 0.57, 1.18, and 1.75 nm based on SAXS results.[417] As temperature was increased, a reduction in CD intensity was observed. For the smallest cluster, it was demonstrated that changes existed in the CD spectra taken at different temperatures in the region where the metal absorbed, even though the linear absorption spectrum was unchanged. This was related to factors impacting the surface stereochemistry, because a change in the gold core should be noticeable on the linear absorption spectrum.

When a phase transfer was performed between water and toluene for the complex, considerable differences were observed between the CD spectra shown in the different solvents. Not only the shape of the CD spectrum but also the peak locations were affected. Shifts of two of the peaks on the CD spectrum differed from the solvent shift of the main absorption peak on the linear absorption spectrum. Based on this evidence and that the linear absorption spectrum was unchanged when temperature increased, the chiral shell around the metal clusters was thought to change indicating that the dissymmetric field was the main factor in the optical activity of these complexes.

Goldsmith et al.[440] applied both TDDFT calculations and a charge-perturbed particle-in-a-box (PIB) model to study the chiroptical response of Au cluster−adsorbate complexes. In the PIB model, the Au cluster was modeled by noninteracting electrons confined to a cubic box, with dimensions defined by the cluster being modeled, while the adsorbates were represented as point charges surrounding the box (see Figure 24). As shown in Figure 24, the arrangement of adsorbates has a small impact on the linear absorption spectrum. However, the CD spectrum is highly sensitive to the chiral field surrounding the metal core. This work also included point charge representations of the adsorbates *R*-methylthiirane and glutathione, which were used to compare between the PIB model system and TDDFT calculations. It was demonstrated that for the $Au_{14}$(*R*-methylthiirane) complex, the form of the CD spectrum and observed Cotton effect were similar for the PIB model and TDDFT, which validated the PIB calculations and that the dissymmetric field model can explain optical activity.

**6.1.3. Chiral Footprint Model.** Humblot et al.[419] introduced the chiral footprint model to explain the observed chirality of a Ni(110) surface with adsorbed (*R*,*R*)-tartaric acid. This study investigated in more detail the work of Ortega Lorenzo et al.[441] where it was shown that adsorption of (*R*,*R*)-tartaric acid or (*S*,*S*)-tartaric acid introduces chirality on a Cu(110) surface. Scanning tunneling microscopy (STM) images indicated that the molecules adsorb in an ordered arrangement on the surface,

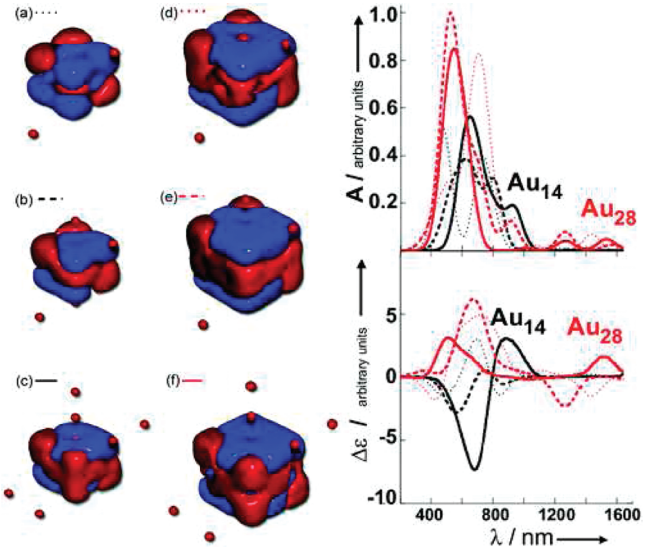


**Figure 24.** Chiral point-charge systems and induced chiral image charges for $Au_{14}$ with 2, 4, and 8 negative point charges (a−c, respectively) and similarly for $Au_{28}$ (d−f, respectively). Linear absorption spectra (top right) and CD spectra (bottom right) are shown, with lines corresponding to the labels next to the PIB figures. Red surfaces in the metal represent regions with increased electron density, and blue indicates regions with reduced electron density. Reproduced from ref 440 by permission of the PCCP Owner Societies. Copyright 2006.

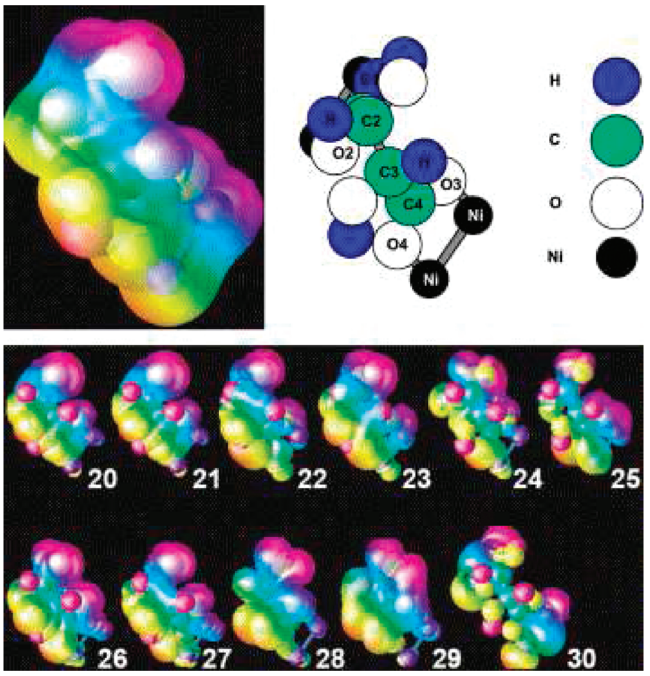


**Figure 25.** Charge distribution for a selection of orbitals for the bitartrate−$Ni_4$ complex (contour has a value of 0.01 electron/Å$^3$). Note that orbital 28 is the highest occupied state in the complex. Reprinted from ref 442 with permission from Elsevier. Copyright 2004.

while reflection−absorption IR spectroscopy confirmed that the molecules adsorbed were bitartrate molecules that bond to the surface via carboxylate groups. DFT calculations of bitartrate on a $Ni_4$ species representing the 4-fold hollow site of the Ni(110) surface showed that the adsorption of bitartrate induces significant reconstruction of the metal surface. Data from the STM and DFT results were compared for the occupied areas of the molecules on the surface, and the good agreement between both demonstrated that a chiral footprint was left on the surface due to bitartrate adsorption.

In 2004, Hofer and co-workers[442] performed a continuation of the previous study where they examined a bitartrate−$Ni_4$ complex using DFT. Compared with free bitartrate, the bitartrate in the complex assumes a skewed geometry that results in the rearrangement of Ni atoms. Interestingly, the chiral footprint was observed to occur not only in the spatial arrangement of atoms but also in the charge distribution of the complex. Examination of charge density contours[442] for both free bitartrate and the bitartrate−$Ni_4$ complex indicated that the orbitals themselves are chiral. Plots of the charge density for a selection of orbitals for the bitartrate−$Ni_4$ complex are shown in Figure 25. These results show that the chiral footprint resides both in the geometrical symmetry and in the electronic structure of the system.

Gautier and Bürgi[420] studied the chirality of gold nanoparticles with adsorbed *N*-isobutyryl-cysteine using both theory and experiment. By use of DFT calculations, several different conformers of *N*-isobutyryl-L-cysteine on a $Au_8$ cluster were studied using their vibrational CD (VCD) spectra. It was shown that the most energetically stable conformer gave poor agreement with the experimentally measured VCD spectrum, while several higher energy structures yield VCD spectra that compare qualitatively with the experimental results. This finding contrasts a similar study by the same authors where the simulated VCD spectrum of the most stable complex of *N*-acetyl-L-cysteine on a $Au_4$ cluster had the best agreement with experimental results.[443] More work may help judge what size of metal cluster is required to represent the metal surface in electronic structure calculations of optical activity.

In ref 420, the higher energy structures arrange *N*-isobutyryl-L-cysteine such that both the thiol and carboxylate groups interact with the gold cluster. While the authors lacked conclusive evidence that only the chiral footprint model was occurring, this two-point interaction with the metal surface is related to that mechanism. In a study by Li et al.,[444] the conversion of cysteine to cysteine methyl ester demonstrated that these two-point interactions are important for maintaining chirality of silver nanoparticles. Conversion between the carboxylic acid to the ester functional group removes the possibility of a two-point interaction, meaning that the loss of optical activity may result from lacking a chiral footprint.

Jadzinsky et al.[14] found that the chiral footprint occurred in gold nanoparticles protected by *p*-mercaptobenzoic acid (*p*-MBA). This study reported the X-ray structure of $Au_{102}$ surrounded by 44 *p*-MBAs. The interior core of the gold particle was a 49 Au atom Marks decahedron with two 20-atom caps with $C_5$ symmetry, and 13 Au atoms with no symmetry along the particle equator. Even though *p*-MBA is not chiral, the interactions between *p*-MBA molecule pairs resulted in staple motifs between molecules in different environments that result in sulfur atoms being chiral centers. The lack of overall symmetry in the gold atoms and chirality of sulfur atoms was used to explain optical activity observed in this system. This work is important in that it is one of the few experimental studies of optical activity in metal clusters where the specific structural details of a gold nanoparticle could be resolved.

Gautier and Bürgi[445] also examined inversion of chirality based on thiolate-for-thiolate exchange on gold nanoparticles. In this

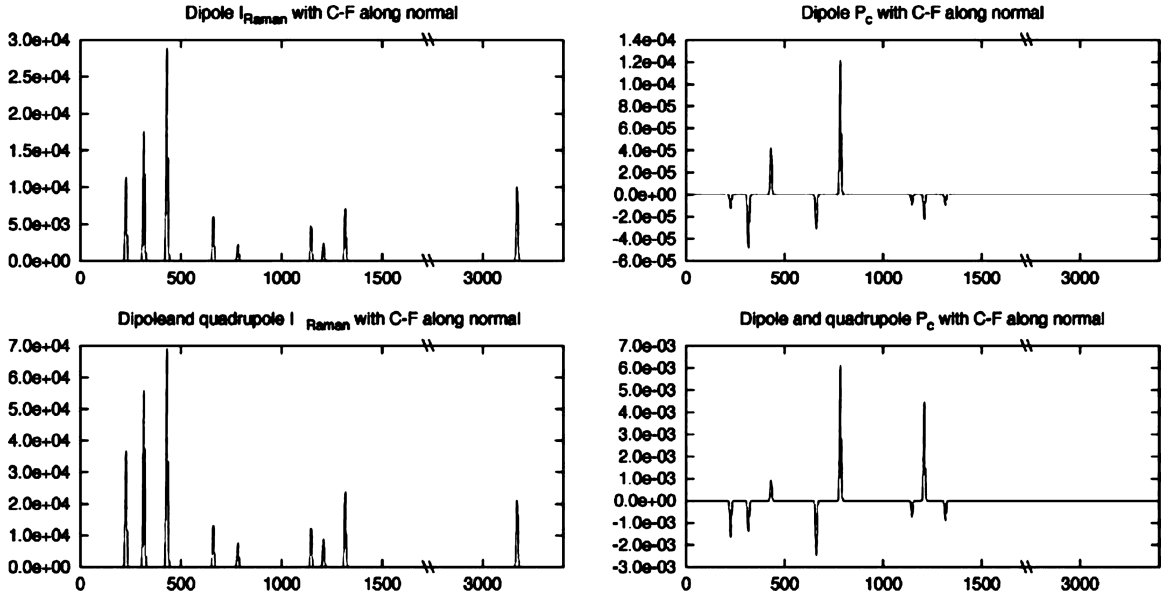


**Figure 26.** SERS spectra using the calculated orientationally averaged Raman intensity ($I_{Raman}$) and SEROA spectra using the calculated degree of circular polarization ($P_c$) for (*R*)-(−)-bromochlorofluoromethane. Results for a dipolar (top left and right) and dipolar/quadupolar (bottom left and right) substrate are shown. Reprinted with permission from ref 455. Copyright 2006 American Institute of Physics.

study *N*-isobutyryl-L-cysteine (NILC) and *N*-isobutyryl-D-cysteine (NIDC) were used to study the optical activity of small gold particles with 10−20 atoms. When gold nanoparticles protected by NILC (NIDC) were exposed to NIDC (NILC), time-evolved CD spectra showed that ligand exchange occurs quickly, which was confirmed by the change in anisotropy factor that indicated an inversion of optical activity. While the optical activity was reversed, the features of the CD spectrum were largely unchanged. Because the arrangement of ligands can cause a dramatic change in the structure of the CD spectrum,[440] it was deemed unlikely that the dissymmetric field model caused the optical activity. Based on the fast inversion of the optical activity, the authors conclude that the ligand brings its own chiral footprint to the gold nanoparticle.

### 6.2. Vibrational Raman Optical Activity

Raman optical activity (ROA) makes use of measuring the small difference in the Raman intensities due to right- and left-circularly polarized incident light. In this way, ROA provides structural information related to the chirality of molecules, which makes it uniquely suited for studying biomolecules by reporting on the secondary and tertiary structures of biomolecules in their native environment.[446−448] However, the signal in ROA is around a thousand times weaker than the already weak Raman intensities, which severely hinders the general applicability of the technique. Large enhancements of the ROA signal can be achieved by surface enhancements (SEROA) from the large electric field and field gradients near the surface of plasmonic metal nanoparticles.[449−458] In comparison to SERS, SEROA is a very new technique and only a few experimental studies have been reported to date.[453−458] The combination of the powerful structural information of ROA with the strong enhancements known for SERS make SEROA a unique technique with a large potential for biosensing applications.

Even though the theoretical foundation for ROA has been known for decades,[406,459−461] much less work has been done in establishing a theoretical understanding of SEROA.[449,450,455,462−466] While our understanding of the different enhancement mechanisms in SERS is fairly advanced,[5,15,24,25,104] much less is known about the enhancements found in SEROA. Similar to SERS, we would expect SEROA to be enhanced by the electromagnetic and chemical interactions between the adsorbate and the metal nanoparticle. However, currently it is not known what the enhancement limit for SEROA is and whether single-molecule SEROA can be achieved.

The first theoretical description of SEROA is due to Efrima, who showed that in addition to enhancement from the local field due to plasmon excitations, a contribution from the electric field gradient at the surface would also result in an enhanced ROA signal.[449,450] Janesko and Scuseria devised a method to determine SEROA by combining the electromagnetic response of orientationally averaged model substrates with Raman optical activity expressions.[455] This model was based on the earlier electromagnetic theory of Efrima.[449,450] Bour[462] later reformulated this in matrix form and generalized it for multiple particles. The work of Janesko and Scuseria also explicitly confirmed the findings of Efrima by explicit calculations on a model system consisting of (*R*)-(−)-bromochlorofluoromethane interacting with different model substrates. This is illustrated in Figure 26 where the SERS and SEROA spectra of (*R*)-(−)-bromochlorofluoromethane interacting with either a dipolar or a quadupolar substrate are plotted. These electromagnetic theories predict that the enhancement of ROA could be larger than SERS for certain substrates, making SEROA and SERS comparable.[449,450,455,462] SEROA from molecules near a spherical metal nanoshell using an extended Mie theory, including both the nanoparticle surface plasmon modes and the radiating molecular multipole fields, has been presented.[465,466]

These theoretical models have only considered the electromagnetic enhancements due to simple geometric particles. Recently, the chemical effect in SEROA was considered using TDDFT based on a short-time approximation for the Raman and ROA cross sections.[463,467] This work showed that for adenine

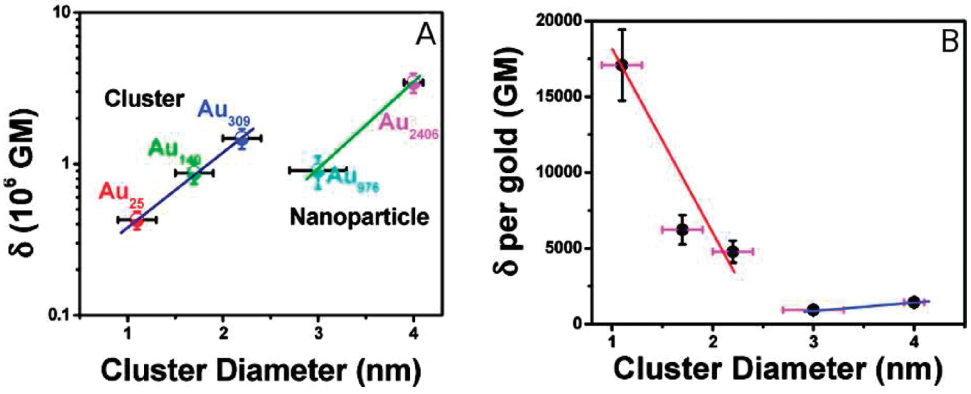


**Figure 27.** Measured absolute two-photon absorption cross sections (a) and two-photon absorption cross sections per gold atom in the cluster (b), in units of Goeppert−Mayer (GM). Reprinted with permission from ref 470. Copyright 2008 American Chemical Society.

interacting with a small silver cluster the total enhancement was on the order of $10^4$ both for SEROA and for SERS. However, the CHEM enhancement is found to be larger for SEROA than for SERS. Also, a recent study using TDDFT has highlighted the strong sensitivity of the SEROA signal to the molecule−metal orientation.[464] Here it was shown that SEROA from different molecules may cancel in ensemble measurements, and it was suggested that future SEROA experiments should use ordered monolayers of chiral molecules to minimize the orientational effects.

## 7. NONLINEAR OPTICAL PROPERTIES

Studies of nonlinear optical properties (i.e., two-photon absorbance, two-photon absorbance followed by fluorescence, second and third harmonic generation, four-wave mixing) of molecules near metal nanoparticles and of the metal nanoparticles themselves have been examined. Experiments have been performed that characterize hyper-Rayleigh scattering of spatially well-defined gold nanoparticle arrays[468] and enhancements of the third-order nonlinear susceptibility of donor−$\pi$−acceptor chromophores on silver nanoparticles.[469] Ramakrishna et al.[470] explored two-photon absorbance for gold clusters in the size regime between $Au_{25}$ (1.1 nm) and $Au_{2406}$ (4 nm). Two-photon cross section results for that study are shown in Figure 27. It was observed that a singularity exists for plots of the absolute two-photon cross section as the size increases, which was attributed to the transition between the discrete electronic structure behavior of clusters to the nanoparticle behavior involving surface plasmon resonance. Amendola et al.[471] studied the stability of nonlinear absorbance measurements of gold nanoparticles with zinc phthalocyanines present during irradiation with intense laser pulses. Zinc phthalocyanines were shown to promote self-healing of the gold nanoparticles, which was indicated by the stability and reproducibility of optical limiting measurements over time. In contrast, unexposed gold nanoparticles underwent fragmentation that was confirmed with optical limiting and UV−vis measurements, which demonstrates that it is possible to maintain the signal of nonlinear processes when intense sources are used.

Other research groups have examined the nonlinear optical properties of nanoparticle aggregates. Nonlinear susceptibilities for large fractal metal clusters were investigated by Shalaev et al.,[472,473] where numerical simulations of optical response properties were performed to better understand the enhancements involved in several nonlinear processes. Zhang and Stroud[474] examined nonlinear susceptibilities using an effective-medium approximation, demonstrating that a large enhancement of the nonlinear susceptibility occurs near the gold plasmon resonance for Au core particles surrounded by a dielectric medium.

Prasad and collaborators[475] investigated the third-order response of *para*-nitroaniline (PNA) near tetrahedral $Au_4$ and $Au_{20}$ clusters using DFT. In this work, data was compared between the exchange−correlation functionals PBE[476] and CAM-B3LYP.[163] Large second hyperpolarizabilities ($\gamma_{av}$) were calculated for systems where PNA was placed near the metal clusters, and it was demonstrated that these enhancements quickly decrease as the PNA−metal cluster distance is increased. This distance dependence indicated that a charge-transfer mechanism was responsible for the increased second hyperpolarizability of the complex. It was also established that the results from CAM-B3LYP and PBE were not consistent (i.e., $\gamma_{av}$ calculated from PBE for PNA near the face of a $Au_{20}$ tetrahedron was $4.53 \times 10^7$ au, whereas CAM-B3LYP found it to be $6.33 \times 10^6$ au for a PNA dimer linked through a $Au_{20}$ tetrahedron). This was attributed to a numerical divergence in the results from the PBE functional, possibly resulting from a resonance near the wavelength used to calculate $\gamma_{av}$ that may be corrected for using damping in the calculations.

A recent thorough examination by Day et al. of the optical properties of gold clusters and gold thiolated clusters was performed using DFT and coupled cluster theory.[477] When examining the two photon absorption cross sections, they observed a strong dependence on the DFT functional chosen. The authors also demonstrated that the optimized geometry, which depends on the DFT functional, can lead to large differences in the optical properties for these clusters.

### 7.1. Surface-Enhanced Hyper-Raman Scattering

Surface-enhanced hyper-Raman scattering (SEHRS) is the two-photon analogue of SERS in which the scattering signal is shifted relative to the second harmonic of the incident radiation ($\omega_s = 2\omega_L - \omega_k$, where $\omega_k$ is the vibrational frequency). SEHRS has predominantly been applied to characterize electronic structure of molecules by comparing to the more established SERS process.[478−487] Hulteen et al.[488] demonstrated that SEHRS for *trans*-1,2-bis(4-pyridyl)ethylene was more sensitive to applied potential than SERS and that only SEHRS was able to detect changes in $\Delta G_{abs}$ and presence of coadsorbed anions that change the surface environment. Other specific applications have included detection of biological molecules[489,490] and investigations

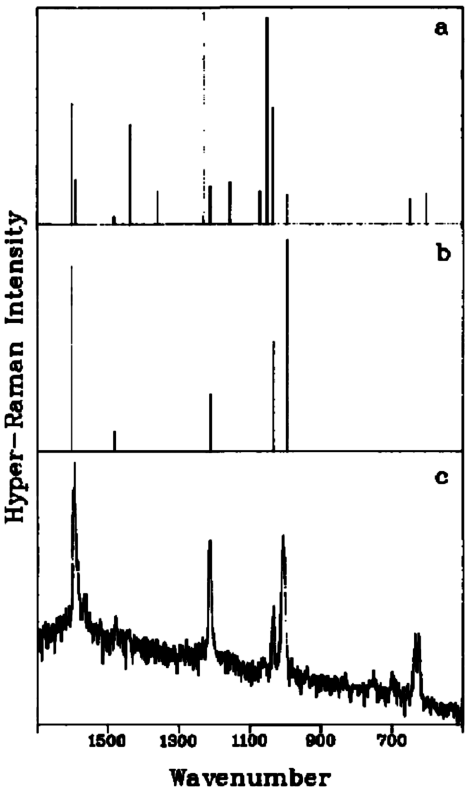


**Figure 28.** Simulated bulk hyper-Raman spectrum (a), simulated SEHRS spectrum (b), and measured SEHRS spectrum (c) of pyridine at 1064 nm. Reprinted with permission from ref 500. Copyright 1988 American Institute of Physics.

of chemical reactions on metal surfaces.[491,492] The effect of the substrate on SEHRS spectra[493−496] has been examined as well, and spectra have been measured using continuous-wave near-infrared lasers instead of more commonly used mode-locked lasers.[497]

While studies involving SEHRS are numerous, there are relatively few that apply theory. A recent study by Milojevich et al.[498] illustrated that SEHRS can be used to probe excited states that are difficult to observe with one-photon excitations in rhodamine 6G. Analysis in that study was complicated because the excited states probed were never simultaneously strong in one- and two-photon absorption. Although surface effects were neglected in this study, the off-resonance hyper-Raman spectrum simulated using DFT was in good agreement with experimental SEHRS spectrum at 1050 nm. The remainder of this section focuses on studies examining the mechanisms and enhancement factor of SEHRS.

The first SEHRS study was performed by Murphy et al.[499] in which $SO_3^{2-}$ molecules were adsorbed on Ag powder. The SEHRS spectrum at 1064 nm excitation exhibited two $a_1$ symmetry modes that coincided with those measured using SERS at 514.5 nm excitation. It was observed that the hyper-Raman signal intensity decreased with time, attributed to morphological changes induced by the laser. An estimate of the enhancement factor for SEHRS was not possible with this work, which motivated future research to incorporate electronic structure calculations and elucidate this enhancement in comparison to the better understood SERS enhancement.

Golab et al.[500] investigated the SEHRS enhancement of pyridine adsorbed to roughened Ag electrodes in a detailed experimental and theoretical study. Excitation of the pyridine molecule involved a mode-locked Nd:YAG laser, allowing for measurements of SERS and SEHRS spectra. Both the SERS and SEHRS spectra had nearly the same dominant peaks, even though the SEHRS spectrum was significantly less intense than the SERS spectrum. However, the most intense peak on the SERS and SEHRS spectra differed, and relative peak intensities were shown to vary between the two methods.

Calculations in this study were performed using the $\pi$-electron model Hamiltonian of Pariser, Parr, and Pople (PPP) to determine the transition polarizability ($\alpha_{ij}$) and first hyperpolarizability ($\beta_{ijk}$) required to simulate Raman and hyper-Raman scattering, respectively. Surface atoms were not explicitly modeled. Instead, calculations of SERS and SEHRS spectra include only the elements of $\alpha_{ij}$ and $\beta_{ijk}$ perpendicular to the "surface" (here assumed to be the $y$-direction), with pyridine oriented perpendicular to the surface with the N atom down. It was demonstrated that the calculations yielded good agreement with measured spectra for relative peak intensities. Results for the simulations of the pyridine SEHRS spectrum compared with the measured SEHRS spectrum are shown in Figure 28. One very interesting finding was that when pyridine is tilted 15° relative to the surface normal, the SERS spectrum remained nearly identical to when pyridine was oriented along the surface normal, but the SEHRS spectrum changes such that several $B_2$ symmetry bands gain significant intensity. It was judged that SEHRS is more sensitive to molecular orientation on the surface than SERS as a result.

An additional feature of this paper was the determination of the SEHRS enhancement factor. The enhancement factor was determined as

$$\frac{I_{HR}^{srf}}{I_{HR}^{bulk}} = \left(\frac{I_{R}^{srf}}{I_{R}^{bulk}}\right)\left(\frac{I_{HR}^{srf}}{I_{R}^{srf}}\right)\left(\frac{I_{HR}^{bulk}}{I_{R}^{bulk}}\right)^{-1} \quad (16)$$

On the right side of the equation, the first term is the SERS enhancement factor taken to be $10^6$. The second term was evaluated using the measured SERS and SEHRS spectra and found to be $4.6 \times 10^{-4}$, while the final term was determined using the PPP calculations for $I_{HR}^{bulk}/I_{R}^{bulk}$ and found to be $1.05 \times 10^{-11}$. Overall, the enhancement factor in this study is $10^{13}$ for SEHRS compared with the $10^6$ for SERS, attributed primarily to increased chemical effects for hyper-Raman scattering compared with Raman scattering.

Yang and Schatz[501] further investigated the enhancement factor of SEHRS, using more rigorous Hartree−Fock (HF) and Zerner's intermediate neglect of differential overlap (ZINDO) methods to evaluate $\alpha_{ij}$ and $\beta_{ijk}$. Like the previous study by Golab et al., the surface was not explicitly modeled in the calculations. It was demonstrated that HF calculations yield more accurate bulk hyper-Raman spectra for benzene and SEHRS spectra for pyridine than the ZINDO method. Also, the most accurate data for $\alpha_{ij}$ and $\beta_{ijk}$ was obtained using basis sets including diffuse functions. Use of eq 16 in this study with the first and second terms on the right side equivalent to what was used by Golab et al. indicated that the SEHRS enhancement factor is on the order of $10^{11}$ to $10^{12}$, meaning PPP calculations overestimated the bulk ratio of hyper-Raman and Raman scattering.

Yang and collaborators[502] examined the centrosymmetric molecule *trans*-1,2-bis(4-pyridyl)ethylene (BPE) on Ag film over nanosphere (AgFON) electrodes. The focus of this study was validating that a three-photon process (SEHRS) was occurring

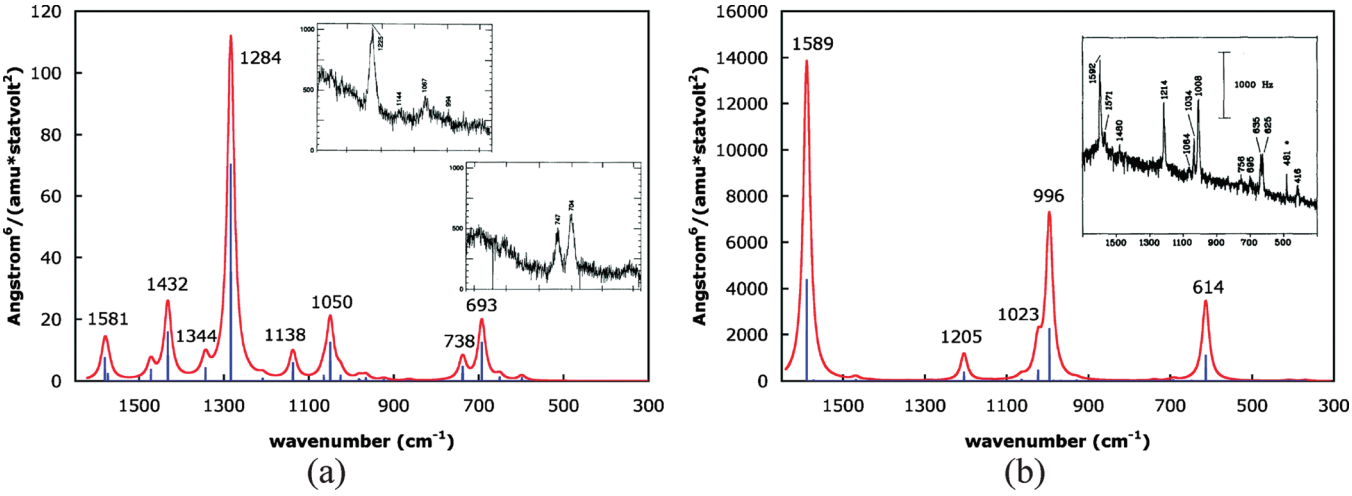


**Figure 29.** Normal hyper-Raman spectrum of pyridine (a) and SEHRS spectrum of pyridine on a tetrahedral $Ag_{20}$ cluster (b), using a Lorentzian with full width at half-maximum of 20 $cm^{-1}$ to broaden the peaks. Insets contain experimental spectra from ref 506 for normal hyper-Raman data and ref 500 for SEHRS data. Reprinted with permission from ref 505. Copyright 2010 American institute of Physics.

instead a two-step process involving second harmonic generation followed by SERS, which may be distinguished by the different selection rules for two- and three-photon processes.[503,504] HF calculations were used for simulating IR, normal Raman, hyper-Raman, SERS, and SEHRS spectra in comparison to measured spectra, where the surface again was not explicitly modeled. In general, it was found that IR, normal Raman, and SERS spectra agree well with experiment in terms of frequencies and relative peak intensities. The simulated SEHRS spectrum was in worse agreement with the measured one, resulting from larger deviations in calculated frequencies and appearance of modes in the measured spectrum that are absent in the calculated one. However, the symmetry of vibrations observed on the SEHRS spectra provided evidence that the process indeed follows three-photon selection rules, ruling out two-step mechanisms.

Li et al.[494] compared measured and simulated normal Raman, hyper-Raman, IR, SERS, and SEHRS spectra in a study of their Ag metal nanoparticles-on-smooth-electrode (NOSE) substrate. DFT calculations were employed to simulate spectra and investigate the molecular orientation of pyridine, pyrazine, and benzene with respect to a nonexplicitly modeled surface. Generally, the simulated normal Raman, IR, and SERS spectra were in good agreement with what was measured. While the simulated SEHRS spectrum for benzene compares well with the measured spectrum, simulated SEHRS spectra for both pyridine and pyrazine are in worse agreement. This was rationalized by the authors by discussing surface selection rules for pyridine and comparing two orientations of pyrazine to measured results also.

Whereas the previous investigations examined the overall SEHRS enhancement factor, Valley et al.[505] focused specifically on estimating the contribution from chemical enhancement to SEHRS. TDDFT was applied to study both substituted and unsubstituted pyridines bonded in different adsorption geometries to tetrahedral $Ag_{20}$ clusters. This is the first study that included a representation of the surface for simulating SEHRS spectra. It was demonstrated that chemical enhancement is important in SEHRS because there were significant differences in relative peak intensities when the simulated (and measured) normal hyper-Raman and SEHRS spectra were compared, as shown in Figure 29. The relative peak intensities from the TDDFT calculations correctly reproduce what is observed experimentally as well. Data for the unsubstituted pyridine adsorbed to the $Ag_{20}$ tetrahedra indicated that the chemical enhancements are on the order of $10^2$ to $10^4$ on average, although the maximum enhancement for an individual peak was on the order of $10^4$ to $10^5$. Combining this with the estimate for the electromagnetic SEHRS enhancement factor on silver[323] of $10^7$, the total SEHRS enhancement factor is $10^9-10^{10}$ on average but can be at large as $10^{11}-10^{12}$.

This study also applies a two-state model for SEHRS chemical enhancement using an analogous series of assumptions proposed by Morton and Jensen[398] for the chemical enhancement of SERS. In this model, the SEHRS chemical enhancement factor is written

$$\mathrm{EF}_{\mathrm{int}}^{\mathrm{model}} = \frac{I_{\mathrm{X-pyr-Ag}}}{I_{\mathrm{X-pyr}}} = A\left(\frac{\omega_{\mathrm{X}}}{\omega_{\mathrm{e}}}\right)^6 \qquad (17)$$

where $\omega_X$ is the HOMO−LUMO gap of the free molecule, $\omega_e$ is the average gap between the $Ag_{20}$ HOMO and molecule LUMO, and $A$ is a constant collecting transition dipole moments, change in permanent dipole moment between the ground and excited state, and derivatives of $\omega_X$ and $\omega_e$ with respect to the normal modes. The correct trend in chemical enhancement for SEHRS is predicted with the model, even though it sometimes yields enhancement factors differing by a factor of approximately four from those directly calculated from TDDFT results. It is clearly demonstrated that there is a large dependence of the SEHRS chemical enhancement on $\omega_X/\omega_e$, which facilitates comparison and understanding of the larger SEHRS chemical enhancement compared with SERS.

## 8. CONCLUSION

In this review, we have described recent advances in applying electronic structure theory to understanding the optical properties of metal clusters and their interactions with molecules. We have highlighted how these methods can provide detailed insights into the microscopic origin of plasmonics. Experimental work on the absorption properties of small metal clusters provide the link between the small molecular-like clusters containing a few metal atoms and the bulk nanoparticles. Electronic structure methods are ideally suited for describing the optical properties of these small clusters due to the importance of quantum size effects.

These kind of studies are likely to becomes even more important in the future as we learn to synthesize a larger range of small nanoclusters containing a precise number of metal atoms as well as ligands. As the size of these clusters increase and bridge the gap with bulk nanoparticles, we will ultimately understand the microscopic origin of plasmonics and electronic structure methods are likely to play an important role in achieving that.

Quantum effects were also shown to be important for correctly describing the enhanced electric field near metal nanoparticles. Since the enhanced local field gives rise to a large number of enhanced molecular spectroscopies it is essential to correctly describe it. Further advances in nanofabrication and the synthesis of nanoparticles will result in an even larger myriad of particle shapes and sizes with well-defined nanometer dimensions. As discussed here, quantum effects start to become important as the features reach a few nanometers. The importance of electronic structure theory is therefore likely to increase, at least to show us when classical electrodynamics methods are reliable.

The area of surface-enhanced spectroscopies greatly benefits from the ever-increasing understanding of the optical properties of nanoparticles and our ability to fabricate structures with well-defined and reproducible optical properties. In contrast to this, our understanding of the optical properties of molecules interacting with larger nanoparticles is still rather rudimentary. This review has highlighted advances in using electronic structure theory to understand surface-enhanced spectroscopies. An important goal for electronic structure methods continues to be the development of new methods that can correctly and efficiently describe the optical properties of molecules interacting with metal nanoparticles. This will finally provide a unified approach to understanding surface-enhanced spectroscopies. However, the major challenge will be to develop efficient methods to treat interactions of an electronically localized system, like a molecule, with an electronically delocalized structure, like a metal particle, that is many nanometers in dimension.

## AUTHOR INFORMATION

### Corresponding Author

*E-mail: jensen@chem.psu.edu.

## BIOGRAPHIES

Seth Morton attended the University of Maine for his undergraduate education where he worked with Dr. Carl Tripp on understanding the UV-crosslinking of liposomes using vibrational spectroscopy. He received his B.S. in Chemistry in 2007, and from there moved to The Pennsylvania State University to perform his postgraduate research under the advisement of Dr. Lasse Jensen. Seth is currently working towards a Ph.D. in Theoretical and Computational Chemistry, and he focuses on developing new computational methods to better simulate molecular optical properties, with the hope of unraveling a unified understanding of surface-enhanced Raman scattering.

Daniel Silverstein received a B.S. degree in chemistry at the University of Colorado at Denver in 2008. He is currently in his third year of graduate studies in chemistry at The Pennsylvania State University in Prof. Jensen's lab. His research interests include simulating resonance Raman and resonance hyper-Raman scattering, vibronic coupling models, photoinduced electron transfer in molecules, and applying quantum mechanics to understand the evolution of plasmons in metal nanoparticles.

Lasse Jensen received his Cand.Scient from the University of Copenhagen, Denmark, in 2000 and his Ph.D. in 2004 from the University of Groningen, The Netherlands. From 2004 to 2007, he was a postdoctoral fellow in the group of George C. Schatz and is currently an Assistant Professor of Chemistry at The Pennsylvania State University. His research interest focuses on developing theoretical methods to understand optical spectroscopy of bio- and nanosystems.

## ACKNOWLEDGMENT

L.J. acknowledges the CAREER program of the National Science Foundation (Grant No. CHE-0955689) for financial support, start-up funds from the Pennsylvania State University,

and support received from Research Computing and Cyberinfrastructure, a unit of Information Technology Services at Penn State. S.M.M. acknowledges the Academic Computing Fellowship from the Pennsylvania State University Graduate School.

## REFERENCES

(1) Faraday, M. *Philos. Trans. R. Soc. London* **1857**, *147*, 145.
(2) Kreibig, U.; Vollmer, M. *Optical Properties of Metal Clusters*; Springer: Berlin, 1995.
(3) Kelly, K. L.; Coronado, E. A.; Zhao, L. L.; Schatz, G. C. *J. Phys. Chem. B* **2003**, *107*, 668.
(4) Halperin, W. P. *Rev. Mod. Phys.* **1986**, *58*, 533.
(5) Link, S.; El-Sayed, M. A. *Annu. Rev. Phys. Chem.* **2003**, *54*, 331PMID: 12626731.
(6) Kalsin, A.; Fialkowski, M.; Paszewski, M.; Smoukov, S. K.; Bishop, K. J. M.; Grzybowski, B. A. *Science* **2006**, *312*, 420.
(7) Stuart, D. A.; Yuen, J. M.; Shah, N.; Lyandres, O.; Yonzon, C. R.; Glucksberg, M. R.; Walsh, J. T.; Duyne, P. V. *Anal. Chem.* **2006**, *78*, 7211.
(8) Huang, X.; El-Sayed, I. H.; Qian, W.; El-Sayed, M. A. *J. Am. Chem. Soc.* **2006**, *128*, 2115.
(9) Xia, Y. N.; Halas, N. J. *MRS Bull.* **2005**, *30*, 338.
(10) Murphy, C. J.; Sau, T. K.; Gole, A. M.; Orendorff, C. J.; Gao, J.; Gou, L.; Hunyadi, S. E.; Li, T. *J. Phys. Chem. B* **2005**, *109*, 13857.
(11) Gates, B. D.; Xu, Q.; Stewart, M.; Ryan, D.; Willson, C. G.; Whitesides, G. M. *Chem. Rev.* **2005**, *105*, 1171.
(12) Zhang, X. Y.; Whitney, A. V.; Zhao, J.; Hicks, E. M.; Van Duyne, R. P. *J. Nanosci. Nanotechnol.* **2006**, *6*, 1920.
(13) Henzie, J.; Barton, J. E.; Stender, C. L.; Odom, T. W. *Acc. Chem. Res.* **2006**, *39*, 249.
(14) Jadzinsky, P. D.; Calero, G.; Ackerson, C. J.; Bushnell, D. A.; Kornberg, R. D. *Science* **2007**, *318*, 430.
(15) Kneipp, K.; Kneipp, H.; Itzkan, I.; Dasari, R. R.; Feld, M. S. *Chem. Rev.* **1999**, *99*, 2957.
(16) Mirkin, C. A.; Letsinger, R. L.; Mucic, R. C.; Storhoff, J. J. *Nature* **1996**, *382*, 607.
(17) Haes, A. J.; Hall, W. P.; Chang, L.; Klein, W. L.; Van Duyne, R. P. *Nano Lett.* **2004**, *4*, 1029.
(18) Yonzon, C. R.; Haynes, C. L.; Zhang, X. Y.; Walsh, J. T., Jr.; Van Duyne, R. P. *Anal. Chem.* **2004**, *76*, 78.
(19) Schultz, D. A. *Curr. Opin. Biotechnol.* **2003**, *14*, 13.
(20) Cao, Y.-W.; Jin, R.; Mirkin, C. A. *Science* **2002**, *297*, 1536.
(21) Penn, S. G.; He, L.; Natan, M. J. *Curr. Opin. Chem. Biol.* **2003**, *7*, 609.
(22) Homola, J.; Yee, S. S.; Gauglitz, G. *Sens. Actuators B* **1999**, *54*, 3.
(23) Haes, A. J.; Haynes, C. L.; McFarland, A. D.; Schatz, G. C.; Van Duyne, R. P.; Zou, S. *MRS Bull.* **2005**, *30*, 368.
(24) Moskovits, M. *Rev. Mod. Phys.* **1985**, *57*, 783.
(25) Campion, A.; Kambhampati, P. *Chem. Soc. Rev.* **1998**, *27*, 241.
(26) Barnes, W. L. *J. Mod. Opt.* **1998**, *45*, 661.
(27) Lakowicz, J. R. *Anal. Biochem.* **2001**, *298*, 1.
(28) Mie, G. *Ann. Phys. (Leipzig)* **1908**, *25*, 377.
(29) Yang, W.-H.; Schatz, G. C.; Van Duyne, R. P. *J. Chem. Phys.* **1995**, *103*, 869.
(30) Draine, B. T.; Flatau, P. J. *J. Opt. Soc. Am. A* **1994**, *11*, 1491.
(31) Bian, R. X.; Dunn, R. C.; Xie, X. S.; Leung, P. T. *Phys. Rev. Lett.* **1995**, *75*, 4772.
(32) Taflove, A.; Hagness, S. C. *Computational Electrodynamics: The Finite-Difference Timedomain Method*; Artech House: Boston, MA, 2005.
(33) de Heer, W. A.; Selby, K.; Kresin, V.; Masui, J.; Vollmer, M.; Châtelain, A.; Knight, W. D. *Phys. Rev. Lett.* **1987**, *59*, 1805.
(34) de Heer, W. A. *Rev. Mod. Phys.* **1993**, *65*, 611.
(35) Wood, D. M.; Ashcroft, N. W. *Phys. Rev. B* **1982**, *25*, 6255.
(36) Liebsch, A. *Phys. Rev. B* **1993**, *48*, 11317.
(37) Coronado, E. A.; Schatz, G. C. *J. Chem. Phys.* **2003**, *119*, 3926.
(38) Han, M.; Li, X.; Li, B.; Shi, N.; Chen, K.; Zhu, J.; Xu, Z. *J. Phys. Chem. C* **2008**, *112*, 17893.
(39) McMahon, J. M.; Gray, S. K.; Schatz, G. C. *Phys. Rev. Lett.* **2009**, *103*, No. 097403.
(40) Zheng, J.; Nicovich, P. R.; Dickson, R. M. *Annu. Rev. Phys. Chem.* **2007**, *58*, 409.
(41) El-Sayed, M. A. *Acc. Chem. Res.* **2001**, *34*, 257.
(42) Alvarez, M. M.; Khoury, J. T.; Schaaff, T. G.; Shafigullin, M. N.; Vezmar, I.; Whetten, R. L. *J. Phys. Chem. B* **1997**, *101*, 3706.
(43) Logunov, S.; Ahmadi, T.; El-Sayed, M.; Khoury, J.; Whetten, R. *J. Phys. Chem. B* **1997**, *101*, 3713.
(44) Schaaff, T. G.; Shafigullin, M. N.; Khoury, J. T.; Vezmar, I.; Whetten, R. L.; Cullen, W. G.; First, P. N.; Gutierrez-Wing, C.; Ascensio, J.; Jose-Yacaman, M. J. *J. Phys. Chem. B* **1997**, *101*, 7885.
(45) Selby, K.; Vollmer, M.; Masui, J.; Kresin, V.; de Heer, W. A.; Knight, W. D. *Phys. Rev. B* **1989**, *40*, 5417.
(46) Wang, C. R. C.; Pollack, S.; Cameron, D.; Kappes, M. M. *J. Chem. Phys.* **1990**, *93*, 3787.
(47) Bonačić-Koutecký, V.; Fantucci, P.; Koutecký, J. *J. Chem. Phys.* **1990**, *93*, 3802.
(48) Selby, K.; Kresin, V.; Masui, J.; Vollmer, M.; de Heer, W. A.; Scheidemann, A.; Knight, W. D. *Phys. Rev. B* **1991**, *43*, 4565.
(49) Pollack, S.; Wang, C. R. C.; Kappes, M. M. *J. Chem. Phys.* **1991**, *94*, 2496.
(50) Bonačić-Koutecký, V.; Fantucci, P.; Koutecký, J. *Chem. Rev.* **1991**, *91*, 1035.
(51) Blanc, J.; Bonačić-Koutecký, V.; Broyer, M.; Chevakeyre, J.; Dugourd, P.; Koutecký, J.; Scheuch, C.; Wolf, J. P.; Wöste, L. *J. Chem. Phys.* **1992**, *96*, 1793.
(52) Bonačić-Koutecký, V.; Fantucci, P.; Fuchs, C.; Gatti, C.; Pittner, J.; Polezzo, S. *Chem. Phys. Lett.* **1993**, *213*, 522.
(53) Brack, M. *Rev. Mod. Phys.* **1993**, *65*, 677.
(54) Heaven, M. W.; Dass, A.; White, P. S.; Holt, K. M.; Murray, R. W. *J. Am. Chem. Soc.* **2008**, *130*, 3754.
(55) Akola, J.; Walter, M.; Whetten, R. L.; Häkkinen, H.; Grönbeck, H. *J. Am. Chem. Soc.* **2008**, *130*, 3756.
(56) Zhu, M.; Aikens, C. M.; Hollander, F. J.; Schatz, G. C.; Jin, R. *J. Am. Chem. Soc.* **2008**, *130*, 5883.
(57) Zheng, J.; Zhang, C.; Dickson, R. M. *Phys. Rev. Lett.* **2004**, *93*, No. 077402.
(58) Yu, J.; Choi, S.; Dickson, R. M. *Angew. Chem., Int. Ed.* **2009**, *48*, 318.
(59) Peyser-Capadona, L.; Zheng, J.; Gonzalez, J. I.; Lee, T.-H.; Patel, S. A.; Dickson, R. M. *Phys. Rev. Lett.* **2005**, *94*, No. 058301.
(60) Zheng, J.; Ding, Y.; Tian, B.; Wang, Z. L.; Zhuang, X. *J. Am. Chem. Soc.* **2008**, *130*, 10472.
(61) Compagnon, I.; Tabarin, T.; Antoine, R.; Broyer, M.; Dugourd, P.; Mitric, R.; Petersen, J.; Bonacic-Koutecky, V. *J. Chem. Phys.* **2006**, *125*, No. 164326.
(62) Mitrić, R.; Petersen, J.; Kulesza, A.; Bonačić-Koutecký, V.; Tabarin, T.; Compagnon, I.; Antoine, R.; Broyer, M.; Dugourd, P. *J. Chem. Phys.* **2007**, *127*, No. 134301.
(63) Edwards, P. P.; Johnston, R. L.; Rao, C. *Metal Clusters in Chemistry*; Wiley-VCH Verlag GmbH: Weinheim, Germany, 2008; pp 1454−1481.
(64) Kubo, R. *J. Phys. Soc. Jpn.* **1962**, *17*, 975.
(65) Kawabata, A.; Kubo, R. *J. Phys. Soc. Jpn.* **1966**, *21*, 1765.
(66) Knight, W. D.; Clemenger, K.; de Heer, W. A.; Saunders, W. A.; Chou, M. Y.; Cohen, M. L. *Phys. Rev. Lett.* **1984**, *52*, 2141.
(67) Knight, W. D.; Clemenger, K.; de Heer, W. A.; Saunders, W. A. *Phys. Rev. B* **1985**, *31*, 2529.
(68) Ekardt, W. *Phys. Rev. Lett.* **1984**, *52*, 1925.
(69) Beck, D. E. *Phys. Rev. B* **1984**, *30*, 6935.
(70) Snider, D. R.; Sorbello, R. S. *Phys. Rev. B* **1983**, *28*, 5702.
(71) Benichou, E.; Antoine, R.; Rayane, D.; Vezin, B.; Dalby, F. W.; Dugourd, P.; Broyer, M.; Ristori, C.; Chandezon, F.; Huber, B. A.; Rocco, J. C.; Blundell, S. A.; Guet, C. *Phys. Rev. A* **1999**, *59*, R1.
(72) Antoine, R.; Rayane, D.; Allouche, A. R.; Aubert-Frécon, M.; Benichou, E.; Dalby, F. W.; Dugourd, P.; Broyer, M.; Guet, C. *J. Chem. Phys.* **1999**, *110*, 5568.
(73) Rayane, D.; Allouche, A. R.; Benichou, E.; Antoine, R.; Aubert-Frecon, M.; Dugourd, P.; Broyer, M.; Ristori, C.; Chandezon, F.; Huber, B. A.; Guet, C. *Eur. Phys. J. D* **1999**, *9*, 243.

(74) Tikhonov, G.; Kasperovich, V.; Wong, K.; Kresin, V. V. *Phys. Rev. A* **2001**, *64*, No. 063202.
(75) Rubio, A.; Balbás, L. C.; Alonso, J. A. *Phys. Rev. B* **1992**, *45*, 13657.
(76) Pacheco, J. M.; Martins, J. L. *J. Chem. Phys.* **1997**, *106*, 6039.
(77) Pecul, M.; Jaszuński, M.; Jørgensen, P. *Mol. Phys.* **2000**, *98*, 1455.
(78) van Gisbergen, S. J. A.; Pacheco, J. M.; Baerends, E. J. *Phys. Rev. A* **2001**, *63*, No. 063201.
(79) Vasiliev, I.; Öğüt, S.; Chelikowsky, J. R. *Phys. Rev. B* **2002**, *65*, No. 115416.
(80) Della Sala, F.; Rousseau, R.; Görling, A.; Marx, D. *Phys. Rev. Lett.* **2004**, *92*, No. 183401.
(81) Blase, X.; Ordejón, P. *Phys. Rev. B* **2004**, *69*, No. 085111.
(82) Röthlisberger, U.; Andreoni, W. *J. Chem. Phys.* **1991**, *94*, 8129.
(83) Moseler, M.; Häkkinen, H.; Landman, U. *Phys. Rev. Lett.* **2001**, *87*, No. 053401.
(84) del Puerto, M. L.; Tiago, M. L.; Chelikowsky, J. R. *J. Chem. Phys.* **2007**, *127*, No. 144311.
(85) Moullet, I.; Martins, J. L.; Reuse, F.; Buttet, J. *Phys. Rev. B* **1990**, *42*, 11598.
(86) Maroulis, G.; Xenides, D. *J. Phys. Chem. A* **1999**, *103*, 4590.
(87) Blundell, S. A.; Guet, C.; Zope, R. R. *Phys. Rev. Lett.* **2000**, *84*, 4826.
(88) Kronik, L.; Vasiliev, I.; Chelikowsky, J. R. *Phys. Rev. B* **2000**, *62*, 9992.
(89) Kümmel, S.; Brack, M.; Reinhard, P.-G. *Phys. Rev. B* **2000**, *62*, 7602.
(90) Solov'yov, I. A.; Solov'yov, A. V.; Greiner, W. *Phys. Rev. A* **2002**, *65*, No. 053203.
(91) Chandrakumar, K. R. S.; Ghanty, T. K.; Ghosh, S. K. *J. Chem. Phys.* **2004**, *120*, 6487.
(92) Maroulis, G. *J. Chem. Phys.* **2004**, *121*, 10519.
(93) Kümmel, S.; Andrae, K.; Reinhard, P.-G. *Appl. Phys. B* **2001**, *73*, 293.
(94) Kümmel, S.; Brack, M. *Phys. Rev. A* **2001**, *64*, No. 022506.
(95) Tiggesbäumker, J.; Köller, L.; Meiwes-Broer, K.-H.; Liebsch, A. *Phys. Rev. A* **1993**, *48*, R1749.
(96) Harbich, W.; Fedrigo, S.; Buttet, J. *Z. Phys. D.* **1993**, *26*, 138.
(97) Harb, M.; Rabilloud, F.; Simon, D.; Rydlo, A.; Lecoultre, S.; Conus, F.; Rodrigues, V.; Félix, C. *J. Chem. Phys.* **2008**, *129*, No. 194108.
(98) Fredigo, S.; Harbich, W.; Buttet, J. *Phys. Rev. B* **1993**, *47*, 10706.
(99) Zhao, J.; Yang, J.; Hou, J. G. *Phys. Rev. B* **2003**, *67*, No. 085404.
(100) Jensen, L.; Autschbach, J.; Schatz, G. C. *J. Chem. Phys.* **2005**, *122*, No. 224115.
(101) Zhao, L.; Jensen, L.; Schatz, G. C. *J. Am. Chem. Soc.* **2006**, *128*, 2911.
(102) Pereiro, M.; Baldomir, D. *Phys. Rev. A* **2007**, *75*, No. 033202.
(103) Idrobo, J. C.; Walkosz, W.; Yip, S. F.; Öğüt, S.; Wang, J.; Jellinek, J. *Phys. Rev. B* **2007**, *76*, No. 205422.
(104) Jensen, L.; Aikens, C. M.; Schatz, G. C. *Chem. Soc. Rev.* **2008**, *37*, 1061.
(105) Bonačić-Koutecký, V.; Veyret, V.; Mitrić, R. *J. Chem. Phys.* **2001**, *115*, 10450.
(106) Bonačić-Koutecký, V.; Pittner, J.; Boiron, M.; Fantucci, P. *J. Chem. Phys.* **1999**, *110*, 3876.
(107) Yabana, K.; Bertsch, G. F. *Phys. Rev. A* **1999**, *60*, 3809.
(108) Idrobo, J. C.; Öğüt, S.; Jellinek, J. *Phys. Rev. B* **2005**, *72*, No. 085445.
(109) Tiago, M. L.; Idrobo, J. C.; Öğüt, S.; Jellinek, J.; Chelikowski, J. R. *Phys. Rev. B* **2009**, *79*, No. 155419.
(110) Silverstein, D. W.; Jensen, L. *J. Chem. Phys.* **2010**, *132*, No. 194302.
(111) Klotzbuecher, W. E.; Ozin, G. A. *Inorg. Chem.* **1980**, *19*, 3767.
(112) Harbich, W.; Fedrigo, S.; Buttet, J.; Lindsay, D. M. *J. Chem. Phys.* **1992**, *96*, 8104.
(113) Fedrigo, S.; Harbich, W.; Buttet, J. *J. Chem. Phys.* **1993**, *99*, 5712.
(114) Handschuh, H.; Ganteför, G.; Bechthold, P. S.; Eberhardt, W. *J. Chem. Phys.* **1994**, *100*, 7093.
(115) Schweizer, A.; Weber, J. M.; Gilb, S.; Schneider, H.; Schooss, D.; Kappes, M. M. *J. Chem. Phys.* **2003**, *119*, 3699.
(116) Gilb, S.; Jacobsen, K.; Schooss, D.; Furche, F.; Ahlrichs, R.; Kappes, M. M. *J. Chem. Phys.* **2004**, *121*, 4619.
(117) Aikens, C. M.; Schatz, G. C. *J. Phys. Chem. A* **2006**, *110*, 13317.
(118) Cottancin, E.; Celep, G.; Lermé, J.; Pellarin, M.; Huntzinger, J. R.; Vialle, J. L.; Broyer, M. *Theor. Chim. Acta* **2006**, *116*, 514.
(119) Fa, W.; Zhou, J.; Luo, C.; Dong, J. *Phys. Rev. B* **2006**, *73*, No. 085405.
(120) Devarajan, A.; Gaenko, A.; Autschbach, J. *J. Chem. Phys.* **2009**, *130*, No. 194102.
(121) Castro, A.; Marques, M. A. L.; Romero, A. H.; Oliveira, M. J. T.; Rubio, A. *J. Chem. Phys.* **2008**, *129*, No. 144110.
(122) Lermé, J.; Palpant, B.; Prével, B.; Cottancin, E.; Pellarin, M.; Treilleux, M.; Vialle, J.; Perez, A.; Broyer, M. *Eur. Phys. J. D* **1998**, *4*, 95.
(123) Wang, J.; Yang, M.; Jellinek, J.; Wang, G. *Phys. Rev. A* **2006**, *74*, No. 023202.
(124) Wu, Z.; Lanni, E.; Chen, W.; Bier, M. E.; Ly, D.; Jin, R. *J. Am. Chem. Soc.* **2009**, *131*, 16672.
(125) Jin, R. *Nanoscale* **2010**, *2*, 343.
(126) Bakr, O.; Amendola, V.; Aikens, C.; Wenseleers, W.; Li, R.; Dal Negro, L.; Schatz, G.; Stellacci, F. *Angew. Chem., Int. Ed.* **2009**, *48*, 5921.
(127) Walter, M.; Akola, J.; Lopez-Acevedo, O.; Jadzinsky, P. D.; Calero, G.; Ackerson, C. J.; Whetten, R. L.; Grönbeck, H.; Häkkinen, H. *Proc. Natl. Acad. Sci. U.S.A.* **2008**, *105*, 9157.
(128) Reimers, J. R.; Wang, Y.; Cankurtaran, B. O.; Ford, M. J. *J. Am. Chem. Soc.* **2010**, *132*, 8378.
(129) Aikens, C. M. *J. Phys. Chem. C* **2008**, *112*, 19797.
(130) Aikens, C. M. *J. Phys. Chem. A* **2009**, *113*, 10811.
(131) Aikens, C. M.; Li, S.; Schatz, G. C. *J. Phys. Chem. C* **2008**, *112*, 11272.
(132) Prodan, E.; Nordlander, P. *Nano Lett.* **2003**, *3*, 543.
(133) Johnson, H. E.; Aikens, C. M. *J. Phys. Chem. A* **2009**, *113*, 4445.
(134) Yan, J.; Gao, S. *Phys. Rev. B* **2008**, *78*, No. 235413.
(135) Yan, J.; Yuan, Z.; Gao, S. *Phys. Rev. Lett.* **2007**, *98*, No. 216602.
(136) Lian, K.-Y.; Salek, P.; Jin, M.; Ding, D. *J. Chem. Phys.* **2009**, *130*, No. 174701.
(137) Prodan, E.; Nordlander, P. *Chem. Phys. Lett.* **2002**, *352*, 140.
(138) Prodan, E.; Nordlander, P.; Halas, N. J. *Nano Lett.* **2003**, *3*, 1411.
(139) Stener, M.; Nardelli, A.; De Francesco, R.; Fronzoni, G. *J. Phys. Chem. C* **2007**, *111*, 11862.
(140) Jensen, L. L.; Jensen, L. *J. Phys. Chem. C* **2008**, *112*, 15697.
(141) Jensen, L. L.; Jensen, L. *J. Phys. Chem. C* **2009**, *113*, 15182.
(142) Mayer, A.; Gonzalez, A. L.; Aikens, C. M.; Schatz, G. C. *Nanotechnology* **2009**, *20*, No. 195204.
(143) Mayer, A.; Schatz, G. C. *J. Phys.: Condens. Matter* **2009**, *21*, No. 325301.
(144) Zuloaga, J.; Prodan, E.; Nordlander, P. *Nano Lett.* **2009**, *9*, 887.
(145) Zhao, K.; Troparevsky, M. C.; Xiao, D.; Eguiluz, A. G.; Zhang, Z. *Phys. Rev. Lett.* **2009**, *102*, No. 186804.
(146) Atay, T.; Song, J.-H.; Nurmikko, A. V. *Nano Lett.* **2004**, *4*, 1627.
(147) Vincenot, J.; Aikens, C. M. In *Quantum Mechanical Examination of Optical Absorption Spectra of Silver Nanorod Dimers*; Springer: Dordrecht, Netherlands, 2009; Vol. 20, pp 253−264.
(148) Lassiter, J. B.; Aizpurua, J.; Hernandez, L. I.; Brandl, D. W.; Romero, I.; Lal, S.; Hafner, J. H.; Nordlander, P.; Halas, N. J. *Nano Lett.* **2008**, *8*, 1212.
(149) Romero, I.; Aizpurua, J.; Bryant, G. W.; García De Abajo, F. J. *Opt. Exp.* **2006**, *14*, 9988.
(150) Troparevsky, M. C.; Zhao, K.; Xiao, D.; Eguiluz, A. G.; Zhang, Z. *Phys. Rev. B* **2010**, *82*, No. 045413.
(151) García de Abajo, F. J. *J. Phys. Chem. C* **2008**, *112*, 17983.
(152) Glass, A. M.; Liao, P. F.; Bergman, J. G.; Olson, D. H. *Opt. Lett.* **1980**, *5*, 368.

(153) Garoff, S.; Weitz, D. A.; Gramila, T. J.; Hanson, C. D. *Opt. Lett.* **1981**, *6*, 245.
(154) Mie, G. *Ann. Phys.* **1908**, *25*, 377.
(155) Craighead, H. G.; Glass, A. M. *Opt. Lett.* **1981**, *6*, 248.
(156) Garnett, J. C. M. *Phil. Trans. R. Soc. A* **1904**, *203*, 385.
(157) Tabarin, T.; Kulesza, A.; Antoine, R.; Mitrić, R.; Broyer, M.; Dugourd, P.; Bonačić-Koutecký, V. *Phys. Rev. Lett.* **2008**, *101*, No. 213001.
(158) Kulesza, A.; Mitrić, R.; Bonačić-Koutecký, V. *J. Phys. Chem. A* **2009**, *113*, 3783.
(159) Corni, S.; Tomasi, J. *J. Chem. Phys.* **2001**, *114*, 3739.
(160) Morton, S. M.; Jensen, L. *J. Chem. Phys.* **2010**, *133*, No. 074103.
(161) Jensen, L.; Åstrand, P.-O.; Mikkelsen, K. V. *Int. J. Quantum Chem.* **2001**, *84*, 513.
(162) Arcisauskaite, V.; Kongsted, J.; Hansen, T.; Mikkelsen, K. V. *Chem. Phys. Lett.* **2009**, *470*, 285.
(163) Yanai, T.; Tew, D. P.; Handy, N. C. *Chem. Phys. Lett.* **2004**, *393*, 51.
(164) Jörgensen, S.; Ratner, M. A.; Mikkelsen, K. V. *J. Chem. Phys.* **2001**, *115*, 3792.
(165) Lopata, K.; Neuhauser, D. *J. Chem. Phys.* **2009**, *130*, No. 104707.
(166) Masiello, D. J.; Schatz, G. C. *J. Chem. Phys.* **2010**, *132*, No. 064102.
(167) Corni, S.; Tomasi, J. *J. Chem. Phys.* **2002**, *117*, 7266.
(168) Chen, H.; McMahon, J. M.; Ratner, M. A.; Schatz, G. C. *J. Phys. Chem. C* **2010**, *114*, 14384.
(169) Hartstein, A.; Kirtley, J. R.; Tsang, J. C. *Phys. Rev. Lett.* **1980**, *45*, 201.
(170) Osawa,M. In *Near-Field Optics and Surface Plasmon Polaritons*; Kawata, S., Ed.; Springer: Berlin/Heidelberg, 2001; Vol. 81, Chapter Surface-Enhanced Infrared Absorption, pp 163−187.
(171) Kosower, E. M.; Markovich, G.; Raichlin, Y.; Borz, G.; Katzir, A. *J. Phys. Chem. B* **2004**, *108*, 12633.
(172) Anderson, M. S. *Appl. Phys. Lett.* **2003**, *83*, 2964.
(173) Xue, X.-K.; Wang, J.-Y.; Li, Q.-X.; Yan, Y.-G.; Liu, J.-H.; Cai, W.-B. *Anal. Chem.* **2008**, *80*, 166.
(174) Nishikawa, Y.; Fujiwara, K.; Ataka, K.; Osawa, M. *Anal. Chem.* **1993**, *65*, 556.
(175) Ataka, K.; Heberle, J. *J. Am. Chem. Soc.* **2003**, *125*, 4986.
(176) Holman, H. Y. N.; Perry, D. L.; Hunter-Cevera, J. C. *J. Microbiol. Methods* **1998**, *34*, 59.
(177) Seelenbinder, J. A.; Brown, C. W.; Pivarnik, P.; Rand, A. G. *Anal. Chem.* **1999**, *71*, 1963.
(178) Rima, F. R.; Nakata, K.; Shimazu, K.; Osawa, M. *J. Phys. Chem. C* **2010**, *114*, 6011.
(179) Krauth, O.; Fahsold, G.; Pucci, A. *J. Chem. Phys.* **1999**, *110*, 3113.
(180) Krauth, O.; Fahsold, G.; Magg, N.; Pucci, A. *J. Chem. Phys.* **2000**, *113*, 6330.
(181) Kundu, J.; Le, F.; Nordlander, P.; Halas, N. J. *Chem. Phys. Lett.* **2008**, *452*, 115.
(182) Priebe, A.; Sinther, M.; Fahsold, G.; Pucci, A. *J. Chem. Phys.* **2003**, *119*, 4887.
(183) Heaps, D. A.; Griffiths, P. R. *Vib. Spectrosc.* **2006**, *41*, 221.
(184) Heaps, D. A.; Griffiths, P. R. *Vib. Spectrosc.* **2006**, *42*, 45.
(185) Krauth, O.; Fahsold, G.; Lehmann, A. *Surf. Sci.* **1999**, *433*−*435*, 79.
(186) Fano, U. *Phys. Rev.* **1961**, *124*, 1866.
(187) Langreth, D. C. *Phys. Rev. Lett.* **1985**, *54*, 126.
(188) Zhang, Z. Y.; Langreth, D. C. *Phys. Rev. B* **1989**, *39*, 10028.
(189) Persson, B. N. J.; Ryberg, R. *Phys. Rev. B* **1981**, *24*, 6954.
(190) Corni, S.; Tomasi, J. In *Surface-Enhanced Raman Scattering: Physics and Applications*; Kneipp, K., Kneipp, H., Moskovits, M., Eds.; Springer Berlin/Heidelberg, 2006; Vol. 103, Chapter Studying SERS from Metal Nanoparticles and Nanoparticles Aggregates with Continuum Models, pp 105−124.
(191) Osawa, M.; Ikeda, M. *J. Phys. Chem.* **1991**, *95*, 9914.
(192) Drexhage, K. H., IV . In *Progress in Optics*; Wolf, E., Ed.; Elsevier: Amsterdam, Netherlands, 1974; Vol. 12, pp 163−192, 192a, 193−232.
(193) Fort, E.; Grésillon, S. *J. Phys. D: Appl. Phys.* **2008**, *41*, No. 013001.
(194) Aslan, K.; Gryczynski, I.; Malicka, J.; Matveeva, E.; Lakowicz, J. R.; Geddes, C. D. *Curr. Opin. Biotechnol.* **2005**, *16*, 55Analytical biotechnology.
(195) Lakowicz, J. R.; Geddes, C. D.; Gryczynski, I.; Malicka, J.; Gryczynski, Z.; Aslan, K.; Lukomska, J.; Matveeva, E.; Zhang, J.; Badugu, R.; Huang, J. *J. Fluoresc.* **2004**, *14*, 425.
(196) Lakowicz, J. R.; Shen, Y.; D'Auria, S.; Malicka, J.; Fang, J.; Gryczynski, Z.; Gryczynski, I. *Anal. Biochem.* **2002**, *301*, 261.
(197) Lakowicz, J. R. *Anal. Biochem.* **2004**, *324*, 153.
(198) Gryczynski, I.; Malicka, J.; Gryczynski, Z.; Lakowicz, J. R. *Anal. Biochem.* **2004**, *324*, 170.
(199) Lakowicz, J. R. *Anal. Biochem.* **2005**, *337*, 171.
(200) Geddes, C. D.; Lakowicz, J. R. *J. Fluoresc.* **2002**, *12*, 121.
(201) Knoll, W.; Yu, F.; Neumann, T.; Niu, L.; Schmid, E. L. In *Radiative Decay Engineering*; Lakowicz, J. R., Geddes, C. D., Eds.; Springer US: New York, 2005; Vol. 8, Chapter 10, pp 305−332.
(202) Geddes, C. D.; Asian, K.; Gryczynski, I.; Malicka, J.; Lakowicz, J. R. In *Radiative Decay Engineering*; Lakowicz, J. R., Geddes, C. D., Eds.; Springer US: New York, 2005; Vol. 8, Chapter 14, pp 405−448.
(203) Gersten, J. I. In *Radiative Decay Engineering*; Lakowicz, J. R., Geddes, C. D., Eds.; Springer US: New York, 2005; Vol. 8, Chapter 14, pp 197−221.
(204) Goulet, P. J. G.; Aroca, R. F. In *Radiative Decay Engineering*; Lakowicz, J. R., Geddes, C. D., Eds.; Springer US: New York, 2005; Vol. 8, Chapter 14, pp 223−247.
(205) Gryczynski, I.; Malicka, J.; Gryczynski, Z.; Lakowicz, J. R. In *Radiative Decay Engineering*; Lakowicz, J. R., Geddes, C. D., Eds.; Springer US: New York, 2005; Vol. 8, Chapter 13, pp 381−403.
(206) Lakowicz, J. R.; Shen, B.; Gryczynski, Z.; D'Auria, S.; Gryczynski, I. *Biochem. Biophys. Res. Commun.* **2001**, *286*, 875.
(207) Sokolov, K.; Chumanov, G.; Cotton, T. M. *Anal. Chem.* **1998**, *70*, 3898.
(208) Attridge, J.; Daniels, P.; Deacon, J.; Robinson, G.; Davidson, G. *Biosens. Bioelectron.* **1991**, *6*, 201.
(209) Dirac, P. A. M. *Proc. R. Soc. London A* **1927**, *114*, 243.
(210) Fermi, E. *Rev. Mod. Phys.* **1932**, *4*, 87.
(211) Weitz, D. A.; Garoff, S.; Gersten, J. I.; Nitzan, A. *J. Chem. Phys.* **1983**, *78*, 5324.
(212) Okamoto, K.; Niki, I.; Shvartser, A.; Narukawa, Y.; Mukai, T.; Scherer, A. *Nat. Mater.* **2004**, *3*, 601.
(213) Gontijo, I.; Boroditsky, M.; Yablonovitch, E.; Keller, S.; Mishra, U. K.; DenBaars, S. P. *Phys. Rev. B* **1999**, *60*, 11564.
(214) Amos, R. M.; Barnes, W. L. *Phys. Rev. B* **1997**, *55*, 7249.
(215) Purcell, E. M. *Phys. Rev.* **1946**, *69*, 681.
(216) Garoff, S.; Weitz, D. A.; Alvarez, M. S.; Gersten, J. I. *J. Chem. Phys.* **1984**, *81*, 5189.
(217) Enderlein, J. *Chem. Phys.* **1999**, *247*, 1.
(218) Enderlein, J. *Biophys. J.* **2000**, *78*, 2151.
(219) Chance, R. R.; Miller, A. H.; Prock, A.; Silbey, R. *J. Chem. Phys.* **1975**, *63*, 1589.
(220) Morawitz, H. *Phys. Rev.* **1969**, *187*, 1792.
(221) Morawitz, H.; Philpott, M. R. *Phys. Rev. B* **1974**, *10*, 4863.
(222) Philpott, M. R. *J. Chem. Phys.* **1975**, *62*, 1812.
(223) Kuhn, H. *J. Chem. Phys.* **1970**, *53*, 101.
(224) Tews, K. H. *Ann. Phys.* **1973**, *29*, 97.
(225) Chance, R. R.; Prock, A.; Silbey, R. *J. Chem. Phys.* **1975**, *62*, 2245.
(226) Chance, R. R.; Prock, A.; Silbey, R. *J. Chem. Phys.* **1974**, *60*, 2744.
(227) Chance, R. R.; Prock, A.; Silbey, R. *J. Chem. Phys.* **1974**, *60*, 2184.
(228) Chance, R. R.; Prock, A.; Silbey, R. In *Advances in Chemical Physics*; I. Prigogine, S. A. R., Ed.; John Wiley & Sons, Inc.: Hoboken, NJ, 1978; Vol. 37, Chapter 1, pp 1−65.

(229) Xu, H.; Wang, X.-H.; Persson, M. P.; Xu, H. Q.; Käll, M.; Johansson, P. *Phys. Rev. Lett.* **2004**, *93*, No. 243002.
(230) Rahmani, A.; Chaumet, P. C.; de Fornel, F. *Phys. Rev. A* **2001**, *63*, No. 023819.
(231) Gersten, J. I.; Nitzan, A. *Surf. Sci.* **1985**, *158*, 165.
(232) Muñoz Losa, A.; Vukovic, S.; Corni, S.; Mennucci, B. *J. Phys. Chem. C* **2009**, *113*, 16364.
(233) Persson, B. N. J. *J. Phys. C: Solid State Phys.* **1978**, *11*, 4251.
(234) Anger, P.; Bharadwaj, P.; Novotny, L. *Phys. Rev. Lett.* **2006**, *96*, No. 113002.
(235) Persson, B. N. J.; Zaremba, E. *Phys. Rev. B* **1985**, *31*, 1863.
(236) Persson, B. N. J.; Lang, N. D. *Phys. Rev. B* **1982**, *26*, 5409.
(237) Avouris, P.; Persson, B. N. J. *J. Phys. Chem.* **1984**, *88*, 837.
(238) Li, X.; Tully, J. C. *Chem. Phys. Lett.* **2007**, *439*, 199.
(239) Pettinger, B. *J. Chem. Phys.* **1986**, *85*, 7442.
(240) Pettinger, B. *Chem. Phys. Lett.* **1984**, *110*, 576.
(241) Johansson, P.; Xu, H.; Käll, M. *Phys. Rev. B* **2005**, *72*, No. 035427.
(242) Nie, S. M.; Emory, S. R. *Science* **1997**, *275*, 1102.
(243) Caricato, M.; Andreussi, O.; Corni, S. *J. Phys. Chem. B* **2006**, *110*, 16652PMID: 16913802.
(244) Corni, S.; Tomasi, J. *J. Chem. Phys.* **2003**, *118*, 6481.
(245) Andreussi, O.; Corni, S.; Mennucci, B.; Tomasi, J. *J. Chem. Phys.* **2004**, *121*, 10190.
(246) Sánchez-González, A.; Muñoz Losa, A.; Vukovic, S.; Corni, S.; Mennucci, B. *J. Phys. Chem. C* **2010**, *114*, 1553.
(247) Vukovic, S.; Corni, S.; Mennucci, B. *J. Phys. Chem. C* **2009**, *113*, 121.
(248) Corni, S.; Cappelli, C.; Cammi, R.; Tomasi, J. *J. Phys. Chem. A* **2001**, *105*, 8310.
(249) Tomasi, J.; Mennucci, B.; Cammi, R. *Chem. Rev.* **2005**, *105*, 2999.
(250) Chowdhury, M. H.; Pond, J.; Gray, S. K.; Lakowicz, J. R. *J. Phys. Chem. C* **2008**, *112*, 11236.
(251) Kneipp, K.; Wang, Y.; Kneipp, H.; Perelman, L. T.; Itzkan, I.; Dasari, R. R.; Feld, M. S. *Phys. Rev. Lett.* **1997**, *78*, 1667.
(252) Xu, H.; Bjerneld, E. J.; Käll, M.; Börjesson, L. *Phys. Rev. Lett.* **1999**, *83*, 4357.
(253) Michaels, A. M.; Nirmal, M.; Brus, L. E. *J. Am. Chem. Soc.* **1999**, *121*, 9932.
(254) Dieringer, J. A.; Lettan, R. B.; Scheidt, K. A.; Van Duyne, R. P. *J. Am. Chem. Soc.* **2007**, *129*, 16249.
(255) *Visualizing Chemistry: The Progress and Promise of Advanced Chemical Imaging*; Committee on Revealing Chemistry through Advanced Chemical Imaging, Board on Chemical Sciences and Technology, Division on Earth and Life Studies, National Research Council: Washington, D.C., 2006.
(256) Kneipp, K.; Kneipp, H.; Kartha, V. B.; Manoharan, R.; Deinum, G.; Itzkan, I.; Dasari, R. R.; Feld, M. S. *Phys. Rev. E* **1998**, *57*, R6284.
(257) Bell, S. E. J.; Sirimuthu, N. M. S. *J. Am. Chem. Soc.* **2006**, *128*, 15580.
(258) Barhoumi, A.; Zhang, D.; Tam, F.; Halas, N. J. *J. Am. Chem. Soc.* **2008**, *130*, 5523.
(259) Kneipp, K.; Haka, A. S.; Kneipp, H.; Badizadegan, K.; Yoshizawa, N.; Boone, C.; Shafer-Peltier, K. E.; Motz, J. T.; Dasari, R. R.; Feld, M. S. *Appl. Spectrosc.* **2002**, *56*, 150.
(260) Sylvia, J. M.; Janni, J. A.; Klein, J. D.; Spencer, K. M. *Anal. Chem.* **2000**, *72*, 5834.
(261) Zhang, X. Y.; Young, M. A.; Lyandres, O.; Van Duyne, R. P. *J. Am. Chem. Soc.* **2005**, *127*, 4484.
(262) Zhang, X. Y.; Zhao, J.; Whitney, A. V.; Elam, J. W.; Van Duyne, R. P. *J. Am. Chem. Soc.* **2006**, *128*, 10304.
(263) Stuart, D. A.; Biggs, K. B.; Van Duyne, R. P. *The Analyst* **2006**, *131*, 568.
(264) Yan, F.; Vo-Dinh, T. *Sens. Actuators B* **2007**, *121*, 61.
(265) Pearman, W. F.; Fountain, A. W. *Appl. Spectrosc.* **2006**, *60*, 356.
(266) *Nanophotonics Accessibility and Applicability*; Committee on Nanophotonics Accessibility and Applicability, Division on Engineering and Physical Sciences, National Research Council: Washington, D.C., 2008.
(267) Ko, H.; Chang, S.; Tsukruk, V. V. *ACS Nano* **2009**, *3*, 181.
(268) Shafer-Peltier, K. E.; Haynes, C. L.; Glucksberg, M. R.; Duyne, R. P. V. *J. Am. Chem. Soc.* **2003**, *125*, 588.
(269) Camden, J. P.; Dieringer, J. A.; Zhao, J.; Van Duyne, R. P. *Acc. Chem. Res.* **2008**, *41*, 1653.
(270) Lyandres, O.; Yuen, J. M.; Shah, N. C.; VanDuyne, R. P.; Walsh, J. T.; Glucksberg, M. R. *Diabetes Technol. Ther.* **2008**, *10*, 257.
(271) Lau, D.; Livett, M.; Prawer, S. *J. Raman Spectrosc.* **2008**, *39*, 545.
(272) Van Elslande, E.; Lecomte, S.; Le Hõ, A.-S. *J. Raman Spectrosc.* **2008**, *39*, 1001.
(273) Brosseau, C. L.; Rayner, K. S.; Casadio, F.; Grzywacz, C. M.; Van Duyne, R. P. *Anal. Chem.* **2009**, *81*, 7443.
(274) Cottingham, K. *Anal. Chem.* **2009**, *81*, 7128.
(275) Chen, K.; Vo-Dinh, K.-C.; Yan, F.; Wabuyele, M. B.; Vo-Dinh, T. *Anal. Chim. Acta.* **2006**, *569*, 234.
(276) Wustholz, K. L.; Brosseau, C. L.; Casadio, F.; Van Duyne, R. P. *Phys. Chem. Chem. Phys.* **2009**, *11*, 7350.
(277) Jurasekova, Z.; del Puerto, E.; Bruno, G.; García-Ramos, J. V.; Sanchez-Cortes, S.; Domingo, C. *J. Raman Spectrosc.* **2010**, *41*, 1455.
(278) Casadio, F.; Leona, M.; Lombardi, J. R.; Van Duyne, R. *Acc. Chem. Res.* **2010**, *43*, 782.
(279) Fleischman, M.; Hendra, P. J.; McQuillan, A. J. *Chem. Phys. Lett.* **1974**, *26*, 163.
(280) Jeanmaire, D. L.; Van Duyne, R. P. *J. Electroanal. Chem.* **1977**, *84*, 1.
(281) Albrecht, M. G.; Crieghton, J. A. *J. Am. Chem. Soc.* **1977**, *99*, 5215.
(282) Anker, J. N.; Hall, W. P.; Lyandres, O.; Shah, N. C.; Zhao, J.; Van Duyne, R. P. *Nat. Mater.* **2008**, *7*, 442.
(283) Prodan, E.; Radloff, C.; Halas, N. J.; Nordlander, P. *Science* **2003**, *302*, 419.
(284) Wang, H.; Brandl, D. W.; Nordlander, P.; Halas, N. J. *Acc. Chem. Res.* **2007**, *40*, 53.
(285) Kneipp, J.; Kneipp, H.; Kneipp, K. *Chem. Soc. Rev.* **2008**, *37*, 1052.
(286) Blackie, E. J.; Ru, E. C. L.; Etchegoin, P. G. *J. Am. Chem. Soc.* **2009**, *131*, 14466.
(287) Etchegoin, P. G.; Le Ru, E. C.; Meyer, M. *J. Am. Chem. Soc.* **2009**, *131*, 2713.
(288) Park, W.-H.; Kim, Z. H. *Nano Lett.* **2010**, *10*, 4040.
(289) Stranahan, S. M.; Willets, K. A. *Nano Lett.* **2010**, *10*, 3777.
(290) Cañamares, M. V.; Chenal, C.; Birke, R. L.; Lombardi, J. R. *J. Phys. Chem. C* **2008**, *112*, 20295.
(291) Etchegoin, P. G.; Ru, E. C. L. *Phys. Chem. Chem. Phys.* **2008**, *10*, 6079.
(292) Fang, Y.; Seong, N.-H.; Dlott, D. D. *Science* **2008**, *321*, 388.
(293) Udagawa, M.; Chou, C.-C.; Hemminger, J. C.; Ushioda, S. *Phys. Rev. B* **1981**, *23*, 6843.
(294) Laor, U.; Schatz, G. C. *Chem. Phys. Lett.* **1981**, *82*, 566.
(295) DiLella, D. P.; Gohin, A.; Lipson, R. H.; McBreen, P.; Moskovits, M. *J. Chem. Phys.* **1980**, *73*, 4282.
(296) Gersten, J.; Nitzan, A. *J. Chem. Phys.* **1980**, *73*, 3023.
(297) Gersten, J. I. *J. Chem. Phys.* **1980**, *72*, 5779.
(298) Otto, A.; Timper, J.; Billmann, J.; Kovacs, G.; Pockrand, I. *Surf. Sci.* **1980**, *92*, L55.
(299) Otto, A. *Surf. Sci.* **1980**, *92*, 145.
(300) Billmann, J.; Kovacs, G.; Otto, A. *Surf. Sci.* **1980**, *92*, 153.
(301) Schatz, G. C.; Van Duyne, R. P. *Surf. Sci.* **1980**, *101*, 425.
(302) Otto, A.; Timper, J.; Billmann, J.; Pockrand, I. *Phys. Rev. Lett.* **1980**, *45*, 46.
(303) Birke, R. L.; Lombardi, J. R.; Gersten, J. I. *Phys. Rev. Lett.* **1979**, *43*, 71.
(304) Burstein, E.; Chen, Y. J.; Chen, C. Y.; Lundquist, S.; Tosatti, E. *Solid State Commun.* **1979**, *29*, 567.
(305) Tsang, J. C.; Kirtley, J. R.; Bradley, J. A. *Phys. Rev. Lett.* **1979**, *43*, 772.

(306) Moskovits, M. *Solid State Commun.* **1979**, *32*, 59.
(307) Hexter, R. M.; Albrecht, M. G. *Spectrochim. Acta A* **1979**, *35*, 233.
(308) Gersten, J. I.; Birke, R. L.; Lombardi, J. R. *Phys. Rev. Lett.* **1979**, *43*, 147.
(309) Moskovits, M. *J. Chem. Phys.* **1978**, *69*, 4159.
(310) Otto, A. *Surf. Sci.* **1978**, *75*, L392.
(311) Van Duyne, R. P. In *Chemical and Biochemical Applications of Lasers*; Moore, B. C., Ed.; Acedemic Press, Inc.: Burlington, MA, 1979; Vol. 4, pp 101−184.
(312) Haynes, C. L.; Yonzon, C. R.; Zhang, X.; Van Duyne, R. P. *J. Raman Spectrosc.* **2005**, *36*, 471.
(313) McQuillan, A. J. *Notes Rec. R. Soc.* **2009**, *63*, 105.
(314) King, F. W.; Duyne, R. P. V.; Schatz, G. C. *J. Chem. Phys.* **1978**, *69*, 4472.
(315) Billmann, J.; Otto, A. *Solid State Commun.* **1982**, *44*, 105.
(316) Billmann, J.; Otto, A. *Anal. Chim. Acta.* **1980**, *6*, 356.
(317) Pettenkofer, C.; Eickmans, J.; Ertürk, U.; Otto, A. *Surf. Sci.* **1985**, *151*, 9.
(318) Otto, A.; Billmann, J.; Eickmans, J.; Ertürk, U.; Pettenkofer, C. *Surf. Sci.* **1984**, *138*, 319.
(319) Tian, Z.-Q.; Ren, B.; Wu, D.-Y. *J. Phys. Chem. B* **2002**, *106*, 9463.
(320) Schatz, G. C. *Acc. Chem. Res.* **1984**, *17*, 370.
(321) McCall, S.; Platzman, P.; Wolff, P. *Phys. Lett. A* **1980**, *77*, 381.
(322) McCall, S. L.; Platzman, P. M. *Phys. Rev. B* **1980**, *22*, 1660.
(323) Zeman, E. J.; Schatz, G. C. *J. Phys. Chem.* **1987**, *91*, 634.
(324) Lombardi, J. R.; Birke, R. L.; Lu, T.; Xu, J. *J. Chem. Phys.* **1986**, *84*, 4174.
(325) Adrian, F. J. *J. Chem. Phys.* **1982**, *77*, 5302.
(326) Otto, A. *Anal. Chim. Acta.* **1980**, *6*, 309.
(327) Otto, A.; Mrozek, I.; Grabhorn, H.; Akemann, W. *J. Phys.: Condens. Matter* **1992**, *4*, 1143.
(328) Hao, E.; Schatz, G. C. *J. Chem. Phys.* **2004**, *120*, 357.
(329) Moskovits, M. In *Surface-Enhanced Raman Scattering - Physics and Applications*; Kneipp, K., Moskovits, M., Kneipp, H., Eds.; Springer-Verlag Berlin: Heidelberg, Germany, 2006; Vol. 103, Chapter 1, pp 1−18.
(330) Schatz, G. C.; Young, M. A.; Van Duyne, R. P. In *Topics in Applied Physics*; Kneipp, K., Moskovits, M., Kneipp, H., Eds.; Springer-Verlag: Berlin, Heidelberg, 2006; Vol. 103, pp 19−46.
(331) Zou, S.; Schatz, G. C. In *Surface-Enhanced Raman Scattering - Physics and Applications*; Kneipp, K., Moskovits, M., Kneipp, H., Eds.; Springer-Verlag Berlin: Heidelberg, Germany, 2006; Vol. 103, Chapter 4, pp 67−87.
(332) Moskovits, M. *J. Raman Spectrosc.* **2005**, *36*, 485.
(333) Lombardi, J. R.; Birke, R. L. *Acc. Chem. Res.* **2009**, *42*, 734.
(334) Otto, A.; Lust, M.; Pucci, A.; Meyer, G. *Can. J. Anal. Sci. Spectrosc.* **2007**, *52*, 150.
(335) Otto, A. *J. Raman Spectrosc.* **2005**, *36*, 497.
(336) Rycenga, M.; Kim, M. H.; Camargo, P. H. C.; Cobley, C.; Li, Z.-Y.; Xia, Y. *J. Phys. Chem. A* **2009**, *113*, 3932.
(337) Le Ru, E. C.; Etchegoin, P. G. *Chem. Phys. Lett.* **2006**, *423*, 63.
(338) Kedziora, G. S.; Schatz, G. C. *Spectrochim. Acta A* **1999**, *55*, 625.
(339) Maniv, T.; Metiu, H. *J. Chem. Phys.* **1980**, *72*, 1996.
(340) Maniv, T.; Metiu, H. *Surf. Sci.* **1980**, *101*, 399.
(341) Maniv, T.; Metiu, H. *Chem. Phys. Lett.* **1981**, *79*, 79.
(342) Pandey, P. K.; Schatz, G. C. *Chem. Phys. Lett.* **1982**, *88*, 193.
(343) Pandey, P. K.; Schatz, G. C. *Chem. Phys. Lett.* **1982**, *91*, 286.
(344) Nakai, H.; Nakatsuji, H. *J. Chem. Phys.* **1995**, *103*, 2286.
(345) Pustovit, V. N.; Shahbazyan, T. V. *Phys. Rev. B* **2006**, *73*, No. 085408.
(346) McFarland, A. D.; Young, M. A.; Dieringer, J. A.; Van Duyne, R. P. *J. Phys. Chem. B* **2005**, *109*, 11279.
(347) Franzen, S. *J. Phys. Chem. C* **2009**, *113*, 5912.
(348) Furtak, T.; Roy, D. *Surf. Sci.* **1985**, *158*, 126.
(349) Jiang, X. D.; Campion, A. *Chem. Phys. Lett.* **1987**, *140*, 95.
(350) Otto, A.; Futamata, M. In *Electronic Mechanisms of SERS*; Kneipp, K., Moskovits, M., Kneipp, H., Eds.; Springer-Verlag: Berlin, Heidelberg, Germany, 2006; Vol. 103, Chapter 8, pp 147−184.
(351) Fromm, D. P.; Sundaramurthy, A.; Kinkhabwala, A.; Schuck, P. J.; Kino, G. S.; Moerne, W. E. *J. Chem. Phys.* **2006**, *124*, No. 061101.
(352) Hildebrandt, P.; Stockburger, M. *J. Phys. Chem.* **1984**, *88*, 5935.
(353) Pettinger, B.; Krischer, K.; Ertl, G. *Chem. Phys. Lett.* **1988**, *151*, 151.
(354) Jensen, L.; Zhao, L. L.; Autschbach, J.; Schatz, G. C. *J. Chem. Phys.* **2005**, *123*, No. 174110.
(355) Pettinger, B.; Gerolymatou, A. *Surf. Sci.* **1985**, *156*, 859.
(356) Pettinger, B.; Gerolymatou, A. *Ber. Bunsen-Ges. Phys. Chem.* **1984**, *88*, 359.
(357) Liang, E.; Kiefer, W. *J. Raman Spectrosc.* **1996**, *27*, 879.
(358) Yoon, J. H.; Park, J. S.; Yoon, S. *Langmuir* **2009**, *25*, 12475PMID: 19817481.
(359) Nikoobakht, B.; Wang, J.; El-Sayed, M. A. *Chem. Phys. Lett.* **2002**, *366*, 17.
(360) Arenas, J. F.; Soto, J.; Pelaez, D.; Fernandez, D. J.; Otero, J. C. *Int. J. Quantum Chem.* **2005**, *104*, 681.
(361) Persson, B. *Chem. Phys. Lett.* **1981**, *82*, 561.
(362) Arenas, J. F.; Woolley, M. S.; Lopez-Tocon, I.; Otero, J. C.; Marcos, J. I. *J. Chem. Phys.* **2000**, *112*, 7669.
(363) Albrecht, A. C. *J. Chem. Phys.* **1961**, *34*, 1476.
(364) Albrecht, A. C. *J. Chem. Phys.* **1960**, *33*, 156.
(365) Lopez-Ramirez, M. R.; Ruano, C.; Castro, J. L.; Arenas, J. F.; Soto, J.; Otero, J. C. *J. Phys. Chem. C* **2010**, *114*, 7666.
(366) Avila, F.; Soto, J.; Arenas, J. F.; Rodríguez, J. A.; Peláez, D.; Otero, J. C. *J. Phys. Chem. C* **2009**, *113*, 105.
(367) Centeno, S.; Lopez-Tocon, I.; Arenas, J.; Soto, J.; Otero, J. *J. Phys. Chem. B* **2006**, *110*, 14916.
(368) Arenas, J. F.; Fernández, D. J.; Soto, J.; López-Tocón, I.; Otero, J. C. *J. Phys. Chem. B* **2003**, *107*, 13143.
(369) Arenas, J. F.; Soto, J.; Tocón, I. L.; Fernández, D. J.; Otero, J. C.; Marcos, J. I. *J. Chem. Phys.* **2002**, *116*, 7207.
(370) Arenas, J. F.; Woolley, M. S.; Otero, J. C.; Marcos, J. I. *J. Phys. Chem.* **1996**, *100*, 3199.
(371) Lombardi, J. R.; Birke, R. L. *J. Chem. Phys.* **2007**, *126*, No. 244709.
(372) Chenal, C.; Birke, R. L.; Lombardi, J. R. *ChemPhysChem* **2008**, *9*, 1617.
(373) Birke, R. L.; Znamenskiy, V.; Lombardi, J. R. *J. Chem. Phys.* **2010**, *132*, No. 214707.
(374) Peticolas, W. L.; Strommen, D. P.; Lakshminarayanan, V. *J. Chem. Phys.* **1980**, *73*, 4185.
(375) Sun, M.; Wan, S.; Liu, Y.; Jia, Y.; Xu, H. *J. Raman Spectrosc.* **2008**, *39*, 402.
(376) Liu, S.; Wan, S.; Chen, M.; Sun, M. *J. Raman Spectrosc.* **2008**, *39*, 1170.
(377) Liu, S.; Zhao, X.; Li, Y.; Chen, M.; Sun, M. *Spectrochim. Acta A* **2009**, *73*, 382.
(378) Sun, M.; Liu, S.; Li, Z.; Duan, J.; Chen, M.; Xu, H. *J. Raman Spectrosc.* **2009**, *40*, 1172.
(379) Sun, M.; Liu, S.; Chen, M.; Xu, H. *J. Raman Spectrosc.* **2009**, *40*, 137.
(380) Sun, M.; Li, Z.; Liu, Y.; Xu, H. *J. Raman Spectrosc.* **2009**, *40*, 1942.
(381) Dong, B.; Liu, L.; Xu, H.; Sun, M. *J. Raman Spectrosc.* **2010**, *41*, 719.
(382) Jensen, L.; Schatz, G. C. *J. Phys. Chem. A* **2006**, *110*, 5973.
(383) Kim, N.-J.; Lin, M.; Hu, Z.; Li, H. *Chem. Commun.* **2009**, 6246–6248.
(384) Maitani, M. M.; Ohlberg, D. A. A.; Li, Z. Y.; Allara, D. L.; Stewart, D. R.; Williams, R. S. *J. Am. Chem. Soc.* **2009**, *131*, 6310.
(385) Wu, D.-Y.; Ren, B.; Jiang, Y.-X.; Xu, X.; Tian, Z.-Q. *J. Phys. Chem. A* **2002**, *106*, 9042.
(386) Wu, D. Y.; Hayashi, M.; Lin, S. H.; Tian, Z. Q. *Spectrochim. Acta A* **2004**, *60*, 137.

(387) Wu, D.-Y.; Ren, B.; Tian, Z.-Q. *Isr. J. Chem.* **2006**, *46*, 317.
(388) Wu, D.-Y.; Duan, S.; Ren, B.; Tian, Z.-Q. *J. Raman Spectrosc.* **2005**, *36*, 533.
(389) Wu, D.-Y.; Liu, X.-M.; Duan, S.; Xu, X.; Ren, B.; Lin, S.-H.; Tian, Z.-Q. *J. Phys. Chem. C* **2008**, *112*, 4195.
(390) Vivoni, A.; Birke, R. L.; Foucault, R.; Lombardi, J. R. *J. Phys. Chem. B* **2003**, *107*, 5547.
(391) Cardini, G.; Muniz-Miranda, M. *J. Phys. Chem. B* **2002**, *106*, 6875.
(392) Muniz-Miranda, M.; Cardini, G.; Pagliai, M.; Schettino, V. *Chem. Phys. Lett.* **2007**, *436*, 179.
(393) Muniz-Miranda, M.; Cardini, G.; Schettino, V. *Theor. Chim. Acta* **2004**, *111*, 264.
(394) Johansson, P. *Phys. Chem. Chem. Phys.* **2005**, *7*, 475.
(395) Zhao, X.; Liu, S.; Li, Y.; Chen, M. *Spectrochim. Acta A* **2010**, *75*, 794.
(396) Morton, S. M.; Ewusi-Annan, E.; Jensen, L. *Phys. Chem. Chem. Phys.* **2009**, *11*, 7424.
(397) Saikin, S. K.; Olivares-Amaya, R.; Rappoport, D.; Stopa, M.; Aspuru-Guzik, A. *Phys. Chem. Chem. Phys.* **2009**, *11*, 9401.
(398) Morton, S. M.; Jensen, L. *J. Am. Chem. Soc.* **2009**, *131*, 4090.
(399) Zhao, L. L.; Jensen, L.; Schatz, G. C. *Nano Lett.* **2006**, *6*, 1229.
(400) Jensen, L.; Zhao, L. L.; Schatz, G. C. *J. Phys. Chem. C* **2007**, *111*, 4756.
(401) Lombardi, J. R.; Birke, R. L. *J. Phys. Chem. C* **2010**, *114*, 7812.
(402) Lombardi, J. R.; Birke, R. L. *J. Phys. Chem. C* **2008**, *112*, 5605.
(403) Masiello, D. J.; Schatz, G. C. *Phys. Rev. A* **2008**, *78*, No. 042505.
(404) Corni, S.; Tomasi, J. *Chem. Phys. Lett.* **2001**, *342*, 135.
(405) Corni, S.; Tomasi, J. *J. Chem. Phys.* **2002**, *116*, 1156.
(406) Barron, L. D. *Molecular Light Scattering and Optical Activity*, 2nd ed.; Cambridge University Press: Cambridge, U.K., 2004.
(407) Schaaff, T. G.; Knight, G.; Shafigullin, M. N.; Borkman, R. F.; Whetten, R. L. *J. Phys. Chem. B* **1998**, *102*, 10643.
(408) Schaaff, T.; Whetten, R. *J. Phys. Chem. B* **2000**, *104*, 2630.
(409) Thilgen, C.; Herrmann, A.; Diederich, F. *Angew. Chem., Int. Ed. Engl.* **1997**, *36*, 2268.
(410) Kessinger, R.; Crassous, J.; Herrmann, A.; Rüttimann, M.; Echegoyen, L.; Diederich, F. *Angew. Chem., Int. Ed. Engl.* **1998**, *37*, 1919.
(411) Newman, M. S.; Darlak, R. S.; Tsai, L. L. *J. Am. Chem. Soc.* **1967**, *89*, 6191.
(412) Yamada, K.-i.; Tanaka, H.; Nakagawa, H.; Ogashiwa, S.; Kawazura, H. *Bull. Chem. Soc Jpn.* **1982**, *55*, 500.
(413) Parks, E. K.; Kerns, K. P.; Riley, S. J. *J. Chem. Phys.* **1998**, *109*, 10207.
(414) Wetzel, T. L.; DePristo, A. E. *J. Chem. Phys.* **1996**, *105*, 572.
(415) Noguez, C.; Garzón, I. L. *Chem. Soc. Rev.* **2009**, *38*, 757.
(416) Kitaev, V. *J. Mater. Chem.* **2008**, *18*, 4745.
(417) Yao, H.; Miki, K.; Nishida, N.; Sasaki, A.; Kimura, K. *J. Am. Chem. Soc.* **2005**, *127*, 15536.
(418) Yao, H.; Fukui, T.; Kimura, K. *J. Phys. Chem. C* **2007**, *111*, 14968.
(419) Humblot, V.; Haq, S.; Muryn, C.; Hofer, W. A.; Raval, R. *J. Am. Chem. Soc.* **2002**, *124*, 503.
(420) Gautier, C.; Brgi, T. *J. Am. Chem. Soc.* **2006**, *128*, 11079.
(421) Tamura, M.; Fujihara, H. *J. Am. Chem. Soc.* **2003**, *125*, 15742.
(422) Yanagimoto, Y.; Negishi, Y.; Fujihara, H.; Tsukuda, T. *J. Phys. Chem. B* **2006**, *110*, 11611.
(423) López-Lozano, X.; Pérez, L. A.; Garzón, I. L. *Phys. Rev. Lett.* **2006**, *97*, No. 233401.
(424) Petty, J. T.; Zheng, J.; Hud, N. V.; Dickson, R. M. *J. Am. Chem. Soc.* **2004**, *126*, 5207.
(425) Shemer, G.; Krichevski, O.; Markovich, G.; Molotsky, T.; Lubitz, I.; Kotlyar, A. B. *J. Am. Chem. Soc.* **2006**, *128*, 11006.
(426) Garzón, I. L.; Artacho, E.; Beltrán, M. R.; García, A.; Junquera, J.; Michaelian, K.; Ordejón, P.; Rovira, C.; Sánchez-Portal, D.; Soler, J. M. *Nanotechnology* **2001**, *12*, 126.
(427) Häkkinen, H.; Moseler, M.; Kostko, O.; Morgner, N.; Hoffmann, M. A.; v. Issendorff, B. *Phys. Rev. Lett.* **2004**, *93*, No. 093401.
(428) Garzón, I. L.; Rovira, C.; Michaelian, K.; Beltrán, M. R.; Ordejón, P.; Junquera, J.; Sánchez-Portal, D.; Artacho, E.; Soler, J. M. *Phys. Rev. Lett.* **2000**, *85*, 5250.
(429) Román-Velázquez, C. E.; Noguez, C.; Garzón, I. L. *J. Phys. Chem. B* **2003**, *107*, 12035.
(430) Buda, A. B.; Mislow, K. *J. Am. Chem. Soc.* **1992**, *114*, 6006.
(431) Hidalgo, F.; Sánchez-Castillo, A.; Garzón, I. L.; Noguez, C. *Eur. Phys. J. D* **2009**, *52*, 179.
(432) Garzón, I. L.; Michaelian, K.; Beltrán, M. R.; Posada-Amarillas, A.; Ordejón, P.; Artacho, E.; Sánchez-Portal, D.; Soler, J. M. *Phys. Rev. Lett.* **1998**, *81*, 1600.
(433) Santizo, I. E.; Hidalgo, F.; Pérez, L. A.; Noguez, C.; Garzón, I. L. *J. Phys. Chem. C* **2008**, *112*, 17533.
(434) Lechtken, A.; Schooss, D.; Stairs, J.; Blom, M.; Furche, F.; Morgner, N.; Kostko, O.; von Issendorff, B.; Kappes, M. *Angew. Chem., Int. Ed.* **2007**, *46*, 2944.
(435) Gu, X.; Bulusu, S.; Li, X.; Zeng, X.; Li, J.; Gong, X.; Wang, L.-S. *J. Phys. Chem. C* **2007**, *111*, 8228.
(436) Car, R.; Parrinello, M. *Phys. Rev. Lett.* **1985**, *55*, 2471.
(437) Huang, W.; Ji, M.; Dong, C.-D.; Gu, X.; Wang, L.-M.; Gong, X. G.; Wang, L.-S. *ACS Nano* **2008**, *2*, 897.
(438) Pessoa, J. C.; Gajda, T.; Gillard, R. D.; Kiss, T.; Luz, S. M.; Moura, J. J. G.; Tomaz, I.; Telo, J. P.; Török, I. *J. Chem. Soc., Dalton Trans.* **1998**, 3587.
(439) Yasui, T.; Hidaka, J.; Shimura, Y. *Bull. Chem. Soc. Jpn.* **1966**, *39*, 2417.
(440) Goldsmith, M.-R.; George, C. B.; Zuber, G.; Naaman, R.; Waldeck, D. H.; Wipf, P.; Beratan, D. N. *Phys. Chem. Chem. Phys.* **2006**, *8*, 63.
(441) Lorenzo, M. O.; Baddeley, C. J.; Muryn, C.; Raval, R. *Nature* **2002**, *404*, 376.
(442) Hofer, W. A.; Humblot, V.; Raval, R. *Surf. Sci.* **2004**, *554*, 141.
(443) Gautier, C.; Bürgi, T. *Chem. Commun.* **2005**, 5393.
(444) Li, T.; Park, H. G.; Lee, H.-S.; Choi, S.-H. *Nanotechnology* **2003**, *125*, S660.
(445) Gautier, C.; Bürgi, T. *J. Am. Chem. Soc.* **2008**, *130*, 7077.
(446) Zhu, F. J.; Isaacs, N. W.; Hecht, L.; Barron, L. D. *Structure* **2005**, *13*, 1409.
(447) Zhu, F. J.; Isaacs, N. W.; Hecht, L.; Tranter, G. E.; Barron, L. D. *Chirality* **2006**, *18*, 103.
(448) Barron, L. D. *Curr. Opin. Struct. Biol.* **2006**, *16*, 638.
(449) Efrima, S. *Chem. Phys. Lett.* **1983**, *102*, 79.
(450) Efrima, S. *J. Chem. Phys.* **1985**, *83*, 1356.
(451) Hecht, L.; Barron, L. D. *Chem. Phys. Lett.* **1994**, *225*, 525.
(452) Hecht, L.; Barron, L. D. *J. Mol. Struct.* **1995**, *348*, 217.
(453) Kneipp, H.; Kneipp, J.; Kneipp, K. *Anal. Chem.* **2006**, *78*, 1363.
(454) Abdali, S. *J. Raman Spectrosc.* **2006**, *37*, 1341.
(455) Janesko, B. G.; Scuseria, G. E. *J. Chem. Phys.* **2006**, *125*, 124704.
(456) Abdali, S.; Johannessen, C.; Nygaard, J.; Nørbygaard, T. *J. Phys.: Condens. Matter* **2007**, *19*, No. 285205.
(457) Johannessen, C.; White, P. C.; Abdali, S. *J. Phys. Chem. A* **2007**, *111*, 7771.
(458) Abdali, S.; Blanch, E. W. *Chem. Soc. Rev.* **2008**, *37*, 980.
(459) Barron, L. D.; Hecht, L.; McColl, I. H.; Blanch, E. W. *Mol. Phys.* **2004**, *102*, 731.
(460) Nafie, L. A. *Annu. Rev. Phys. Chem.* **1997**, *48*, 357.
(461) Hug, W. In *Handbook of Vibrational Spectroscopy*; Chalmers, J. M., Griffiths, P. R., Eds.; JohnWiley and Sons, Ltd: Chichester, 2002; Vol. 1, pp 745−758.
(462) Bour, P. *J. Chem. Phys.* **2007**, *126*, No. 136101.
(463) Jensen, L. *J. Phys. Chem. A* **2009**, *113*, 4437.
(464) Janesko, B. G.; Scuseria, G. E. *J. Phys. Chem. C* **2009**, *113*, 9445.
(465) Acevedo, R.; Lombardini, R.; Halas, N. J.; Johnson, B. R. *J. Phys. Chem. A* **2009**, *113*, 13173.
(466) Lombardini, R.; Acevedo, R.; Halas, N. J.; Johnson, B. R. *J. Phys. Chem. C* **2010**, *114*, 7390.

(467) Jensen, L.; Autschbach, J.; Krykunov, M.; Schatz, G. C. *J. Chem. Phys.* **2007**, *127*, No. 134101.
(468) Novak, J. P.; Louis, C.; Brousseau, I.; Vance, F. W.; Johnson, R. C.; Lemon, B. I.; Hupp, J. T.; Feldheim, D. L. *J. Am. Chem. Soc.* **2000**, *122*, 12029.
(469) Li, J.; Guo, L.; Zhang, L.; Yu, C.; Yu, L.; Jiang, P.; Wei, C.; Qin, F.; Shi, J. *Dalton Trans.* **2009**, 823.
(470) Ramakrishna, G.; Varnavskit, O.; Kim, J.; Lee, D.; Goodson, T. *J. Am. Chem. Soc.* **2008**, *130*, 5032.
(471) Amendola, V.; Dini, D.; Polizzi, S.; Shen, J.; Kadish, K. M.; Calvete, M. J. F.; Hanack, M.; Meneghetti, M. *J. Phys. Chem. C* **2009**, *113*, 8688.
(472) Shalaev, V. M. *Phys. Rep.* **1996**, *272*, 61.
(473) Shalaev, V. M.; Poliakov, E. Y.; Markel, V. A. *Phys. Rev. B* **1996**, *53*, 2437.
(474) Zhang, X.; Stroud, D. *Phys. Rev. B* **1994**, *49*, 944.
(475) Rinkevicius, Z.; Autschbach, J.; Baev, A.; Swihart, M.; Ågren, H.; Prasad, P. N. *J. Phys. Chem. A* **2010**, *114*, 7590.
(476) Perdew, J. P.; Burke, K.; Ernzerhof, M. *Phys. Rev. Lett.* **1996**, *77*, 3865.
(477) Day, P. N.; Nguyen, K. A.; Pachter, R. *J. Chem. Theor. Comput.* **2010**, *6*, 2809.
(478) Brehm, G.; Sauer, G.; Fritz, N.; Schneider, S.; Zaitsev, S. *J. Mol. Struct.* **2005**, *735*−*736*, 85.
(479) Johnson, C. K.; Soper, S. A. *J. Phys. Chem.* **1989**, *93*, 7281.
(480) Kneipp, H.; Kneipp, K.; Seifert, F. *Chem. Phys. Lett.* **1993**, *212*, 374.
(481) Kneipp, K.; Kneipp, H.; Seifert, F. *Chem. Phys. Lett.* **1995**, *233*, 519.
(482) Leng, W.; Kelley, A. M. *J. Am. Chem. Soc.* **2006**, *128*, 3492.
(483) Li, W.-H.; Li, X.-Y.; Yu, N.-T. *Chem. Phys. Lett.* **1999**, *305*, 303.
(484) Li, W.-H.; Li, X.-Y.; Yu, N.-T. *Chem. Phys. Lett.* **1999**, *312*, 28.
(485) Nie, S.; Lipscomb, L. A.; Feng, S.; Yu, N.-T. *Chem. Phys. Lett.* **1990**, *167*, 35.
(486) Palonpon, A.; Ichimura, T.; Verma, P.; Inouye, Y.; Kawata, S. *J. Raman Spectrosc.* **2009**, *40*, 119.
(487) Yu, N.-T.; Nie, S.; Lipscomb, L. A. *J. Raman Spectrosc.* **2005**, *21*, 797.
(488) Hulteen, J. C.; Young, M. A.; Duyne, R. P. V. *Langmuir* **2006**, *22*, 10354.
(489) Kneipp, J.; Kneipp, H.; Wittig, B.; Kneipp, K. *Nano Lett.* **2007**, *7*, 2819.
(490) Kneipp, J.; Kneipp, H.; Kneipp, K. *Proc. Natl. Acad. Sci. U.S.A.* **2006**, *103*, 17149.
(491) Baranov, A. V.; Bobovich, Y. S.; Petrov, V. I. *J. Raman Spectrosc.* **1993**, *24*, 695.
(492) Li, W.-H.; Li, X.-Y.; Yu, N.-T. *Chem. Phys. Lett.* **2000**, *327*, 153.
(493) Leng, W.; Yasseri, A. A.; Sharma, S.; Li, Z.; Woo, H. Y.; Vak, D.; Bazan, G. C.; Myers Kelley, A. *Anal. Chem.* **2006**, *78*, 6279.
(494) Li, X.-Y.; Huang, Q.-J.; Petrov, V. I.; Xie, Y.-T.; Luo, Q.; Yu, X.; Yan, Y.-J. *J. Raman Spectrosc.* **2005**, *36*, 555.
(495) Ikeda, K.; Takase, M.; Sawai, Y.; Nabika, H.; Murakoshi, K.; Uosaki, K. *J. Chem. Phys.* **2007**, *127*, No. 111103.
(496) Itoh, T.; Yoshikawa, H.; Yoshida, K.; Biju, V.; Ishikawa, M. *J. Chem. Phys.* **2009**, *130*, No. 214706.
(497) Itoh, T.; Ozaki, Y.; Yoshikawa, H.; Ihama, T.; Masuhara, H. *Appl. Phys. Lett.* **2006**, *88*, No. 084102.
(498) Milojevich, C. B.; Silverstein, D. W.; Jensen, L.; Camden, J. P. *ChemPhysChem* 2010, *12*, 101.
(499) Murphy, D. V.; Raben, K. U. V.; Chang, R. K.; Dorain, P. B. *Chem. Phys. Lett.* **1982**, *85*, 43.
(500) Golab, J. T.; Sprague, J. R.; Carron, K. T.; Schatz, G. C.; Van Duyne, R. P. *J. Chem. Phys.* **1988**, *88*, 7942.
(501) Yang, W.-H.; Schatz, G. C. *J. Chem. Phys.* **1992**, *97*, 3831.
(502) Yang, W.-H.; Hulteen, J.; Schatz, G. C.; Van Duyne, R. P. *J. Chem. Phys.* **1996**, *104*, 4313.
(503) Cyvin, S. J.; Rauch, J. E.; Decius, J. C. *J. Chem. Phys.* **1965**, *43*, 4083.
(504) Christie, J. H.; Lockwood, D. J. *J. Chem. Phys.* **1971**, *54*, 1141.
(505) Valley, N.; Jensen, L.; Autschbach, J.; Schatz, G. C. *J. Chem. Phys.* **2010**, *133*, No. 054103.
(506) Neddersen, J. P.; Mounter, S. A.; Bostick, J. M.; Johnson, C. K. *J. Chem. Phys.* **1989**, *90*, 4719.